DESIGN OF A 3D PRINTED

TENDON GRAFT SLEEVE

FOR OSTEOINTEGRATION

ENHANCEMENT

PNG SI NING

NATIONAL UNIVERSITY OF SINGAPORE

2017

DESIGN OF A 3D PRINTED

TENDON GRAFT SLEEVE

FOR OSTEOINTEGRATION

ENHANCEMENT

PNG SI NING

(B.Eng. (Hons.), NUS)

A THESIS SUBMITTED FOR THE DEGREE OF MASTER OF ENGINEERING

DEPARTMENT OF BIOMEDICAL ENGINEERING
NATIONAL UNIVERSITY OF SINGAPORE

2017

Supervisors:
Professor James Goh Cho Hong

Examiners:
Associate Professor Leo Hwa Liang
Dr Yeow Chen Hua

Declaration

I hereby declare that this thesis is my original work and it has been written by me in its entirety. I have duly acknowledged all the sources of information which have been used in the thesis.

The thesis has also not been submitted for any degree in any university previously.

_____
PNG SI NING

20/04/2017

Acknowledgement

The author would like to take this opportunity to express her deepest gratitude to the following people who have made the completion of this thesis possible.

To Prof James Goh, I would like to express my heartfelt gratitude for the opportunity and your invaluable guidance rendered throughout the course of my masters. You have been more than just my supervisor but also a mentor that I always look up to.

To Dr Thomas Teh and Dr Neo Puay Yong, a big heartfelt thank you for all your selfless mentoring and sharing of knowledge and advice during the various stages of my masters. I would also like to specially thank Yee Wei and Rahiem for the support you have given in order to bring this project to fruition.

To all my friends and colleagues from the NUS Tissue Engineering Programme and Tissue Repair Lab, thank you for the encouragement and support for the past 2 years. The camaraderie and friendships we have forged will be always be one of my most cherished memories.

To the staff at the Department of Biomedical Engineering (Jacqueline, Melinda, Annie, Kun Song), a huge thank you for all the help that you have given for all these years.

Last but not least, to my family and friends, no amount of words is enough to express my thanks. Thank you for all your understanding and support and for being my unwavering pillar of strength throughout my studies.

Table of Contents

Summary

ACL tears are known to have a high rate of incidence amongst athletes. Due to its low vascularization and thus low healing ability, ACL tears eventually lead to degenerative joint diseases. The current gold standard for ACL tears is ACL reconstruction surgery with hamstring autografts. However, the primary focus is on mechanical fixation instead of the histological osteointegration of the graft within the bone tunnel; leading to inferior integration and graft pull-out and the need for a subsequent revision ACL surgery.

The aim of this thesis is therefore to design and develop a 3D printed device as a graft sleeve in the promotion of osteointegration at the bone – graft interface within the bone tunnel for ACL reconstruction surgery applications. Using Solidworks, various designs were explored, tested and evaluated for its efficacy as a graft sleeve device. Concurrently, silk and silk-based materials were explored for their potential in being 3D printable bioinks for translation of the design from current non-biocompatible 3D printing materials to a biocompatible silk – based material. Studies for this thesis were separated into 2 phases, the design phase and the material phase:

In the design phase, various tubular designs with locking or latching mechanisms and features like teethed protrusions along the inner walls of the sleeve were explored. Results showed that a full hollow tube structure with regular teethed protrusions along the inner wall of design had the best grip strength on the tendon graft enclosed within and also allowed for the successful pull-through of the graft – sleeve construct through the bone tunnel.

The form of the device (i.e. shape and structure) is closely dependent on its intended function. Hence, whether the design of the device is translatable for a clinical ACL reconstruction surgery application is dependent on the biocompatibility, cell supporting ability, mechanical and structural properties of the material. In the material phase, pure silk solutions were first explored for their compatibility as a bioink material. However, results showed extruded pure silk solutions   had long gelation times and weak mechanical properties and were thus not compatible as bioinks. Following that, various silk-polymer composites were explored for their compatibility and silk/SDS/Pluronic composite showed the most promise as a future biocompatible bioink compatible with current 3D printing technologies.

With the current work, it can be concluded that the final graft sleeve design is a reproducible alternative for current tissue augmentation devices and that the silk/SDS/Pluronic composite material may be a prospective biocompatible bio ink for the printing of such a graft sleeve device for application in ACL reconstruction.

List of Tables

List of Figures

ii

List of Abbreviations and Symbols

β	Beta
3D	3 – Dimensional
ACL	Anterior Cruciate Ligament
ANOVA	Analysis of Variance
bFGF	basic fibroblast growth factor
BMP	Bone morphogenetic proteins
BMSCs	Bone marrow mesenchymal stem cells
BPTP	Bone-patella tendon-bone
CAD	Computer-aided design
dH_2O	Distilled water
DLP	Digital light processing
ECM	Extracellular matrix
EGF	Epithelial growth factor
FDA	Food and Drug Administration
G-CSF	Granulocyte colony-stimulating factor
H_2O_2	Hydrogen Peroxide
HRP	Horseradish Peroxidase
MMPs	Matrix Metalloproteinases
MSCs	Mesenchymal stem cells
Na_2CO_3	Sodium carbonate
PEG	Poly(ethylene)glycol
PCL	Polycaprolactone
PDGF	Platelet-derived growth factor

PDS	Polydioxanone
PLA	Polylactic acid
PGA	Polyglycolic acid
PLGA	Poly(lactide-coglycolide)
PLLA	Poly L-lactic acid
PRP	Platelet-rich plasma
PTFE	Polytetrafluoroethylene
PVA	Poly(vinyl alcohol)
SDS	Sodium dodecyl sulfate
SF	Silk fibroin
TGFβ	Transforming growth factor beta
TIMPs	Tissue Inhibitor of Metalloproteinase
VEGF	Vascular endothelial growth factor

1 Background

1.1. Anterior Cruciate Ligament

The anterior cruciate ligament (ACL) is one of the four major ligaments in the human knee joint that coordinates function and promotes stability [1]. Consisting of a band of dense connective tissues, the ACL is made up of two major fiber bundles - the anteromedial and posterolateral bundles. The ACL originates at the medial side of the lateral femoral condyle and passes obliquely through the intercondylar fossa before insertion at the medial tibial eminence [2, 3]. Being a key structure in the human knee joint, the ACL restrains anterior tibial translation with regards to the femur and resists abnormal rotational loads of the tibia. This helps in ensuring the stability of the knee joint and reduces the likelihood of ACL rupture [4].

ACL injuries are one of the most common injuries of the knee and typically occur amongst athletes during high impact or high-pivoting sport activities when there is a sudden deceleration, twisting, cutting or jumping action [1, 5]. Over 200 000 patients are diagnosed with ACL tears annually with an incidence rate of 1 in 3000 [6, 7]. Due to the lack of sufficient vascularization resulting in the poor healing ability of the ACL, the instability in the knee persists and eventually results in degenerative joint diseases [1, 8]. Therefore, surgical intervention in the form of reconstruction with biological tissue grafts is required [2, 6].

1.2. Clinical Treatment of ACL Injury

In the past, there were many different methods of treating ACL tears; from non-operative techniques to surgical procedures. In the 1970s, primary repair of the torn ACL in the form of suturing was used but was later abandoned because of poor clinical results. In the 1980s, prosthetic grafts made of synthetic materials were used. However, these prosthetic

1

grafts had complications such as increased wear debris and inferior clinical data. The current gold standard of surgical reconstruction of ACL is using local autografts or allografts because of their potential of undergoing remodelling and hence integration into the native joint [9-11].

During ACL reconstruction surgery, bone tunnels that pass through the original attachments of the native ACL are drilled through the tibia and femur. After suturing the harvested grafts into double bundle, the final graft is then passed through the two bone tunnels and then fixed using commercial fixation devices like interference screws. This fixation point is the weakest point of the graft and will remain the weakest point until healing in the bone tunnel occurs [8].

1.2.1. Autografts and Allografts

The two most common autografts used clinically are the bone-patella tendon-bone (BPTP) and the hamstring tendon grafts. Traditionally, the BPTP autograft was preferred especially for young and active patients and was harvested generally from the middle one third of the patellar tendon with a portion of bone at each end. Thereafter, interference screws were used for fixation of the bone plugs in place [8].

Compared with the hamstring tendon grafts, BPTP autografts were found to have better tissue-to-bone fixation strength and mechanical properties, improved bone-to-bone integration at the insertion sites and thus, faster healing with the native tissues. However, it has been found that the morbidity rates of knee ligaments using BPTB autografts were much higher and there were other implications such as weakness in the quadriceps, pain or fracture of the patella and the inability to kneel [1, 12-15]. Comparatively, hamstring autografts have the advantages of lesser donor site complications, a smaller incision site,

decreased pain in the knee during kneeling and a thicker tendinous graft within the bone tunnel [9, 13-15].

Alternatively, allografts have many advantages such as the elimination of donor site morbidity, smaller incision sizes and no limitations to its size. Nonetheless, allografts have their complications like limited supply due to a finite pool of donors, delayed biological incorporation and risk of transmission of blood-borne diseases. Possible host immune response, decreased mechanical strength due to sterilization processes required have also led to higher failure rates of ACL reconstructions using allografts [6, 7, 10, 13-15].

1.2.2. Synthetic Ligaments

Synthetic grafts date back to the early 1970s as substitutes for ACL replacement grafts due to the shortcomings of autografts and allografts. They can be classified as grafts, stents or augmentation devices and prosthesis [16, 17].

Currently, Food and Drug Administration (FDA) approved synthetic grafts in the market include grafts made of materials like polypropylene, polyethylene terephthalate and polytetrafluoroethylene (PTFE) [18]. However, though these grafts had satisfactory initial strength and provided initial stability to the knee, clinical success was limited because of foreign body response to the wear debris of the implant and the lack of integration with native tissues which resulted in mechanical fatigue and subsequent graft rupture or failure [6, 19].

The stent approach focused on the role of augmentation; where a mechanically inferior material was wrapped around the autologous implant to form a composite structure such

3

as the Kennedy ligament augmentation device. This method aimed to protect the autologous graft during early stage vascularisation when the artificial material performed its role as a load carrier so that there was gradual load transfer to the healing tissues [17, 19, 20]. Unfortunately, such grafts may have an unintended stress-shielding effect on the autogenous tissue and prevent adequate mechanical strength development [17].

Lastly, prosthetic implants had been proven to have very limited success. These were usually in the form of scaffolds which induced fibrous tissue ingrowth and the formation of a neo-ligament at the intra-articular region which led to the subsequent increase in the ultimate strength of the synthetic ligament. Nonetheless, these prosthetics did not last because of their inability in replicating the native mechanical properties. Very often, repeated elongation caused permanent deformation and they were also associated with complications such as chronic effusions and synovitis caused by wear debris [16, 18].

1.2.3. Tissue Engineered Constructs

Tissue engineered constructs thus are developed to address the problem of long term efficacy of synthetic grafts. These constructs are capable of restoring normal joint kinematics to the native knee due to their improvement in mechanical properties over time [17]. In general, these scaffolds are designed to be implantable and at the same time, encourage the ingrowth of tissue and formation of neoligament. They may be seeded with cells from an autograft or allograft or surface modified for enhanced biocompatibility[7].

(a)　　Biological Materials

i.　　　　Collagen Scaffolds

90% of the native ACL is made up of type I collagen. As such, extensive research had been done on the use of collagen-based scaffolds [6]. Initial studies with scaffolds made of collagen fibrils showed fibroblasts adherence to the scaffold and viability *in vitro* and

in vivo. However, collagen degrades rapidly and loses its mechanical properties over time. Hence, various techniques such as using collagen-glycosaminoglycan or collagen-elastin composites, cross-linked collagen or a twisted collagen braid were used for improved mechanical strength of the scaffold [6, 10, 15, 20]. Unfortunately, the improved mechanical strength still did not match that of native ACL and other concerns with leaching of crosslinking agents and immunogenicity with the use of collagen harvested from animals had pushed for the use of other materials with more favourable properties [6, 10, 21].

ii.   Silk Scaffolds

Silk, an inexpensive and biocompatible material, is an improvement to collagen. With its outstanding and tailorable mechanical properties, silk fibres when braided into a rope-like geometry, has mechanical properties matching those of native functional ACL [22]. At the same time, it has a slow degradation rate *in vitro* and *in vivo*, undergoes complete degradation in 2 years *in vitro* [6, 20] and is able to maintain long term mechanical tensile integrity [15]. Compared with collagen scaffolds, the slow degradation rate of silk scaffolds is very critical in ensuring primary stability to the knee during the time for ingrowing cells to generate neoligamentous tissue [10]. When seeded with human bone marrow mesenchymal stem cells (BMSCs), silk scaffolds were found to support the regeneration of ligament 24 weeks after implantation in a porcine animal model [23].

iii.   Other Biological Materials

Other biological materials used in ACL tissue engineering include hyaluronic acid [24], chitosan [25-27] and alginate [28-31]. Though these materials are highly biocompatible with the human body, the general disadvantage is that they lack mechanical strength [24-31]. In addition, chitosan scaffolds also have limited cell adhesion [25-27].

(b) Synthetic Polymer Scaffolds

Synthetic biodegradable scaffolds are versatile alternatives to scaffolds made from biological materials like silk and collagen. With different fabrication techniques and the wide selection of materials, scaffolds with the exact adaptation of native ACL's mechanical properties and tissue response as well as degradation rate can be fabricated [10]. Biodegradable materials like polylactic acid (PLA), polyglycolic acid (PGA) and poly(lactide-coglycolide) (PLGA) were found to be unsuitable materials as ACL grafts as they are biologically inert and their degradation rates and hence loss in mechanical properties are too rapid for the remodelling rate of native tissues [21]. In addition, lactic acid and wear debris which are the byproducts of hydrolytic degradation of biodegradable materials, caused pH changes at the degradation site and bone resorption [32]. To improve the degradation rate, PGA scaffolds coated with polycaprolactone (PCL) to improve the degradation rate were demonstrated to have improved fibroblast attachment and proliferation [6, 10, 33]. Braided polydioxanone (PDS) scaffolds were considered but were found to have an early loss of their mechanical properties in *in vivo* animal studies. Poly L-lactic acid (PLLA) scaffolds manufactured in braid-twist manner had the best viscoelastic properties and cellular proliferation [6, 10].

1.3. Unmet Clinical Need

Despite the platitude of natural and synthetic grafts and scaffolds that can be used for ACL reconstruction, graft failure due to lack of healing at the bone-graft interface is still common [8]. The attachment site of the graft is very often the weak link post-surgery and is the reason for the delay in early return to function [34]. Hence, the integration between tendon graft and host bone is critical in ensuring a shorter healing time, improved fixation strength and therefore less risk of graft loosening and pull-out and the eventual need for a

revision surgery [8, 35]. However, current techniques focus primarily on mechanical fixation alone and not on the histological tendon osteointegration.

1.4. Aim

Therefore, the aim of this thesis is to design and develop a 3D printed device that will have its future application in ACL reconstruction surgery; as a graft sleeve which helps in the promotion of osteointegration at the bone-tendon-graft interface within the bone tunnel. This device will act as a scaffold for support and mediation of bone growth at the interface and also potentially as a carrier for the osteoconductive factor, nanohydroxyapatite.

1.5. Objectives and Scope

This thesis has two main focus for the development of a successful ACL graft sleeve; design and material of the graft sleeve. Chapter 1 provided a brief introduction of the anterior cruciate ligament in the human knee joint, the current gold standard of ACL regeneration and the current clinical problem of such a treatment method. Chapter 2 will provide the literature review for the current state of the art in improved osteointegration within the bone tunnel in ACL reconstruction, the different methods of scaffold fabrication with specific focus on 3D printing, its current technology and the bioinks currently available.

The aim of the focus on design is to explore and develop the different scaffold designs for the purpose of enveloping the ACL graft like a sleeve and will be addressed in Chapter 3. In this chapter, the device design development will be addressed with the introduction of various scaffold designs developed using CAD drawings on Solidworks and printed with a commercial 3D printer. Thereafter, bench testing and Instron testing of the printed designs will be conducted and the results and feasibility of each design will be discussed.

Chapter 4 addresses the aim of the material of the device; which is to explore the possibility of developing silk as a 3D printable "ink" for its subsequent use as a biocompatible material for fabrication of the ACL graft sleeve. This chapter will address silk as a 3D printable "ink" and explore other silk-polymer composites that could be the next novel material for use as a biocompatible 3D printable "ink".

A comparative discussion and conclusion will then be made in Chapter 5 where the potential bioink materials will be compared and the best material to be recommended for future works. Lastly, Chapter 6 will conclude the key results in this thesis and provide recommendations for future works and development.

2 Literature review
2.1. Background of the Enthesis

In the human body, soft tissues like tendons and ligaments insert into hard tissues like bone, forming the enthesis which is very critical for musculoskeletal motion [36]. This functional integration zone has a very complex structure with graded mechanical properties to facilitate transmission and dissipation of physiological loads and stress concentrations; therefore ensuring smooth joint motion [37, 38]. The enthesis takes two forms, fibrous or fibrocartilaginous. Fibrous enthesis or indirect insertions have the characteristics of tendon incorporation to the periosteum during development while direct insertions or fibrocartilaginous enthesis have direct incorporation to the epiphysis or apophysis of a bone via a complex transitional tissue [39, 40].

2.1.1. Structure of the Enthesis

In the knee joint, studies have shown that there are four continuous transitional zones in the fibrocartilaginous enthesis; namely the ligament, the fibrocartilage, mineralized fibrocartilage and bone. These four zones have their characteristic spatial arrangement of cell types and composition of matrix; representing a gradual transition in composition, biochemical and structural elements. The ligament is made up of interspersed fibroblasts within a matrix of collagen I and III fibers in parallel [36, 39, 41]. The fibrocartilage interface in zone 2 is unmineralized, has more random collagen bundles of collagen types II and III and chondrocyte-like cells arranged in rows or pairs in lacunae of extracellular matrix [37, 39, 41-43]. The deeper region of the fibrocartilage layer becomes calcified to form the mineralized fibrocartilage layer (Zone 3) and is made up predominantly of collagen type II and type X [36, 41, 43]. Zones 2 and 3 are separated from bone by the tidemark, a perpendicularly transversing line separating the two regions[38]. Lastly, Zone 4 is made of trabecular bone and this layer has osteoblasts, osteocytes and osteoclasts

embedded within a highly calcified matrix made up predominantly of type I collagen [39, 42].

2.1.2. Development of the Enthesis

In early human development, the ligament is attached to the hyaline cartilage which forms the anlagen for future bone [44, 45]. Type I, II and X collagen is localized at these ligament-to-bone insertion sites. The enthesis mineralization process acts similarly to that of chondrocyte hypertrophy at the growth plates. The type II collagen-expressing chondrocytes present in hyaline cartilage undergoes the cellular process of endochondral ossification. Very simply, bone microvessels penetrate into the cartilage and results in gradual bone tissue development along the blood vessels. This bone tissue expansion via ingrowth of blood vessel stops when no hyaline cartilage remains. Eventually, the undersurface of cartilage is eroded and replaced with bony trabeculae [46-48]. During this remodeling process, the collagen fibers and mineral continues to develop via fibroblast metaplasia and eventually, a well-organised and mature transitional tissue is formed [45]. On the other hand, the ligament cells at the ligament side undergo metaplasia into cartilage cells, thereby producing a layer of fibrocartilage [46-48].

2.1.3. Importance of Enthesis for ACL reconstruction

Enthesis development is very crucial for ACL reconstruction surgeries because the most common reason for graft failure is the lack of healing between the tendon graft and bone within the bone tunnel [8]. After implantation of the tendon graft, a layer of fibrovascular scar tissue forms between the graft and bone tunnel interface [8, 49] with no collagen continuity between the graft and bone. Then, new bone formation occurs along the bone tunnel [50]. Subsequent bone growth into the interface tissue with the resulting integration of the outer portion of the graft enhances the attachment strength of the graft [51]. Collagen forming perpendicular fibres, which resembles that of Sharpey's fibres

found in fibrous enthesis, connects the graft to the surrounding bone. Eventually, an interfacial tissue like a fibrous enthesis is formed, with continuity of collagen fibres between the graft and surrounding bone throughout the length of the bone tunnel [50, 51]. The graft can now be described as osteointegrated with native bone since the formation of such a fibrous enthesis prohibits any relative movement between the graft and the bone it has direct contact with [52]. However, this healing process is extremely slow because the fibrocartilage zone formed is avascular in nature and is further aggravated by the loss of bone at the site of injury when a bone tunnel is artificially created [40, 53]. In addition, the different healing rates of the tendon graft and native bone could be a potential reason for the lack of tissue integration. Tendons have low vascularity and cellularity and typically require a year of healing before return to its normal function whereas bone healing only takes 12 weeks [45]. Moreover, the native structure and composition of the enthesis is also not reformed during healing and this result in an interface that is mechanically and structurally inferior [38, 40, 45, 51, 53]. This often causes stress concentrations at the insertion sites and therefore high rates of failure [45].

2.2. Current state of the art for ACL enthesis development

The mechanical strength of the bone-graft attachment has been shown to correlate with the degree of osseous ingrowth and mineralization of the healing tissue [54, 55]. Till date, there is no optimal technique or method for improving osteointegration at this interface. Currently, there are various approaches for enhancing bone formation and bone loss reduction in order to promote interfacial osteointegration [49]. These methods can be classified into six approaches; they are growth factors, biomaterial, chemical and biological agents, cell therapy, biophysical modalities and lastly gene transfer and therapy [45, 53].

2.2.1. Molecular Approach

(a) Growth Factors

During tendon and bone healing, a large number of growth factors and cytokines are secreted [45] which helps in the regulation of collagen production. Specifically, insulin-like growth factors I and II (IGF-1 and II), transforming growth factorβ (TGFβ), vascular endothelial growth factor (VEGF), platelet-derived growth factor (PDGF) and basic fibroblast growth factor (bFGF) are found to be upregulated and synergistically direct the healing process [50]. Other growth factors such as epithelial growth factor (EGF) combined with TGFβ, granulocyte colony-stimulating factor (G-CSF) and bone morphogenetic proteins (BMP) have also been employed at the insertion site [45, 53, 56]. BMP, members of the TNFβ superfamily, is the most potent osteoinductive growth factor with BMP-2 having the best positive results on bone formation and remodelling at the interface [50, 57]. Increasingly, platelet-rich plasma (PRP), an autologous derivative of blood high in platelets concentration, has been proposed as a novel and non-invasive treatment method for ACL repair. The theoretical benefit of this treatment method is that

being rich in growth factors and cytokines in a physiological combination, it provides an ideal local tissue healing and regeneration environment for improved osteointegration at the interface [50, 58].

In general, with the introduction of these growth factors, an upregulation of osteogenic factors, increased cell proliferation, extracellular matrix (ECM) synthesis and deposition and increased collagen production has led to the enhanced osteointegration at the interface [6, 7, 10, 38, 45, 50, 53, 56, 58]. Nonetheless, concerns such as their short life span and the delivery and maintenance at the treatment site have limited the efficacy of these growth factors [6, 7, 10, 58].

(b) Chemical and Biological Agents

After ACL injury and reconstruction, the intra-articular environment is critical in the healing of the ACL. Matrix Metalloproteinases (MMPs) and Tissue Inhibitor of Metalloproteinase (TIMPs) are important enzymes in the process of tissue remodelling. Post injury, the levels of MMPs and TIMPs are observed to increase in the synovial fluid [59, 60]. Moreover, the balance of the levels of the two may affect the susceptibility to cartilage destruction [59]. α2-macroglobulin, a MMP inhibitor, was observed to enhance bone healing and increase collagen levels when applied at the bone tendon insertion site in animal models [45].

The depletion of macrophages post-injury also plays a role in inflammation and tissue fibrosis, therefore affecting ligament healing. Liposome-encapsulated clodronate, an inhibitor of macrophages, when injected into mice models, demonstrated improved healing [53, 61].

During the healing process, neovascularization and angiogenesis occurs. Hence, with hyperbaric oxygen treatment, neovascularization at the interface, collagen organization and tendon osteointegration was also similarly observed [53].

2.2.2. Cellular Approach

Stem cells are often used in tissue regeneration because of their potential for self-renewing and multi-differentiation with the application of endogenous and exogenous factors [51]. Particularly, the use of mesenchymal stem cells (MSCs) in cellular therapies for musculoskeletal diseases has emerged as the current gold standard. MSCs are easy to expand and because of their multipotency and their ability to secrete bioactive growth factors and cytokines, they can provide a regenerative microenvironment and have the potential of restoring the native tissue structure [38, 60]. MSCs applied either via intravascular injections to graft surfaces or seeded in scaffolds were found to upregulate type II collagen production [62] and improve osteointegration of the graft to bone [59]. Synovial MSCs, which has a higher proliferation and differentiation potential when compared with BMSCs, showed accelerated fibrous structure formation and enhanced collagen fibres formation at the interface [51]. Bone marrow aspirates or periosteal progenitor cells introduced into bone tunnels with the tendon graft or wrapped as a piece of cell sheet around the tendon graft showed the extensive formation of new bone and fibrocartilage at the interface with excellent integration in between [8, 60, 63].

2.2.3. Gene Therapy Approach

Gene therapy in ligaments typically uses nonviral gene delivery vectors or viruses-derived vectors where the viruses have natural entry pathways in the cell. Such a method allows the mediation of specific gene expressions to alter the synthesis of tissue endogenous proteins [58]. The primary advantage of this approach is that delivery of the gene to the target tissue now allows for a sustained and prolonged release of growth

factors. As such, by infecting tendon grafts with an adenovirus-BMP-2 gene, the integration of the tendon graft to the bone tunnel is shown to be improved [53]. BMSCs genetically modified with growth factors such as bFGF and BMP2 and transplanted to injury sites in rabbit models have revealed that healing is augmented. There were cartilage-like cells formed at the bone-graft interface, smaller bone tunnel area and improved ultimate load and stiffness [64]. Using an adenoviral vector-laden collagen hydrogel, growth factors like TGF-β1 and genes like IGF-1 cDNA can be transferred *in situ* to the injury site. Increased cellularisation and deposition of collagen I and III demonstrated enhanced osteointegration of the interface [65, 66]. Nonetheless, gene therapy has its disadvantages such as the high risk of mutagenesis, malignancy and toxicity. The loss or decrease in the expression of the transferred gene after a short period of time is also equally challenging [40, 53, 58, 64].

2.2.4. Tissue Engineering Approach

(a) Biophysical Modalities

Low-intensity pulsed ultrasound has been demonstrated to be clinically beneficial for accelerating bone fracture healing and cartilage defects [45, 53, 67]. Not only is osteoblast activity and vascularization upregulated, tendon-to-bone healing is accelerated and the resulting interface morphology is similar to that of the native enthesis. The interface is also mechanically superior with an improved peak load to failure and stiffness when compared with controls in a sheep model [40, 68]. However, this approach is a time intensive procedure [40].

Extracorporeal shockwave treatment is thought to affect the healing of bone through exerting direct pressure or causing cavitation. Less time is required as compared with low-intensity pulsed ultrasound because a higher amount of energy is used [40]. The high

15

pressure shockwaves alter the interface's surround biochemical environment. This helps in the upregulation of growth factors, the creation of an environment with ingrowth of neovascularization and angiogenesis and increased formation of bone and collagen [69-71]. Till date, the optimal parameters of use of this technique are still unclear [40].

The use of mechanical loading for the regeneration of a functional bone-tendon interface has only been recently explored. It is postulated that during the process of endochondral ossification, mechanical loading is necessary for the continued maturation of mineralized bone [60, 72]. Physiological loading in the form of multidimensional mechanical strains when applied showed enhanced MSCs proliferation, upregulation of types I and II collagen and promoted ligament fibroblast induction of the cells within scaffolds [73, 74]. Other studies with delayed application of cyclic loading showed improved mechanical properties and biological parameters for enhancement of bone-tendon healing [40]. However, studies with short and low levels of controlled loading showed a decrease in the number of trabecular at the interface though tendon-bone healing was not affected [75]. This indicates that till date, there is no ideal mechanical stimulation regime in terms of type, magnitude, and duration of mechanical stimuli for enhancement of bone-graft integration [73, 74, 76, 77].

(b) Biomaterial

Having a similar composition to native bone, calcium and magnesium phosphate biocements or adhesives are used to enhance osteointegration at the interface [53]. These bone cements together with brushite calcium phosphate cement (dicalcium phosphate dihydrate) provides a biocompatible and osteoconductive environment for enhanced cell proliferation and recruitment of growth factors [40]. Tricalcium phosphate and hydroxyapatite [78, 79], either in injectables form, as bone cements or as additives and

16

coatings to tissue engineered scaffolds, were observed to induce bone development and osteointegration at the interface. The precipitation of calcium phosphates onto the tendon graft forming a "hybridized" graft has also been shown to enhance tendon-bone healing more quickly and the mechanical strength of the interfacial tissue was also much stronger [8, 40, 45, 49, 53]. Demineralized bone matrix is another alternative that has been shown to induce the growth of more fibrocartilaginous tissue and mineralized fibrocartilage and possibly an enthesis interface which is physiologically similar. However, the mechanical strength of such an interface has yet to be determined [8, 45].

(c)   Synergistic Approach

As discussed above, the regeneration of the native tendon-bone interface is extremely challenging. It is necessary to reconstruct the complex tissue gradient of native interface *ex vivo* and subsequently maintain this gradient through the application of growth factors at the insertion site in vivo. Therefore, a synergistic approach of using cells and scaffold is the proposed approach to successfully promote osteointegration at this interface [38].

2.3.   Current state of the art – Scaffold Fabrication for Tissue Engineering Applications

In tissue engineering, a well-designed three-dimensional scaffold with the appropriate geometry and physical structure is critical for enhancing cell penetration and guiding tissue formation *in vitro* and *in vivo*. Conventional scaffold fabrication techniques include solvent casting and particulate leaching, phase separation, gas foaming and freeze drying [80-83]. However, these techniques are limited in the control of pore sizes geometry, interconnectivity and spatial distribution [84, 85]. Moreover, the scaffolds produced with conventional methods have weak physical and mechanical properties and are prone to deformation[83]. Hence, more advanced techniques such as electrospinning,

rapid prototyping [85] and biofabrication [86] have evolved so as to provide chemical, mechanical, structural and biological supports [84].

2.3.1. Conventional Techniques

(a) Solvent Casting & Particulate Leaching

There are two methods of solvent casting: the first method is to dip the prepared mould into a polymeric solution and allow the mould to dry while the second method involves pouring of the polymeric solution onto the mould and the subsequent slow evaporation of the solvent. Both methods create a polymeric membrane that adheres to the mould after the evaporation of the solvent [84]. For the creation of porous scaffolds, the solvent casting method is typically used together with the particulate leaching method. Briefly, the polymer is dissolved in an organic solvent before the addition of porogens (i.e. salts or sugars of desired sizes). The mixture is then cast onto a mould and the solvent is allowed to evaporate. Following that, the scaffold is immersed in water for the leaching out of the salt crystals, creating porous scaffolds [82]. While these methods are simple in obtaining desired pore size percentages and crystallinity, the shapes and interconnectivity of the pores created, the internal architecture and topology are uncontrollable and the maximum membrane thickness that was obtained was only 3mm [82, 84, 87].

(b) Phase Separation

This method involves the separation of the polymeric solution into the polymer-rich and polymer-poor phase via a change in temperature or with a non-solvent. Phase separation via the use of a non-solvent is not optimal for tissue engineering applications as a heterogeneous pore structure is created. The polymer solution is first quenched at low temperatures and becomes thermodynamically unstable. Hence, it undergoes a phase separation of the liquid-liquid phase into a polymer-rich phase and a polymer-poor phase.

The polymer-rich phase solidifies and forms a matrix whilst the polymer-poor phase forms pores from the removal of solvent [81, 82, 84].

(c) Gas Foaming

During this process, gas-foaming agents such as carbon dioxide and nitrogen, water or fluoroform are used. The polymers are pressurized at high pressures with the gas-foaming agents till saturation and this result in the nucleation and growth of gas bubbles in the polymers which creates pores in the polymer volume. The extent of porosity is dependent upon the porogens used. One major advantage of this technique is that organic solvents do not need to be used. However, the final scaffold fabricated yields a structure with largely unconnected pores and an external surface that is non-porous [81, 82, 84].

(d) Freeze Drying

Freeze drying process is typically carried out in 2 phases. In the initial freezing phase, the polymer is cooled down till ice crystals are formed in the solvent, forcing the aggregation of polymer molecules into the interstitial spaces. Subsequently, removal of the solvent is done via the application of a partial vacuum pressure and a dry interconnected random porous scaffold is formed when all solvent is sublimated and unfrozen water is removed by desorption [81, 82].

2.3.2. Advanced Techniques

(a) Electrospinning

This widely used technique uses electrical charges in the fabrication of nano-scale or micro-scale fibers with small pore sizes and high surface area to volume ratios. Firstly, a high voltage source is applied to a polymer solution or melt filled capillary tube. By surface tension, the solution or melt is held at the tip of the capillary. Upon application of an electric field, a mutual charge repulsion opposite to that of the surface tension is induced within the solution or melt. By increasing the electrical field intensity, the charge

19

repulsion overcomes the surface tension, forming a jet. Lastly, as the ejected jet travels to the collector where collection of fibres occurs, repulsion between the solution and melt occurs, causing solvent evaporation to form fibres [81, 82, 84]. The process is advantageous mainly due to its versatility and non-invasiveness, and coagulating agents or high temperatures are not required [84]. Moreover, scaffolds fabricated via electrospinning have been proven to promote cell adhesion, growth and proliferation and binding [88, 89]. Nonetheless, complex topography and structures and homogenous pore distribution through the scaffold is still non-achievable via electrospinning [81].

(b) Rapid Prototyping

Solid freeform fabrication is a fabrication technique which produces freeform solid objects from a computer model directly; without any human intervention or tooling [90] and rapid prototyping is one of the advanced forms of this technique[84]. Basically, rapid prototyping reads the information from computer-aided design (CAD) drawings, converts the information to an STL type file format and then into a series of cross-sectional layers to be read by the printer. This bottom-up approach manufactures three-dimensional scaffolds in a layer-by-layer fashion according to the drawing; with each layer glued or bonded to the previous layer [85, 91]. Based on the type of scaffold biomaterial that is required, the ideal type and technology of rapid prototyping is selected. Generally, for tissue engineering applications of biological material deposition and patterning, the main technologies used are inkjet, extrusion and light-assisted. Selection of the technology is based on the surface resolution and cell viability of the printed scaffold and the biological bioink for printing [92].

i. Inkjet Printing

Inkjet printing is the most commonly used technique for both non-biological as well as biological applications. Ink cartridges loaded with biological materials are used and controlled volumes of protein or cell solutions are dispensed onto an electronically controlled elevator stage. Thermal or acoustic forces are used to eject liquid droplets onto a substrate which is a support or part of the final scaffold [87, 92, 93].

In thermal inkjet printers, the printer head is electrically heated, producing pressure pulses and forcing the droplets from the nozzle. Inkjet printers are cheap, widely available and have high print speeds. Nonetheless, there are concerns with non-uniform droplet size, exposure of the biological materials to thermal and mechanical stresses and frequent nozzle clogging.

Acoustic forces are generally produced by a piezoelectric crystal or by application of a voltage to a piezoelectric material. The pressure pulses generated ejects the droplets from the nozzle. Comparatively, this technique produces droplets of uniform sizes and controllable rate of ejection and avoids thermal or mechanical stresses on cells [87, 92].

ii. Extrusion Printing

This technique of printing focuses on the principle of extruding continuous material filaments through a fluid dispensing system. A pneumatic or mechanically driven pressure system is used to generate continuous beads of materials for the continuous deposition of filaments in the xy plane. As such, this technique provides better structural integrity to the scaffold [93, 94]. The stage or the extrusion head is then moved along the z-axis for deposition on the previous layer. One example of this technique is Fused Deposition Modelling which originated in the late 1980s. The polymer material being

21

used is heated at the extrusion nozzle head to the melting temperature of the polymer material. Upon extrusion, the intrinsic property of the polymer material causes the immediate hardening of the material to form layers [84]. In tissue engineering applications, very often the bioinks have shear thinning properties to allow for easy flow through the nozzle yet have high viscosities upon deposition. Materials that can flow at room temperature but undergoes cross-linking and gelation at physiologically suitable temperature or vice versa have also been used [92, 93]. Other bioink materials are crosslinked by light and chemical stimulus upon deposition. This technique is the most convenient for creating porous scaffolds and for tissue and organ fabrication [94]. However, the printing resolution and speed is inferior and cell viability after printing is low due to high shear stresses within the nozzle [92, 94].

iii.   Light Assisted Printing

Light assisted printed involves the process of photo-polymerisation of the biomaterials and can be classified into two subgroups: digital light processing (DLP)-based printing and laser-based printing[87, 93].

In DLP-based bioprinting, a digital micromirror device is used for UV light modification. An entire plane of optical pattern (i.e. the mask image) is then projected onto the photopolymer solution which significantly reduces printing time. At the same time, artificial interfaces such as between droplets in inkjet printing and lines in extrusion printing are avoided and the mechanical integrity of the printed scaffolds is enhanced; allowing for complex structures to be printed [87].

On the other hand, laser based printing is based on the Laser-Induced Forward Transfer principle, which uses a pulsed laser beam for transfer of the bioink to the substrate [95].

Briefly, the laser pulse is focused on the absorbing layer of either gold or platinum which creates a higher pressure bubble in the bioink layer. This induces shock waves, generated by the bubble formation, to transfer the bioink onto the collector substrate [92, 94, 95]. The technology of using lasers was first formulated in 1986 and is known as stereolithography. In this technique, a UV laser traces a cross section of the patterns on a curable photopolymer resin. The solidified layers are able to join together when the resin-filled blade is refilled [84]. One special type of laser-based printing, two-photon polymerization uses a near-infrared femtosecond laser to trigger a nonlinear optical effect in the bioink. The bioink then undergoes polymerization and produces scaffolds of extremely high resolution[87].

In general, laser based printing is an emerging technology with many advantages over inkjet and extrusion printing; there is no nozzle clogging because no nozzles are required, it has high precision for the formation of intricate microscale features. However, due to the use of lasers, cell viability in these bioinks is generally low and there are limitations to printability in the z-direction. In addition, fast gelating bioinks are a requirement, there may be possible contamination from the use of photoinitiators and fabrication time is generally longer [87, 92, 94, 95].

iv.   Direct Write Assembly

This printing method is primarily used to achieve fine feature sizes. Through a microscale orifice, beads of materials are dispensed directly into an environment which initiates the curing of the material via temperature, light, humidity gradients or other chemical polymerization techniques into their desired programmed geometries [91].

2.3.3. 3D Printing – Bio-inks

As discussed in previous sections, 3D printing is increasingly being adopted for scaffold fabrication in tissue engineering as it allows for the reproducible and large-scale fabrication of complex and physiologically relevant geometries of extremely high precision that were previously impossible. There are many designs and technologies of 3D printing and similarly, there are many materials that could be used for 3D printing. Very often, properties of these materials that enhance its printability have an opposite effect on its biocompatibility with the human body [96].

(a)   Properties of a bio-ink

Ideally, printable biomaterials must have properties that allows for both printing efficacy and cytocompatibility [97]. This compromise of having cell viable bioinks to have passable yet suboptimal print fidelity is termed as the biofabrication window. In the selection of the optimal materials as a bioink, the material, rheological, chemical and biological characteristics are very critical [98].

i.   Material Properties

The hydration, degradation rate, mechanical stability and permeability of the bioink are important material properties that have to be considered. Besides influencing the eventual viscosity of the bioink, the hydration and permeability of the material also affects the oxygen and nutrient transport to cells within the printed scaffold, the mechanical strength and viscoelasticity of the final construct and its swelling properties [96-98]. However, there is a trade-off between porosity or hydration and mechanical strength; with increased pore sizes or water content, the mechanical strength of the final construct decreases [97]. The mechanical properties and degradation rate of the material also influence the cellular proliferation and differentiation within the scaffold, extracellular matrix production and remodelling and the scaffold's long term biocompatibility [96, 98].

ii.   Rheological Properties

The consistency, printability, extrusion rate, resolution and eventual shape retention of the bioink are highly dependent on its viscosity. Too high a viscosity will result in clogging or fracture at the dispensing tip whilst an inadequate viscosity imparts detrimental shear forces on the cells. Hence, materials that exhibit shear-thinning properties are best used in printing; there is reduced nozzle-clogging while the cells remain viable and uniformly encapsulated in the low viscosity biomaterial solution [96-98]. The initial viscosity of the bioink also affects the subsequent cross-linking mechanisms for an eventual stable construct [91].

iii.   Chemical Properties

The chemical properties of the material affects its gelation kinetics and in turn, its mechanical properties, biocompatibility, print resolution and structural integrity [96]. Sufficient cross-linking within a single layer has to occur to achieve structural integrity and the challenge is in achieving it without application of cytotoxic processing [91]. The polymer backbone chain mobility and concentration affect the type of cross-linking mechanism (i.e. physical or chemical crosslinking) that can be used. In general, temperature- based crosslinking provides a fast yet unstable construct while chemical dependent crosslinking such as photonic, ionic, electrostatic and pH provides a slower but more permanent construct. The degree and mechanism (i.e. temperature and solvents used) of crosslinking can influence the printing resolution, mechanical properties and cytotoxicity of the construct [96, 97].

iv.   Biological Properties

The biological interactivity of the bioink material is dependent on its eventual applications. The tissue engineered printed constructs should allow for cellular attachment, proliferation, differentiation and subsequent integration with the host tissue.

Moreover, the degradation rate of the biomaterial also affects the remodelling and cytocompability of the scaffold [91].

(b) Types of bio-ink

There are three main categories of bioink: matrix, sacrificial and support. Depending on each category, the bioink properties required has its own specific characteristics [96]. Matrix bioinks are usually media suspended cell slurries or cell-encapsulated synthetic or natural hydrogels. Hence, during the printing process, it is critical for the bioink to shield the cells from shear stresses. A quick, non-toxic gelation mechanism is also required to achieve optimal print resolution and shear thinning biomaterials are often used. Finally, the biomaterial should be degradable, biologically interactive and have hydration, porosity and mechanical properties similar to that of the native extracellular matrix [91, 96]. Examples of such bioinks include collagen, fibrin, silk fibroin, gelatin and its functionalized variations, alginate and chitosan [96, 97, 99].

Sacrificial bioinks offer temporary support or are a part of an intricate 3D printed geometry and are often used with matrix bioinks. High viscosity or shear thinning biomaterials are preferred for smooth extrusion and high print fidelity. In addition, it should be cytocompatible and easy to remove. Common sacrificial bioinks include gelatin, Pluronic [100], agarose [101] and carbohydrate glass [96].

Support bioinks are a more permanent support as compared to sacrificial bioinks. These bioinks together with matrix bioinks enhances the mechanical properties and structure of the printed construct. Hence, these biomaterials should have high mechanical strength and high viscosity to achieve high print fidelity and be cytocompatible and biodegradable.

Examples of support biomaterials are polylactic acid, poly(l-lactic acid), poly(lactic-co-glycolic acid) and polycaprolactone [96, 99, 102].

(c) Silk-based bioinks

There are many materials that are being explored as potential bioinks. These range from natural materials such as polysaccharides (i.e. agarose, alginate, chitosan, dextran, starch), proteins (collagen, fibrin, gelatin, silk fibroin) and glycosaminoglycans (i.e. chondroitin sulfate and hyaluronan) to synthetic polymers such as polyethers (i.e. poly(ethylene glycol), polyesters (i.e. poly(caprolactone), poly(glycolic acid), poly(lactic-co-glycolic acid)), other polymers such as poly(vinyl alcohol) and poloxamers like Pluronic F127 [91, 96-99, 101, 103]. The following literature review shown in Table 1 will be focused on silk-based bioinks as silk is the only protein that matches the native mechanical properties of the ACL and is thus deemed suitable for this application [22].

Table 2- 1: Silk-based bioinks for Tissue Engineering Application

	Bioink	Crosslinking Mechanism	Advantages	Disadvantages	References
Pure Silk	Silk fibroin	Self-assembly	Control over microscale structures and composition	Risk of nozzle clogging	[104-106]
	Silk fibroin	Photonic	Formation of high resolution microstructures	Presence of photo-reactive groups	[107]
	Silk fibroin	Physical	Simple	Time consuming, slow gelation	[108]
Recom-binant silk	Spider Silk Fibroin	Physical	No crosslinking additives or thickeners required	Fabrication of recombinant silk	[109]
Silk Additive Composite	Silk/HRP/H_2O_2	Enzymatic	Low injection force required	Slow gelation	[110-113]
	Silk/Riboflavin	Photonic	Precise control over mechanical properties of gel	Slow gelation and use of lasers required	[114]
	Silk/methylene blue	Photonic	Low damage to cells	Use of lasers is required	[115]
Silk Polymer Composite	Silk/Hydroxyapatite	Chemical	Controlled pore size and porosity gradients	Risk of nozzle clogging	[116]
	Silk/polyethylene glycol	Physical	Rapid gelation; good cell adherence	Weak mechanical properties of construct	[117]
	Silk/gelatin	Chemical, Enzymatic	Temperature sensitive; improved printability	Decreased resolution and weak mechanical properties	[118, 119]
	Silk/Alginate	Chemical, Enzymatic	Fast gelation, Easy removal of alginate	Lack of cell adherence and potential of demixing	[120, 121]
	Silk/Polyol	Self-assembly	Metabolizable, non-toxic polymer; no harsh crosslinking mechanisms required	Risk of buckling of printed constructs	[122]
	Silk/gelatin/glycerol	Physical, Self-assembly	Excellent shape retention, Non-toxic printing and post printing curing	Potential of phase separation of components of blend	[123]

3. Device Design Process

As covered in Chapter 2, there has been extensive research ongoing in the field of enhancing osteointegration at the bone-ligament interface. Nonetheless, current techniques primarily focus on mechanical fixation of the graft and not on the regeneration of the native enthesis to enhance recovery. Hence, there is a critical need to address the histological osteointegration at the bone-ligament interface and it is hypothesized that a graft sleeve at the interface will help address this clinical problem.

3.1. User Needs

In the design of such a graft sleeve device, the identification of the requirements of the user is important. Ultimately, the product should be designed to have features that will fulfil the user needs and also address existing constraints and their importance. In addition, the user needs have to be ranked with the most general primary needs at the top. This ranking of the need importance is essential for subsequent trade-off analysis in the design process and will determine which features are more critical for the successful design of the device [124, 125]. Below is the table of user needs identified for the graft-sleeve device and its importance.

Table 3- 1: User Needs

No	User Needs	Importance
1	Biocompatible with the body	1
2	No micro movements of graft within bone tunnel	2
3	Enhances osseointegration between graft and bone	3
4	Does not break apart during passage through bone tunnel	4
5	Does not slip off the graft during passage through bone tunnel	4
6	Allows cellular and fluid exchange between bone tunnel and graft	5
7	Biodegradable over time	6
8	Sterile for use	7
9	Easy to use	8

3.2. Metric Table

The user needs in Table 2.1 are then translated into measurable characteristics that can reflect the extent to which the product will satisfy the user needs. The underlying assumption is that this translation is possible and that each need is specified by only one metric. Fulfilling this one metric will then ensure that the user need is met. However, it is often difficult to represent one user need with only one metric. Hence, a few metrics may be used to describe a particular user need [125].

Table 3- 2: Metrics

No	Metrics	Units	Importance
1	Extent of irritation when implanted into the body	Qualitative	1
2	Thickness of wall of device	mm	2
3	Length of device	mm	2
4	Diameter of device	mm	2
5	Average time before increased cell proliferation is observed	Days	3
6	Average time before increased cell differentiation is observed	Days	3
7	Pull through strength	N	3
8	Radial extension of device before failure	%	4
9	Tensile strength of device before failure	N	4
10	Porosity of device	%	5
11	Average diameter of pore sizes and its range	µm	5
12	Degradation rate of device	Years	6
13	Material safe for sterilization methods	Yes/No	7
14	Average time taken to load graft into device	minutes	8

3.3. Needs-metrics Matrix

The needs-metric matrix is a common tool used in the representation of the relationship between the user needs and the specified metrics. This helps in ensuring that all user needs are met in the design process. Very simply, the user needs are represented in the rows of the matrix while the metrics are represented in the columns. A cross in the cell in the matrix indicates that the need is related to the metric associated with the cell [125].

Table 3- 3: Needs-Metric Matrix

Needs		Extent of irritation when implanted into the body (1)	Thickness of device wall (2)	Length of device (3)	Diameter of device (4)	Average time before increased cell proliferation is observed (5)	Average time before increased cell differentiation is observed (6)	Pull through strength (7)	Radial extension of device before failure (8)	Tensile strength of device before failure (9)	Porosity of device (10)	Average diameter of pore sizes and its range (11)	Degradation rate of device (12)	Material safe for sterilization methods (13)	Average time taken to load graft into device (14)
Biocompatible with the body	1	x													
No micro movements of graft within bone tunnel	2		x	x	x										
Enhances osseointegration between graft and bone	3					x	x								
Does not break apart during passage through bone tunnel	4							x	x	x					
Does not slip off the graft during passage through bone tunnel	5							x	x	x					
Allows cellular and fluid exchange between bone tunnel and graft	6										x	x			
Biodegradable over time	7												x		
Sterile for use	8													x	
Easy to use	9														x

3.4. Benchmarking with current device

Lastly, benchmarking was done with a similar device, the tissue interface augmentation device for ligament or tendon reconstruction [126] to determine the design specifications of the design to match up to a similar device that is currently available. This process allows for the assigning of target specifications (i.e. optimal values) to each metric for easy design verification and validation in the later stages of device design [125, 127].

Table 3- 4: Metrics Benchmarking

Metric No.	Need No.	Units	Importance	Optimal Values	Minimum Acceptable Value
1	1	Qualitative	1	Moderate irritant	Moderate irritant
2	2,3	mm	2	0.99	1
3	2	mm	2	30	35
4	2,3	mm	2	5	6
5	3	Days	3	7	10
6	3	Days	3	14	20
7	3	N	3	0.952 ± 0.0010	0.8
8	5	%	4	12	10

9	4	N	4	8.08 ± 2.22	7.5
10	6	%	5	70	65
11	6	µm	5	150 ± 20	200 ± 20
12	7	Years	6	1	1.5
13	8	Yes/No	7	Yes	Yes
14	9	minutes	8	30	35

3.5. Design Rationale & Verification

Based on the user needs, the biocompatibility of the material is critical. As covered in Chapter 2, although silk is an excellent material for ACL regeneration applications, there are currently no silk or silk-based biomaterials with properties suitable for printing with conventional 3D printers while having similar mechanical properties as silk braided fibres. Hence, a reverse approach was adopted; to develop an optimal and reproducible 3D printable design with conventional 3D Rapid Prototyping materials before developing a silk-polymer composite with the suitable mechanical properties which match the properties of the Rapid Prototyping material for the optimal design.

The below mentioned designs were printed with the Objet260 Connex3 3D printer from Stratasys, USA. A range of additive manufacturing Stratasys materials (Stratasys PolyJet Materials Data Sheet) were used to print the designs below:

(a) Transparent material (VeroClear-RGD810)

(b) Rubber-like black material (TangoGray FLX950)

(c) Rubber-like black material with different ratios of Veroclear Material and TangoBlack material as per Table 3.5

Table 3- 5: Rubber-like material with different ratios of transparent veroclear material

Primary Material: TangoBlackPlus FLX 980 Secondary Material: Veroclear RGD810					
Material	FLX9040	FLX9050	FLX9060	FLX9070	FLX9085	FLX9095
Ratio of Primary Material	80	70	60	50	40	30

Ratio of Secondary Material	20	30	40	50	60	70

3.5.1. Design Iteration 1
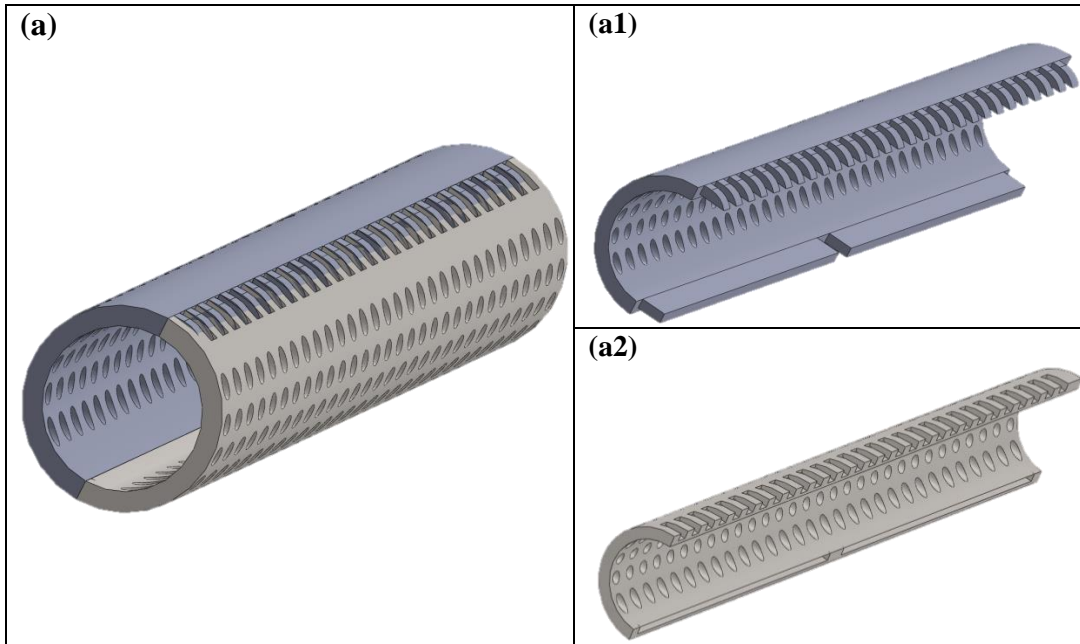
Figure 3- 1. Solidworks Images of Design 1 with length 30mm, diameter 5mm, wall thickness 1mm and pore diameter 1.5mm. Design 1 works on the principle of a snap fit of 2 components to form a hollow cylinder (a). The locking component with teethed edge at the top and a slotting component at the bottom (a1) fit into the adjacent "docking" component with teethed slots and bottom slotting component (a2).

Design 1 is based on the principle of a snap fit assembly method of attaching 2 different components to form the final cylindrical shape by pushing the 2 components' interlocking features together **(Figure 3- 1)**. The rationale is because snap fit assembly methods can be done very easily and quickly and do not have any loose parts unlike assembly methods using nails or screws. There are 2 opposite components in this design; the teeth on the top edge and the slotting component at the bottom edge of component B which will interlock with the empty or "docking" slots of component C.

Initial benchtesting with printed designs of either pure Veroclear material or TangoGray material showed that both these 2 materials were not feasible for this design. Veroclear is too stiff for the snap fit assembly to work and resulted in breaking of the components while TangoBlack material is too soft and the components break when too much mechanical force is applied. Moreover, as the scale of the resolution of the features (i.e. teeth and slots for the teeth to fit into) is in the millimetre range, the strength of the snap fit assembly is not that strong and the two opposite components are not able to interlock and hold together. Hence, this design was considered to be not very feasible.

3.5.2. Design Iteration 2
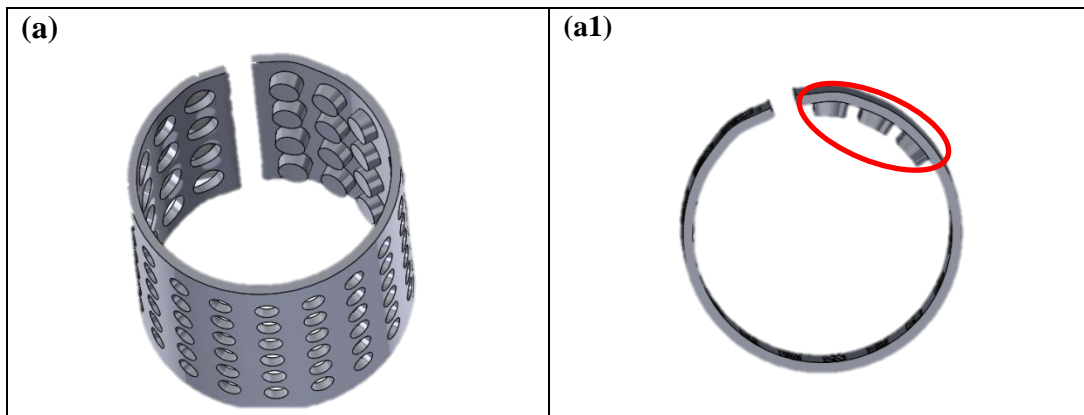
Figure 3- 2. Solidworks Images of Design 2 with breadth 30mm, diameter 5mm, wall thickness 1mm and pore diameter 1.75 mm. Design 2 works on the principle of a press fit assembly with the "buttons" diameter 2mm circled in red (a1) press fit into their corresponding adjacent slots (a).

Design 2 is based on the principle of a press fit assembly method of pulling the edge with the "buttons" over to the edge with the slots and then pushing the buttons into the slots to fix the shape (**Figure 3- 2**). The rationale is because the press fit assembly method allows for a simple securing of the 2 edges to form a smaller diameter cylinder when the buttons are held in place in their slots via friction. The shrinkage of the overall diameter of the cylinder helps in the eventual securing of the tissue graft within the cylinder.

Similar to Design 1, initial benchtesting with printed designs of either pure Veroclear material or TangoGray material showed that both these 2 materials were not feasible for this design. Veroclear is too stiff for the compression from a bigger diameter cylinder to that of a smaller diameter and resulted in breaking of the material (see **Figure 3- 3**) while TangoGray material is too soft and the components break when too much mechanical force is applied. Moreover, a major limitation is that with this design, there is an overlapping thickness at the region where the buttons sit into their respective slots. The increase in double the thickness will result in a decreased osteointegration at this region and therefore an overall non-uniform osteointegration effect when this device is used in the bone tunnel.

	(b2)
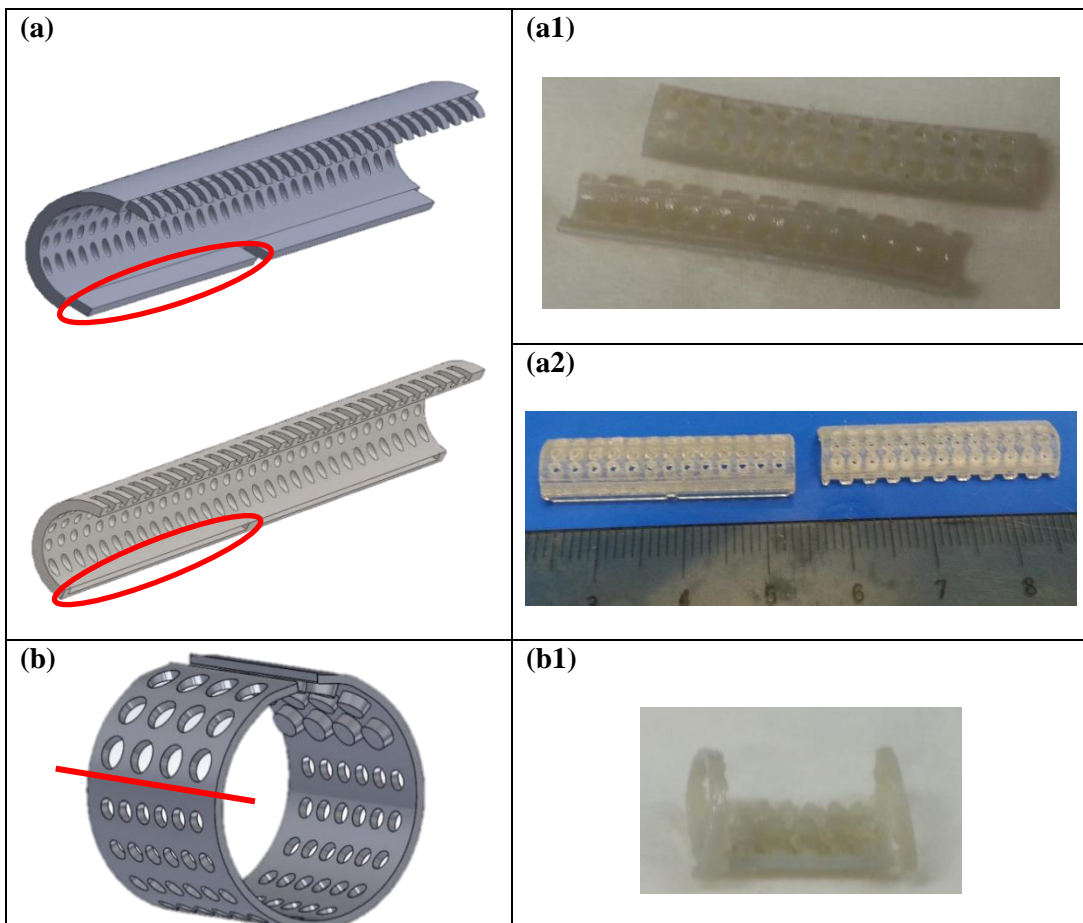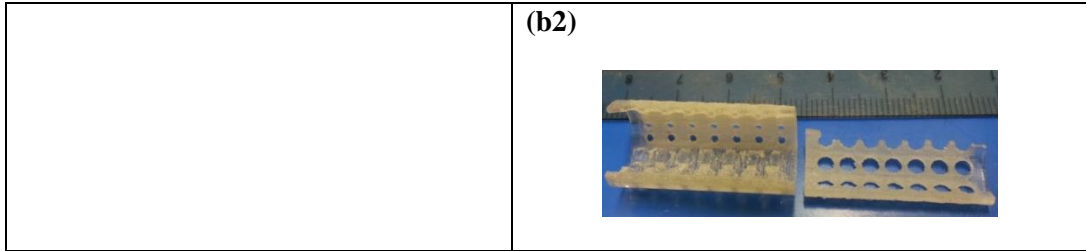
Figure 3- 3. Points of failure of Designs 1 and 2. The first design printed with TangoGray material (a1) and Veroclear material (a2) breaks and cracks at the red circled areas when the slots are being pressed into their corresponding docking slots (a). Similarly, the second design printed with TangoGray material (b1) and Veroclear material (b2) fractures along the red line in a longitudinal manner.

3.5.3. Design Iteration 3

<u>**Overview of Design**</u>	<u>**Details of Design**</u>
(a)	**(a1)**
(b)	
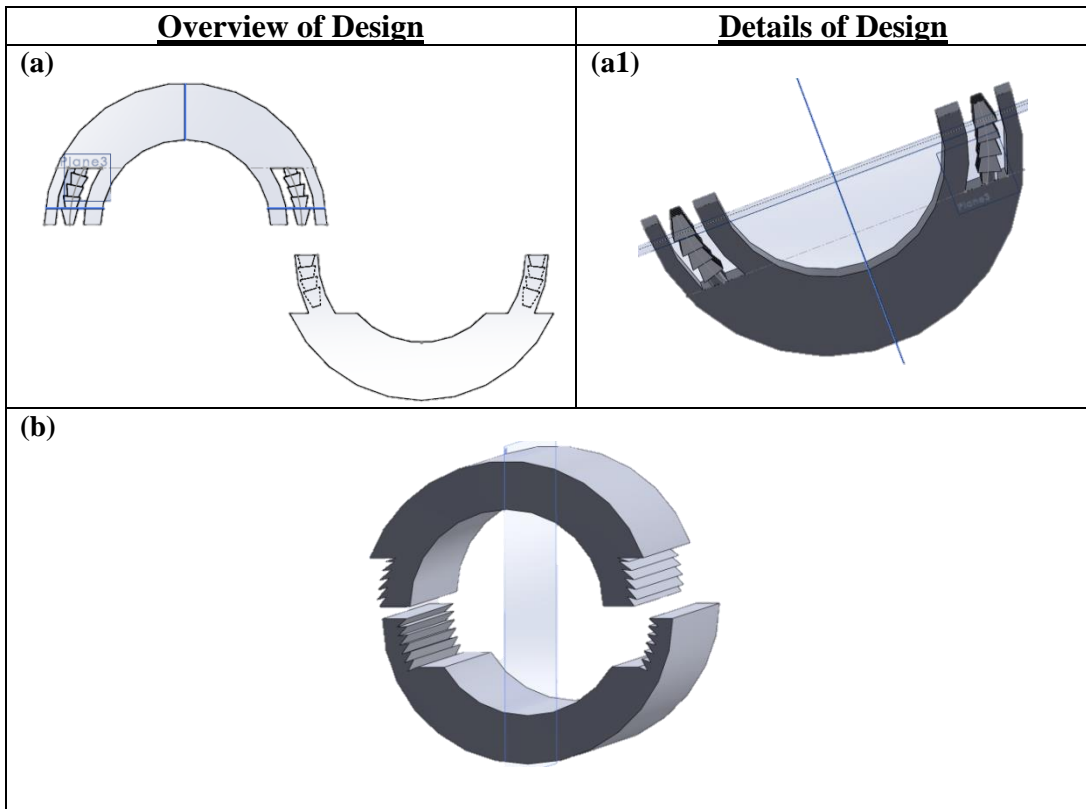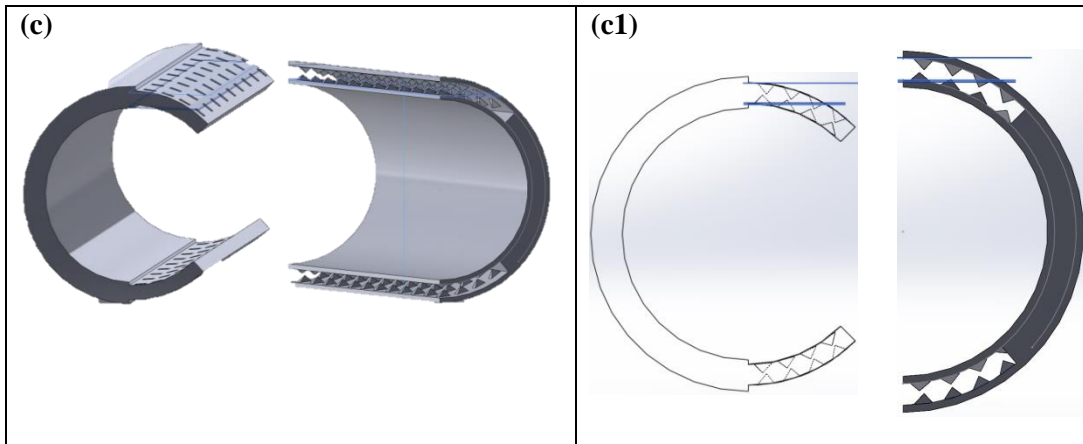
Figure 3- 4. Other Designs based on the rationale of 2 interlocking halves. The top half of semi-circle with diameter 3mm and wall thickness 1mm with its protruding slots (a1) is to be pressed fit into the slots in the bottom half of the semi-circle design (a) through the press-fit mechanism. The second design uses jagged edges along the sides of the wall to hold the two halves of the cylinder of diameter 5mm and wall thickness 1mm together (b). The third design with teeth of height 0.4mm on the shorter part of one half of a circle of diameter 5mm and wall thickness 1mm (c1) slotting into the empty slots of the longer half of the circle (c) in a sideways manner.

The above 3 designs (**Figure 3- 4**) are based upon the idea of 2 interlocking halves of a cylinder being fitted to each other via various assembly methods to form a full hollow cylinder that resembles a sleeve. For Design A, the upper half of the hollow cylinder has protruding features that will act as the anchorage holding the upper half and bottom half together when the protruding features sit into the empty slots at the bottom half. For Design B, a similar anchorage and assembly method is adopted; in replacement of the protruding features, jagged edges opposite in direction are present along the sides of the wall to hold the two halves of the cylinder together. Lastly, in Design C, the pointed teeth-like features of the semi-circle fit into the empty slots of the half-circle with a longer arc length, thereby locking the 2 halves together.

However, one major recurring limitation with such a design that aims to assemble two interlocking halves together is the strength of the interlocking mechanism. Due to the micro-scale dimensions of the printed designs and the features responsible for the

interlocking mechanism, the strength of the interlocking mechanism is not strong enough

for the two halves to hold together. A typical observation is that the slots are too shallow

because of the limited thickness of the designs of 0.5mm and this resulted in the easy

slippage of the protruding features, jagged edges or teeth-like features out from their

respective slots.

3.5.4. Design Iteration 4
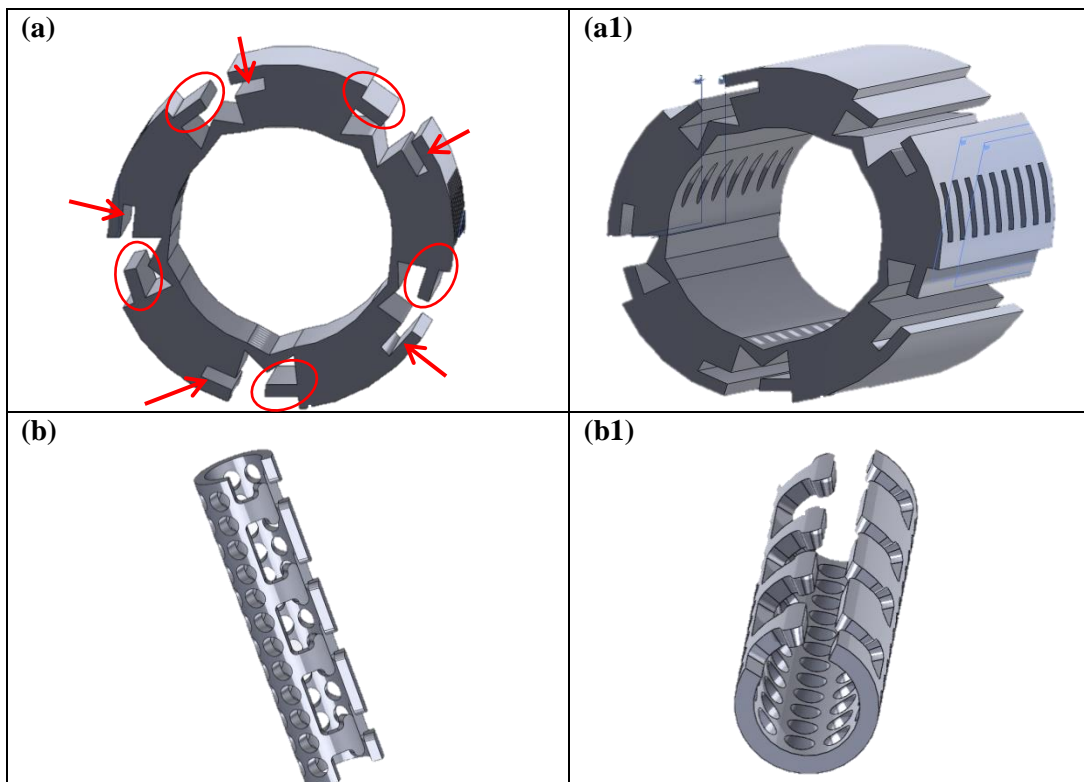
Figure 3- 5. Solidworks images of designs that fold into itself. The first design works on the principle of a bigger diameter of 7mm folding into a smaller diameter circle of 4.5mm through the protruding slotted edges of thickness 0.25mm folding sideways seen from the front view (a) and the side view (a1) with total wall thickness of 1.25mm. The second design follows the principle behind jigsaw puzzles where the interlocking features of breadth 4mm and 5mm apart at both of the longitudinal edges of length 30mm (see side view (b)) catch onto each other to form a full circle of diameter 6mm (b1).

In iteration 4, the above 2 designs (**Figure 3- 5**) are based upon the idea of designs that

will fold into itself and be held in place. In Design A, when the protrusions (circled in red)

sit into the adjacent slots (indicated by the red arrows), the pointed edges in the inner

diameter of the hollow cylinder will compress towards each other. This forces the diameter of the lumen of the hollow cylinder to shrink and will exert a mechanical constrictive force on the graft hence holding it in place. On the other hand, Design B is based on the rationale behind how jigsaw puzzles are able to fit and hold onto each other. Design B is printed as a flat piece before bending the edges of this piece towards each other so that the interlocking features at the two corresponding edges can fit into each other.

When conducting bench testing on both designs, a persistent limitation occurs similar as in iteration 3. Due to the micro-scale dimensions of the printed designs and the features responsible for the interlocking mechanism, the strength of the interlocking mechanism is not strong enough for the two halves to hold together. In Design A, the protrusions tend to slip out of their slots and the inner circle expands outwards while in Design B, the interlocking features do not hold onto each other and tend to unroll back to its original flat shape.

3.5.5. Design Iteration 5
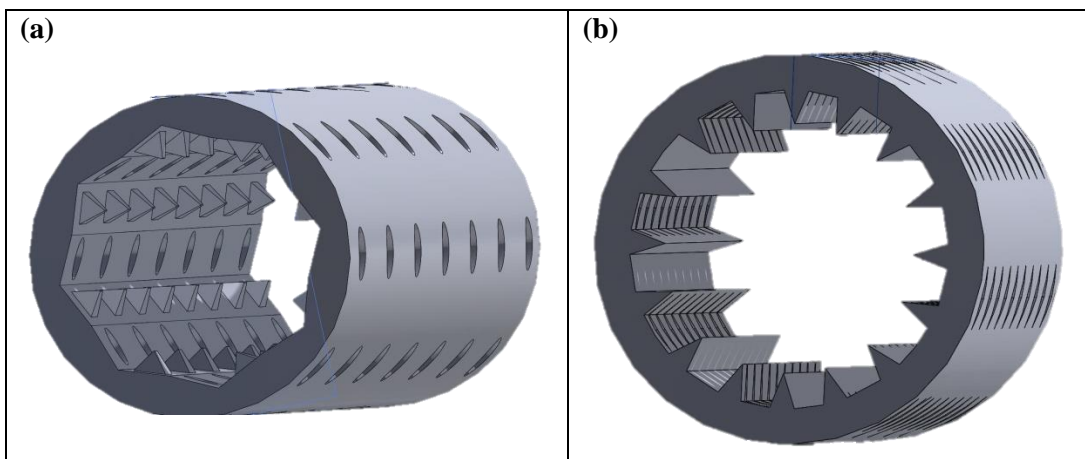
Figure 3- 6. Solidworks Images of full hollow cylinder designs. Both designs are of the same inner diameter of 5mm and wall thickness 1mm with differing shapes of the cross-section (i.e. hexagaonal (a) and circular (b)) of the lumen of the hollow cylinder with pore diameters of 1mm.

In the last iteration, the above 2 designs (**Figure 3- 5**) are full hollow cylinder designs that are of a smaller diameter than the graft size. Based on the elasticity of the material, it can be expanded circumferentially for the insertion of the tendon graft before it returns to its original diameter and hence, exerting a circumferential constriction force inwards onto the tendon graft. Previous 4 design iterations have showed that there is limited interlocking strength exerted by the interlocking features to hold two halves of a hollow cylinder together due to the micro-dimensions of the device. Hence, a full hollow cylinder design was considered. At the same time, the optimal 3D PolyJet Material to be used is FLX 9095; any increasing ratios of TangoBlack material results in the material being too soft to be manipulated and breaks very easily. The hexagonal design was chosen over that of the circular design because the sharp protrusions within the interior walls of the circular design tend to break off during removal of support material due to its small surface area.

3.6.   Design Validation

There are a few parameters of the full hollow cylinder design that has to be considered. For each parameter, experiments with 3D printed designs using FLX9095 Rapid Prototyping material were conducted to determine their optimal values and statistical analysis involving multiple comparisons were evaluated using a one-way analysis of variance (ANOVA) test and post-hoc Tukey correction using OriginPro 9 (OriginLab). A p-value of less than 0.05 was taken as significant and all experimental data were expressed as means ± standard deviation.

3.6.1. Internal Diameter of Hollow Cylinder

There are two considerations for the internal diameter of the hollow cylinder; the elasticity of the material and the diameter of the tendon graft. In typical human ACL reconstruction surgeries, quadrupled-strand hamstring autografts with diameters equal or

greater than 8mm were found to have decreased failure rates [128-130]. However, in a current preclinical study with a total of 30 porcine models, the tendon graft made from 2 harvested porcine flexor digitorum profundus tendons sutured together along its length were found to have an average diameter of 6mm. With the same source of flexor digitorum profundus tendons being used for bench testing of the 3D printed designs, the internal diameter of the hollow cylinder were therefore determined to have a maximum of 6mm in diameter. At the same time, uniaxial tensile testing of a 1mm thickness FLX9095 material (see **Table 3- 5**), used for printing of the 3D device, with the Instron 3345 machine (Instron, Norwood, MA, USA) has showed a 36.08 ± 7.81 % elongation at break. Hence, taking both limits into consideration, the internal diameter of the device is 4.4 – 6mm.

3.6.2. Thickness of Device

The optimal thickness of the device should satisfy the requirements of being relatively thin so as not to interfere with the osteointegration function of the device yet relatively thick to allow for easy loading of graft onto the device without failure. Hence, the devices, with an internal diameter of 4.5mm, were printed with a series of different thickness (i.e. 0.4mm, 0.5mm, 1mm, 1,2mm, 1,5mm, 1,8mm and 2mm). These thickness values were chosen to determine the upper and lower limits for this sleeve application. Bench test with the radial expansion of the internal diameter of the device with forceps and a vernier caliper showed that that a thickness of 0.4mm is not feasible as the device breaks even at the initial stage of removal of support material from the lumen of the design. From **Figure 3- 7**, the maximum percentage change in diameter of $36.89 \pm 1.22\%$ was observed for devices of thickness 1mm. This is significantly higher than devices with thickness of 0.5mm, 1.5mm, 1.8mm and 2mm (i.e. when the difference in thickness is more than or equals to 0.5mm). The larger percentage change in diameter is indicative of

the extensibility of the material and thus the ease of loading the tendon graft into the device. Hence, the thickness of the material was determined to be that of 1mm.
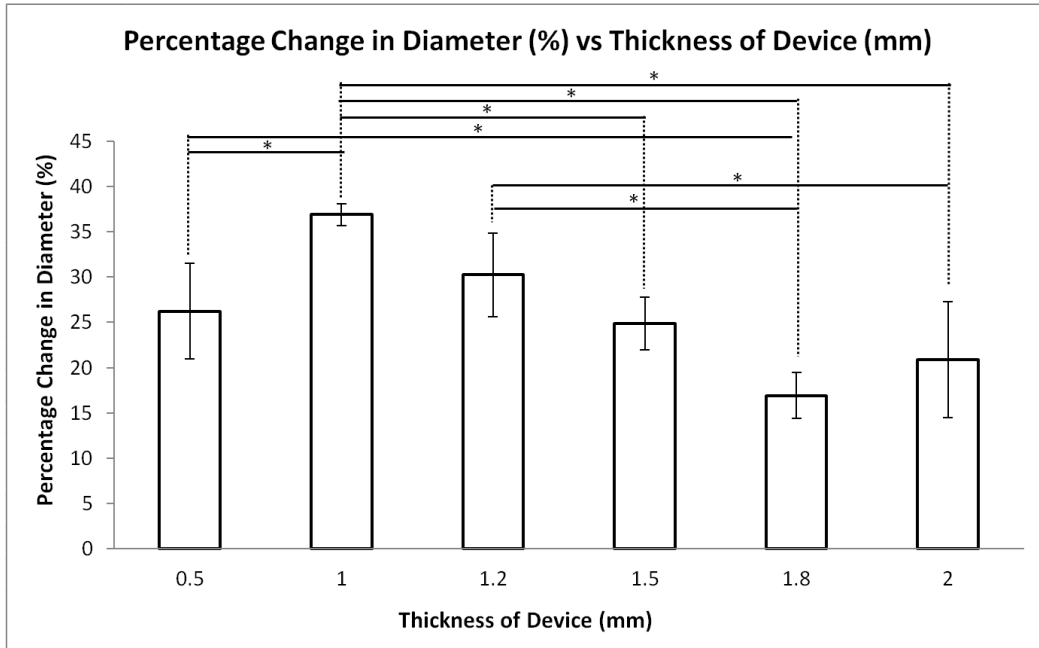
Figure 3- 7. Percentage change in diameter versus the thickness of the device (n = 3). For thickness of 0.5mm, significantly larger percentage change in diameter was only observed when the thickness is doubled and when the difference is between 1mm – 1.5mm. For thickness between 1mm – 1.2mm, significantly larger percentage change in diameter was observed when the thickness difference is ≥ 0.5mm. Beyond a device thickness of 1.5mm, there is no significant change in the percentage change in diameter. *p<0.05

3.6.3. Length of Device

In a study by Yang *et al*. in a porcine model, it was found that a graft length of 2cm within the tibial tunnel would be safe and have sufficient strength for adequate rehabilitation following ACL reconstruction surgery. In addition, with a longer graft length of 4cm within the tibial tunnel, ultimate tensile strength was found to be greater as compared to the group with 2cm length. However, between both groups, there was no difference in either graft slippage or total graft movement [131]. Hence, based on the reported findings, the length of the device (to fit the tunnel) was determined to be 3cm in length.

3.6.4. Porosity of Device

Following the previous study in the optimal thickness of the device (see **above**), where the optimal thickness of the device is determined to be 1mm, the porosity of devices of thickness 1mm and 0.5mm were compared with the porosity of the tissue augmentation silk sleeve device (see **Benchmarking with current device**).

Briefly, the porosity of the devices (i.e. tissue augmentation silk sleeve device or 3D printed devices with thickness 0.5mm and 1mm) were determined using the liquid displacement method reported in literature [132-134]. The displacement liquid used was ethanol because of its ease of penetration into the pores of the device and being a non-solvent of Veroclear, TangoBlack or silk, it does not induce shrinkage or swelling of the device. The devices were first immersed in a measuring cylinder with a known volume of ethanol (*V1*). After 5 minutes of immersion, the device was then pressed to force air from the device and for the penetration of ethanol into the device to fill the pores. This total volume of ethanol and ethanol-impregnated device was recorded as *V2*. After removal of the device, the residual volume of ethanol was recorded as *V3*. Finally the porosity of the device was calculated as per Equation (1) [132].

$$porosity, p = \frac{V1 - V3}{V2 - V3} \text{---------------------------- (1)}$$

The porosity of the silk sleeve tissue augmentation device was found to have a significantly higher porosity of 69.84 ± 2.75 % compared with devices of thickness 0.5mm and 1mm (see **Figure 3- 8**). In 3D printed parts, there are two types of pores; pores by design and pores generated during the process [135]. Since both devices of either thickness 0.5mm and 1mm have the same pore design and it is observed that there is no significant difference in the porosity between both devices, this indicates that the

porosity of the Polyjet Veroclear and TangoBlack blend does not contribute to the overall porosity of the device with the current printing parameters of strut thickness and density.
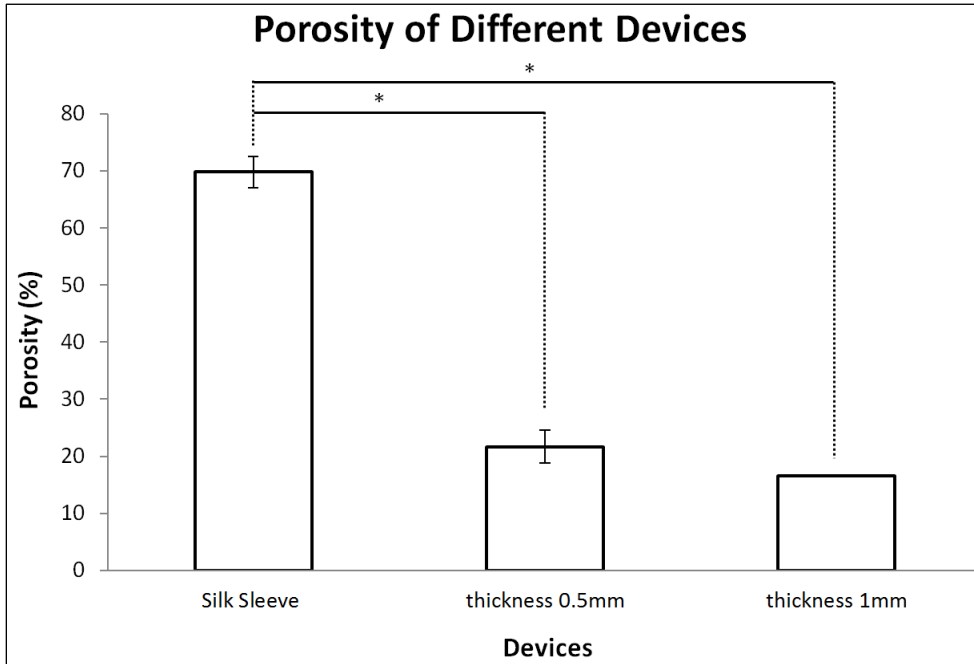
Figure 3- 8. Porosity of the tissue augmentation silk sleeve device (see *Benchmarking with current device*) versus 3D printed designs of thickness 0.5mm and 1mm (n = 3). The porosity of the silk sleeve tissue augmentation device has a significantly higher porosity of 69.84 ± 2.75 % compared with devices of thickness 0.5mm and 1mm.

3.7.   Instron Pull-through Test

The printed devices were then put through a pull-through test with the Instron 3345 machine. Briefly, a 6.5mm bone tunnel was drilled through 15 pcf cellular foam sawbone blocks (Pacific Research Laboratories, Vashon Island, WA, USA). Two porcine flexor digitorum profundus tendons were harvested and then sutured together along its length to form the tendon graft. The tendon grafts were then loaded onto the device and then pulled through the 6.5mm bone tunnel at a speed of 10mm/s with an Instron 3345 machine (Instron, Norwood, MA, USA) (see **Figure 3- 9**) and the efficacy of the device was evaluated from any slippage of the graft from the device during pull through. Videos of the graft loading onto the device and the subsequent pull through test are attached. The

results showed that with the device, it was much easier to load the tendon graft into the device as compared with loading it onto the tissue interface augmentation device. At the same time, the pull through strength required for the printed device was also approximately half that of the pull through strength required as compared to when the tissue augmentation device is used (see **Table 3- 6**).
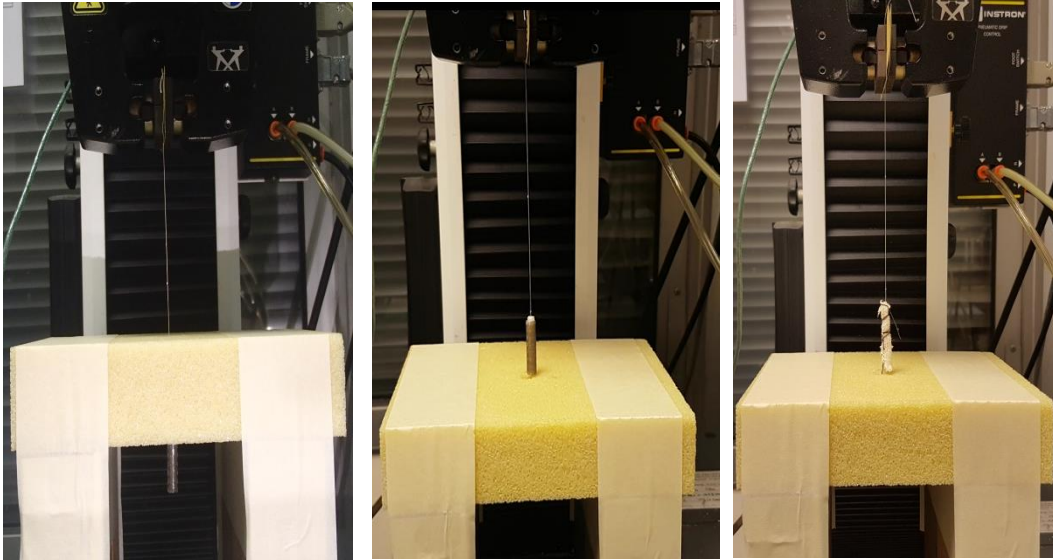
Figure 3- 9. Pull through test of porcine graft/sleeve construct (left and middle) and tissue augmentation device (left) with Instron machine (n = 3). The graft/sleeve construct is pulled at 10mm/s through the bone tunnel of 4cm (left) and is observed to remain intact after pull through (middle).

Table 3- 6. Pull through strength (N) of tissue augmentation device and printed device (n= 3).

	Tissue Augmentation Device	Printed Device
Pull through Strength (N)	0.952 ± 0.001	0.494 ± 0.075

3.8.   Design Specifications

As per the results above, a design freeze was adopted and the design specifications are listed below. These specifications were determined to be between the optimal values and the minimum acceptable value so as to allow for trade-offs.

No.	User Needs	Specifications	Units
1	Extent of irritation when implanted into the body	Moderate	Qualitative
2	Thickness of wall of device	1	mm
3	Length of device	3	cm
4	Diameter of device	4.5	mm
5	Pull through strength	0.9	N
6	Radial extension of device before failure	10	%
7	Tensile strength of device before failure	7.5	N
8	Porosity of device	65	%
9	Average diameter of pore sizes and its range	200	µm
10	Degradation rate of device	1.5	Years
11	Material safe for sterilization methods	Yes	N.A.
12	Average time taken to load graft into device	35	Minutes

4. Material Selection Process

4.1. Silk – Biomaterial for ACL applications

As previously described in Chapter 1 **Section 1.2.3(a)ii**, silk is a cheap and biocompatible material. In ACL reconstruction surgery, silk is primarily chosen from amongst all the synthetic and natural fibres because it is the only protein-based biocompatible fiber which matches the mechanical properties of native ACL, is not associated with bioburdens commonly present for mammalian-derived materials, maintains its long term mechanical tensile integrity *in vitro* [15] and has a slow *in vivo* degradation rate [6, 20] which allowed for optimal host tissue infiltration and integration [22].

4.2. Silk as a 3D printable bioink

As covered in **Silk-based bioinks** in Chapter 2 and **Table 2- 1**, there are various pure silk or silk-polymer/additive composites that are currently being investigated. A common limitation with using silk is the slow gelation process, weak mechanical properties and most importantly, the risk of clogging the nozzle head during the printing process. Hence, new silk formulations has to be investigated that would be ideal for printing yet at the same time, is a biocompatible biomaterial which supports cell growth and proliferation.

4.3. Rationale for material selection

Since silk has been ascertained to be an optimal natural fiber for ACL tissue engineering applications and its potential for its development to be a silk printable bioink, it may be possible that the 3D printed sleeve designs in Chapter 3 could be fabricated with a replacement biocompatible silk-based bioink for *in vivo* implantation. Hence, uniaxial tensile testing of the PolyJet materials (see **Table 3- 5**) and that of silk films were conducted with the Instron 3345 machine (Instron, Norwood, MA, USA) to determine if the mechanical properties of silk matches up to that of the PolyJet materials. Briefly, with a 1000N load cell and a tensile extension rate of 10mm/second, in line with a previously

published study on mechanical properties of silk films by Lu *et al.* [136], mechanical tensile tests were conducted on both silk films and PolyJet Materials FLX 9070, FLX 9085 and FLX 9095.

Bombyx Mori silk fibres were degummed, dissolved and dialysed following a modified protocol which was adapted from Kaplan [137]. Briefly, unwanted sericin was removed via degumming by boiling raw silk fibres in 0.02M Na_2CO_3 (Sigma Aldrich). Thereafter, any residual Na_2CO_3 (Sigma Aldrich) were removed by washing the silk threads in distilled water (dH_2O). Degummed silk fibres were then air-dried before being dissolved in 9.3M lithium bromide solution (Sigma Aldrich) at 60°C for 4hours to obtain 20% (w/v) silk fibroin (SF) solutions. SF solutions were then dialyzed against dH_2O for 48hrs with at least six changes of dH_2O using SnakeSkinTM dialysis tubing (3500 MWCO; Thermo Fisher Scientific, Rockford, IL, USA). Dialyzed SF solutions were then centrifuged at 2000g for 10 minutes to remove impurities, and the supernatant containing the purified SF stock solution was collected and kept at 4°C for further processing. The final concentration of SF stock aqueous solution was approximately 6% (w/v). To fabricate the silk films, 6% SF solution was casted onto 6 well polystyrene plates and left to dry in the fumehood. Upon drying, another layer of 6% SF solution was added upon the first layer. This process was repeated and lastly, the silk films were methanol treated. Specimens (i.e. fabricated silk films and 3D printed PolyJet films) were pre-soaked in distilled water for an hour prior to mechanical testing. The specimens were clamped at both ends by the pneumatic clamps and then stretched along their longitudinal axis till failure (see **Figure 4- 1**).

Results from the mechanical testing (see **Table 4- 1**) demonstrated that the tensile modulus of the silk to be much higher than that of FLX 9070 and FLX 9085. However,

the tensile modulus and ultimate tensile strength of silk was still lower than that of FLX

9095, which was previously determined in Chapter 3 that it was the optimal PolyJet

Material for the designed devices to work. Hence, silk/polymer composites were

considered to improve the mechanical properties of silk to match those of FLX 9095 for a

translatable biocompatible device.

Table 4- 1: Mechanical Properties of Silk Films and PolyJet Materials (n = 5)

Material	Silk	FLX9070	FLX9085	FLX9095
Tensile Modulus (MPa)	18.22 ± 0.97	5.85 ± 0.34	11.57 ± 0.62	29.72 ± 2.16
Ultimate Tensile Strength (MPa)	2.19 ± 1.05	0.93 ± 0.22	2.03 ± 0.21	3.57 ± 0.61
Elongation at Break (%)	72.90 ± 80.39	29.05 ± 5.38	36.61 ± 6.11	36.02 ± 7.81

Figure 4- 1. Mechanical Testing with Instron Machine. Specimens (i.e. silk films and PolyJet Materials; circled in red) were clamped between the pneumatic clamps and

were tested under uniaxial tensile loading along the longitudinal axis (left) till failure (right) (n = 5).

4.3.1. Pure Silk "ink"

i. High concentration silk

(a) Material and Methods

Bombyx Mori silk fibres were degummed, dissolved and dialysed following a modified protocol which was adapted from Kaplan [137]. Briefly, unwanted sericin was removed via degumming by boiling raw silk fibres in 0.02M Na_2CO_3 (Sigma Aldrich). Thereafter, any residual Na_2CO_3 (Sigma Aldrich) were removed by washing the silk threads in distilled water (dH_2O). Degummed silk fibres were then air-dried before being dissolved in 9.3M lithium bromide solution (Sigma Aldrich) at 60°C for 4hours to obtain 20% (w/v) SF solutions. SF solutions were then dialyzed against dH_2O for 48hrs with at least six changes of dH_2O using SnakeSkinTM dialysis tubing (3500 MWCO; Thermo Fisher Scientific, Rockford, IL, USA). Dialyzed SF solutions were then centrifuged at 2000g for 10 minutes to remove impurities, and the supernatant containing the purified SF stock solution was collected and kept at 4°C for further processing. The final concentration of SF stock aqueous solution was approximately 5% (w/v). To obtain SF solutions with higher concentrations, 10ml of the 5% SF solution was dialyzed against 400ml of poly(ethylene)glycol (PEG) solutions (10 000g/mol, Sigma Aldrich) of different concentrations for varying durations using Slide-A-Lyzer™ dialysis cassettes (3500 MWCO; Thermo Fisher Scientific, Rockford, IL, USA) at room temperature [138]. The concentrated silk solutions of different concentrations were then loaded into syringes and preliminarily extruded via various nozzle tips of various sizes (i.e. 18G, 22G, 27G and 31G) using a syringe pump (New Era, Farmingdale, NY, USA).

(b)   Results

Table 4- 2: SF Concentrations and Volumes after dialysis with different PEG concentrations

Duration of Dialysis (Hours)	PEG Concentrations (%)					
	15		20		25	
	Final SF Concentration (%)	Final Volume (ml)	Final SF Concentration (%)	Final Volume (ml)	Final SF Concentration (%)	Final Volume (ml)
2	8.60	2.4	9.40	2.0	10.00	1.8
3	7.67	8.0	10.67	1.0	11.00	0.7
4	9.67	1.5	18.20	0.5	33.50	0.2

Table 4- 3: Final SF concentration after dialysis against 20% (w/v) PEG solution

Duration of Dialysis (Hours)	Final SF Concentration (%) (Dialysis against 20% (w/v) PEG)	
	Initial SF concentration: 5.6%	Initial SF concentration: 6.4%
4	16.9	21.2
5	22.2	28.3
7	26.0	57.9
9	15.8	gelation of silk solution

Extrusion Rate	SF Concentration (%)	
	22.2%	26.0%
30µl/minute		
50µl/minute		

Figure 4- 2. Silk "constructs" formed from concentrated SF solutions. SF solutions of 22.2% (w/v) (left) and 26% (w/v) (right) were extruded onto glass slides at different rates (i.e. 30µl/minute (top row) and 50µl/minute (bottom row)).

With the same starting concentration of 5% (w/v) SF solution and initial volume of 10ml, it can be seen from **Table 4- 2** that with the same duration of dialysis, SF solutions dialyzed against higher PEG concentrations yield a higher final concentration of SF. This trend was similarly observed for increasing duration of dialysis when the PEG concentration was held constant. Concurrently, as the concentration of SF solution increased, the final volume of the concentrated SF solution was observed to decrease over time. Moreover, when these concentrated SF solutions were loaded into syringes and subsequently extruded via the 18G, 22G, 27G and 31G nozzle tips, the only SF concentration that yielded a fibre-like filament was 33.50%. However, at 33.50%, the volume of the SF solution was too little (i.e. 200µl) for the formation of any visible filaments for any post-fabrication treatment. On the other hand, the rest of the SF concentrations were observed to have too high a water content for any formation of the filamentous shape upon extrusion from the nozzle tip and was observed to spread on the glass surface. Rapid evaporation of the SF solution was also observed after extrusion (see **Figure 4- 2**).

(c)   Discussion

The observed increase in concentration of SF solution was to be expected as the much higher salt concentration in the surrounding PEG dialysis solution resulted in the movement of water molecules in the SF solution across the membrane of the dialysis cassette into the PEG dialysis solution by osmotic stress [139]. The movement of the higher molecular weight PEG molecules across the membrane into the SF solution was restricted due to the smaller molecular weight cutoff (MWCO) of the dialysis cassette membrane. Hence, with the decrease in the amount of water, the concentration of the SF solution increased over time and when higher salt concentrations of dialysis solutions were used. One major limitation of the current method of obtaining concentrated SF

solution was the repeatability of this method. While concentrations as high as 33.50% were achievable, the volume reduction was 50 times. Attempts to increase the initial volume or initial concentration before dialysis induced premature and spontaneous gelation within the dialysis cassette (see **Table 4- 3**) [139]. In addition, high concentrations of SF solution had rapid gelation within a span of 48 hours at $4\degree$C and therefore it was not feasible to store the SF solution to have an increased yield. The rapid gelation of SF solutions with the increase in SF content had also been similarly confirmed in other studies [139, 140].

For silk concentrations below 33.50%, the shear rate of the SF solutions was highly dependent on its viscosity and it behaved like a non-Newtonian fluid. This shear thinning behaviour indicated the presence of aggregate formation due to hydrophobic/ hydrophilic interactions within the SF solution because of silk's amphiphilic structure [106]. Hence, this resulted in non-uniform extrusion and the merging of adjacent structures that were extruded. Though 33.50% SF concentration supported the formation and shape retention of filament – like fibres, these filaments did not have the adequate mechanical strength for further processing. Attempts with methanol treatment resulted in the disintegration of the filaments.

(d)   Conclusion

Hence, it can be concluded that it was neither practical nor feasible to use highly concentrated SF solutions as a 3D printable ink. Low SF concentrations did not undergo gelation fast enough for shape retention after extrusion while the process of obtaining high SF concentrations was not reproducible and had low yields that underwent rapid gelation upon storage. In addition, the resultant constructs also did not have enough

mechanical strength for post-printing processing with methanol to induce a more robust construct.

ii.   Temperature sensitive silk

(a)   Material and Methods

Bombyx Mori silk fibres were degummed, dissolved and dialysed following a modified protocol which was adapted from Kaplan [137]. Briefly, unwanted sericin was removed via degumming by boiling raw silk fibres in 0.02M Na_2CO_3 (Sigma Aldrich). Thereafter, any residual Na_2CO_3 (Sigma Aldrich) were removed by washing the silk threads in dH_2O. Degummed silk fibres were then air-dried before being dissolved in 9.3M lithium bromide solution (Sigma Aldrich) at 60°C for 4hours to obtain 20% (w/v) SF solutions. SF solutions were then dialyzed against dH_2O for 48hrs with at least six changes of dH_2O using SnakeSkinTM dialysis tubing (3500 MWCO; Thermo Fisher Scientific, Rockford, IL, USA). Dialyzed SF solutions were then centrifuged at 2000g for 10 minutes to remove impurities, and the supernatant containing the purified SF stock solution was collected and kept at 4°C for further processing. The final concentration of SF stock aqueous solution was approximately 5% (w/v). To obtain SF solutions with higher concentrations, 10ml of the 5% SF solution was dialyzed against 400ml of PEG solutions (10 000g/mol, Sigma Aldrich) of different concentrations for varying durations using Slide-A-Lyzer™ dialysis cassettes (3500 MWCO; Thermo Fisher Scientific, Rockford, IL, USA) at room temperature [138]. The concentrated SF solutions of different concentrations were then loaded into syringes and preliminarily extruded through 27G nozzle tips onto slides pre-cooled at -20˚C at an ambient temperature of -20˚C before removal to room temperature for methanol treatment post extrusion.

(b)   Results
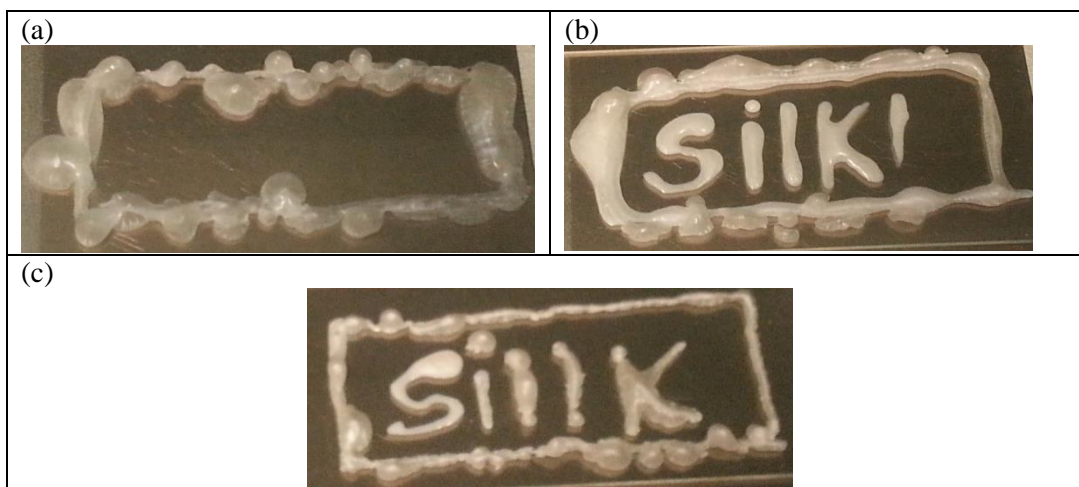
Figure 4- 3. Extrusion of different concentration of SF solutions onto a pre-cooled glass slide at -20°C. No uniform fibre formation was observed for 5% (w/v) SF concentration (a), 7.5% (w/v) SF concentration (b) and 10% (w/v) SF concentration (c).

It can be seen in **Figure 4- 3** that with increasing SF concentrations, the finer the fibres formed and the faster the freezing and solidification of the SF fibres when extruded under temperatures of -20˚C onto pre-cooled slides. Furthermore, when a second layer of SF solution was extruded upon the first layer of SF solution, the silk fibres did not fuse but instead accumulated to form globules at points along the first layer. Hence, there was no uniform fibre formation especially for extrusion of second layer onwards. At the same time, the solidified structures thawed rapidly upon removal from the -20˚C environment and lost its preliminary solidified structure and shape before any further post-processing treatment (i.e. methanol treatment) could be done on the constructs.

(c)   Discussion

The reason for the formation of the different fibers was due to the differing water content in the different concentrations of SF solution. During normal freezing process, the water crystals grew at a controllable rate while the silk molecules became less stable, phase separated and coagulated with each other and were excluded from the frozen water till the

freezing process was complete [141, 142]. As the extruded SF solution was very small in volume (given the volume extrudable through a 27G needle of 0.21mm diameter), the freezing process was very rapid. Hence, the extruded silk "filament" was able to hold its frozen shape on the glass slide. However, the rate of ice nucleation increased with increasing water content [141] (i.e. more dilute silk concentration) and this was observed when the filaments from the 5% SF solution tend to have a phase separation between silk and water because of the non-uniform freezing rates. This was seen from the globular – like structures atop the surface of the denser silk solution on the glass slide surface. The difference in water content, with more concentrated SF solutions having lower concentration of water, determined the morphology of the filaments being formed. For a more lamellar-like filament formation, the ice crystals formed within the SF solution had to assume a stable dendritic morphology without any side branches. This could only be achieved for SF concentrations more than 6% (w/v) or at temperatures below $-80\,^{\circ}$C [143]. As per observed in **Figure 4- 3**, as the SF concentration increased from 5% (w/v) to 7.5% (w/v) and finally to 10% (w/v), the morphology of the SF filaments changed from a globular structure to a more lamellar-like filament. However, upon removal from the $-20\,^{\circ}$C environment to ambient room temperature, the constructs underwent rapid thawing and spread out on the glass slide. This was primarily because the filament formation was not stable yet; a freezing duration of $6 - 7$ days was usually required for the elongation of the folded micelles which aggregated to form stable filaments [144].

Another limitation of this approach was the ink's inability in building a 3D structure. Due to the hydrophobicity of the initial frozen layer and the low temperature at which the extrusion was conducted, the second layer froze too rapidly for any merging with the first layer.

(d)   Conclusion

As discussed above, it can be preliminarily concluded that this approach was no more feasible than the one above. The time that was required for stable filament formation was too long and a major concern was its inability to build upwards to form a 3D construct. Moreover, the construct was not stable and disintegrated even with minor changes in the surrounding temperature. Hence, silk – polymer composites instead of just pure SF solutions should be considered as pure SF solutions have weak mechanical properties and their compatibility with current 3D printing technologies cannot match up to that of commercial 3D printable inks.

4.3.2. Silk-Polymer Blend "ink"

i.   Silk-PVA

(a)   Material and Methods

6% (w/v) Poly(vinyl alcohol) (PVA, average mol wt 30,000–70,000, 87–90% hydrolyzed) solution was made by dissolving PVA Powder (Sigma Aldrich, St. Louis, MO) in dH_2O from the Milli-Q system (Millipore, Billerica, MA) and autoclaving the mixture at 120˚C for 2hours. Thereafter, 6% (w/v) PVA solution was blended with 6% (w/v) SF solution in different ratios (i.e. silk/PVA: 90/10, 80/20 and 70/30) [145] and then cast onto 6 well polystyrene cell culture plates. Upon drying, another layer of the silk/PVA solution was cast above the first layer and then left to dry. This process was repeated a third time before the cast films were methanol treated. Following the methanol treatment, the silk/PVA films were first soaked in dH_2O before being subjected to uniaxial tensile testing with an Instron 3345 machine (Instron, Norwood, MA, USA), with a 1000N load cell and at a tensile loading rate of 10mm/minute [136]. Samples were mounted and placed in a gold coat sputter (JEOL, Tokyo, Japan) before viewing for layer delamination with a scanning electron microscope from

JEOL (JSM-5610/JSM6510; JEOL, Tokyo, Japan). Images were taken from 500x to

4000x magnification.

(b)   Results
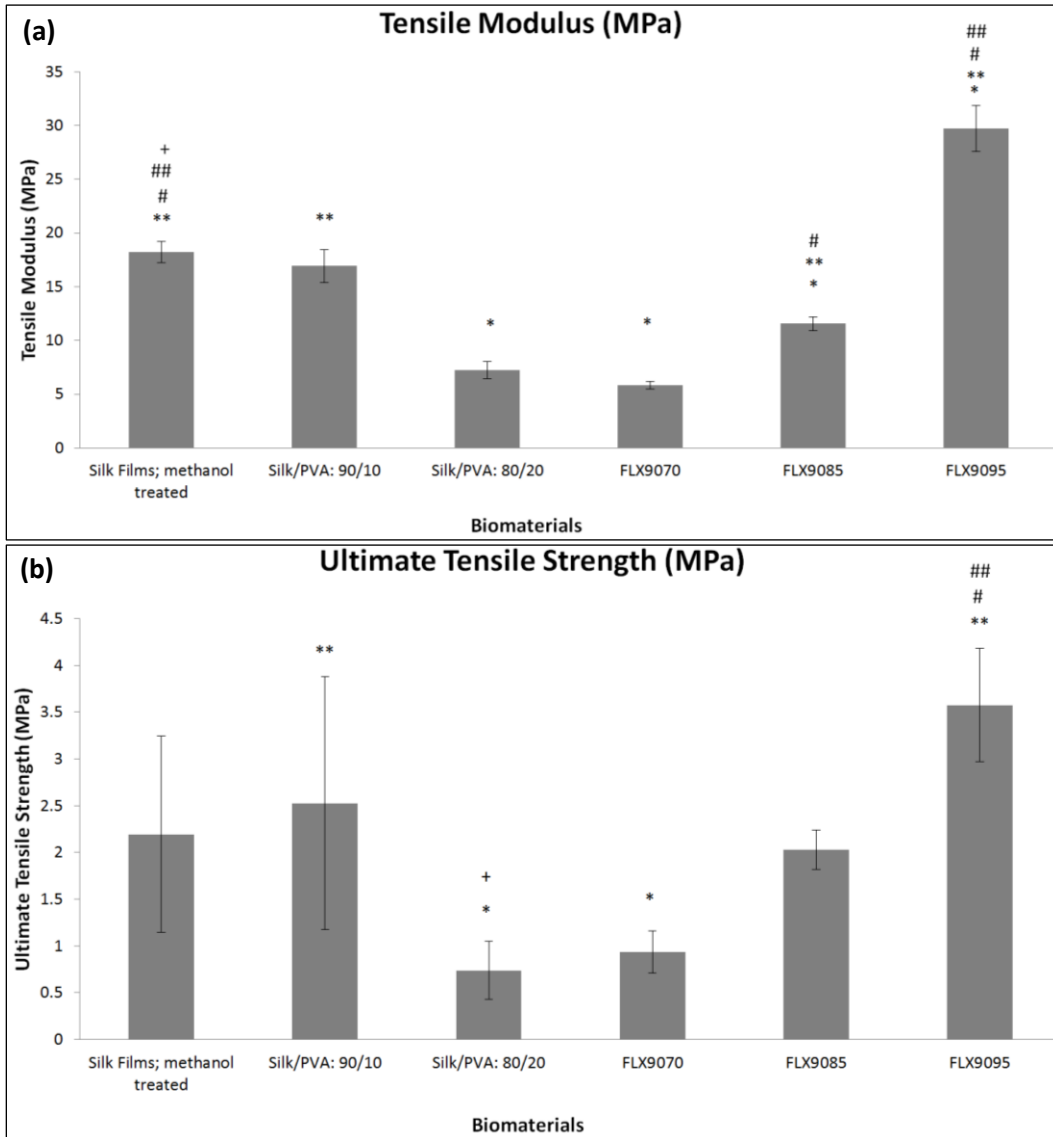
Figure 4- 4. Mechanical properties (i.e. tensile modulus (a) and ultimate tensile strength (b)) of biomaterials of pure silk films, silk/PVA films (with ratios 90/10 and 80/20) and PolyJet materials of different stiffness (FLX 9070, 9085 and 9095). Significantly higher tensile modulus was observed for pure silk films and PolyJet materials FLX9085 and 9095 over silk/PVA films of the ratio 80/20 (**p<0.05), PolyJet material FLX 9070 (#p<0.05), PolyJet material FLX 9085 (##p<0.05) and PolyJet material FLX9095 (+p<0.05). The tensile modulus and ultimate tensile strength of 80% silk/20% PVA films was significantly lower than that of the other sample groups (*p<0.05).

Pure Silk	Silk/PVA: 90/10	Silk/PVA: 80/20
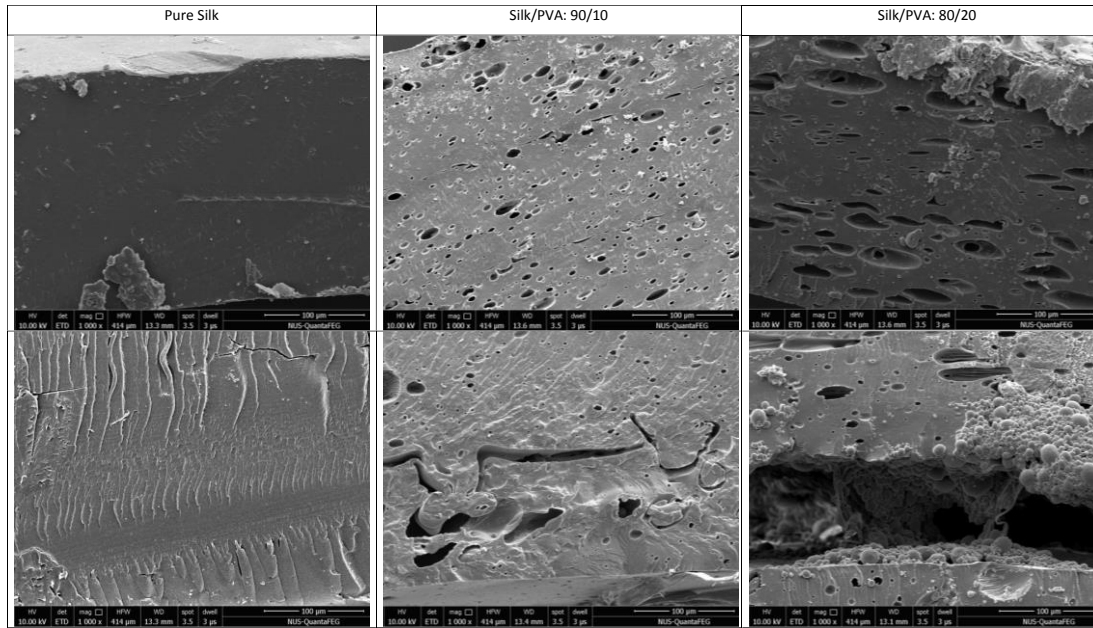
Figure 4- 5. SEM images of pure silk, silk/PVA films of ratios 90/10 and 80/20 at 1000x magnification showed increasing porosity (top) and delamination (bottom) between the layers as PVA ratio increased.

The tensile modulus of the pure silk films was observed to be significantly higher than that of silk/PVA films with PVA content of 20%. However, as compared to the PolyJet material FLX9060, the mechanical properties of the pure silk films were still significantly weaker. There was no significant difference in mechanical properties when the composition of the TangoBlack material decreased (i.e. FLX9050 and FLX9040).

(c)   Discussion

Silk films become dry and brittle when dried or left in ambient exposure. Hence, in order to improve the inferior tensile properties of silk films, synthetic polymers especially PVA have been used to mix with silk to form silk/PVA composites with improved mechanical properties [146-148]. However, contrary to what was reported in literature, **Figure 4- 4** showed that not only was there no improvement in tensile modulus, there was a significant decrease in tensile modulus when the PVA content increased to 20%. This could be possibly be due to the macrophase separation of the silk and PVA into a 2 phase structure (sea/island) [149] when the silk/PVA composites were cast onto 6 well

polystyrene plates and left to dry. The separation of the two layers was confirmed in studies which reported on the spontaneous phase separation of silk and PVA when the two solutions were blended and subsequently cast into films [145, 148] and also from the SEM images (see **Figure 4- 5**). As the proportion of PVA increased to 20%, the tensile modulus of the silk/PVA: 80/20 films decreased significantly as compared to pure silk films. This was to be expected as with the increase in the proportion of PVA within the blend, the phase separation would be more distinct with a more irregular microstructure, weave structures and spherical particles of non-uniform sizes [149]. There was also increased pore density from studies working with freeze dried silk/PVA sponges [147] and this was also observed from the SEM images (see **Figure 4- 5**). Literature also reported that due to the immiscibility of silk and PVA resulting in phase segregation of the two [146], the surface of the cast silk/PVA films was rough and round-sphere like particles suspected to be silk particles were also observed on the surface [148]. This was similar to the surface morphology observed under SEM in **Figure 4- 5.**

(d)   Conclusion

In conclusion, the current method of mixing PVA with silk did not yield a uniform film formation. To form a homogenous formulation of silk and PVA required repeated freeze thaw cycles, which resulted in the formation of irreversible silk/PVA gels and not films. In addition, the silk/PVA films also had inferior mechanical properties as compared to pure SF films. Therefore, PVA is not the ideal synthetic polymer to mix with silk in the formulation of a homogenous and stable bioink suitable for 3D printing applications.

ii.   Silk-PEG

(a)   Material and Methods

Polyethylene glycol (PEG) solution was made by dissolving PEG Powder (8000 MW, Sigma Aldrich, St. Louis, MO) in dH_2O to constitute various concentrations of 50% (w/v),

65% (w/v), 75% (w/v) and 80% (w/v). Thereafter, different concentrations of SF solution (i.e. 4% (w/v), 5% (w/v) and 6% (w/v)) were blended with various concentrations of PEG in ratios of 1:1 and 2:1 and triplicates of each silk/PEG condition at a volume of 300µl were pipetted to a 24-well plate (Corning® Costar®, NY, USA). For monitoring of the gelation process and the determination of gelation time, turbidity of the silk/PEG composite during gelation was measured spectrophotometrically at the absorbance mode (wavelength of 550nm) with defined intervals using a microplate reader (Turner Bio-systems, Sunnyvale, CA) at a temperature of 25˚C over a period of 5 days (i.e. till no change in optical density was observed). SF solutions of concentrations 4% (w/v), 5% (w/v) and 6% (w/v) and PEG solutions of concentrations 50% (w/v), 65% (w/v), 75% (w/v) and 80% (w/v) were the negative controls for this study. The opacity of the silk/PEG gels will increase over time and the change in optical density will quantify the turbidity change [150] and hence the gelation time of the silk/PEG gels. For each silk/PEG condition, the optical density values were averaged to obtain the change in optical density over time. The gelation time was then determined as the time at which the optical density reached a value corresponding to half of the maximum optical density obtained [150, 151]. At the same time, the silk/PEG composites were loaded into 3ml syringe – moulds for the eventual formation of silk/PEG gels and left to undergo complete gelation at room temperature. Using an adapted test tube inversion method, the determination of gel formation was assessed by the fluidity or the presence of liquid accumulation at the bottom of the inverted syringe after 5 days [152]. Thereafter, the silk/PEG gels (n = 5) were removed from their moulds and subjected to unconfined compression testing with an Instron machine (Instron, Norwood, MA, USA) between 2 compression platens with a 10N load cell and at a compression loading rate of 1mm/minute till fracture (**Figure 4- 6**). After normalizing to sample geometries, the compressive modulus was determined from the slope of the initial linear region of the

stress-strain curve generated and yield strength determined using a 2% strain offset from

the initial linear region [138, 153].
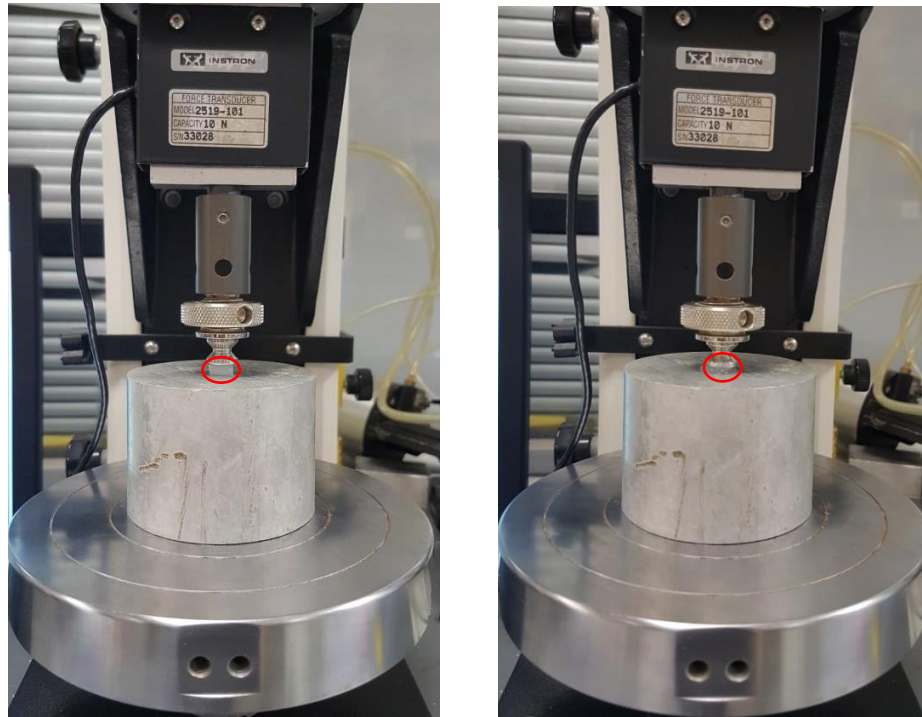
Figure 4- 6. Mechanical Testing with Instron Machine. Specimens (i.e. silk blend gels; circled in red) were sandwiched between compression platens and were tested under uniaxial unconfined compression loading along the longitudinal axis (left) till failure (right) (n = 5).

(b)   Results
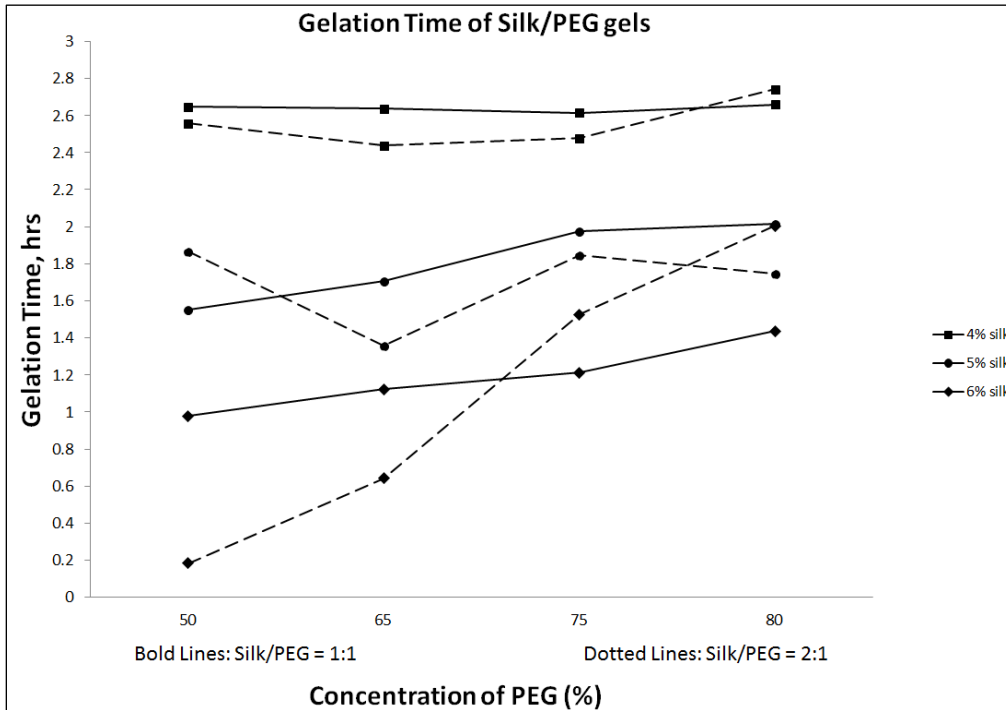
Figure 4- 7. Gelation times of silk/PEG composites of ratio 1:1 (represented by bold lines) and ratio 2:1 (represented by broken lines). For silk/PEG ratio of 1:1, the gelation time decreased as the silk concentration increased from 4% to 6%. However, as PEG concentrations increased, the gelation time increased or remained approximately constant. No observable trend was observed for silk/PEG composites of ratio 2:1 except for 6% silk concentration, where increasing the concentration of PEG increased the gelation time.

Comparing across the 3 different silk concentrations (i.e. 4%, 5% and 6%), it can be

observed (**Figure 4- 7**) that the gelation time of the silk/PEG composites decreased as

silk concentration increased. For 4% silk/PEG composites blended in the ratio of 1:1, the

gelation time remained approximately the same as PEG concentration increased from 50%

to 80%. On the other hand, there was a slight increase in the gelation time as PEG

concentration increased from 50% to 80% for the groups with 5% silk/PEG composites

and 6% silk/PEG composites blended in the ratio of 1:1. Comparing the 2 different ratios

in which silk was blended with PEG, there was no distinct relationship between the 2

groups; other than the gelation time was generally lower for silk/PEG composites of ratio

2:1. Amongst the silk/PEG composites of 2:1, there was no observable relationship between the increase in PEG concentration and gelation time when 5% silk was used for the silk/PEG composite. The gelation time for 4% silk/PEG composites remained approximately the same as PEG concentration increased from 50% to 75% before increasing when the PEG concentration was increased to 80%. The most significant relationship between gelation time and concentration of PEG was observed when 6% SF solution was used; the shortest gelation time of 11 minutes (**Figure 4- 7**) was observed for 6% silk/50% PEG composites while the gelation time increased sharply with increasing PEG concentrations from 65% to 80%.
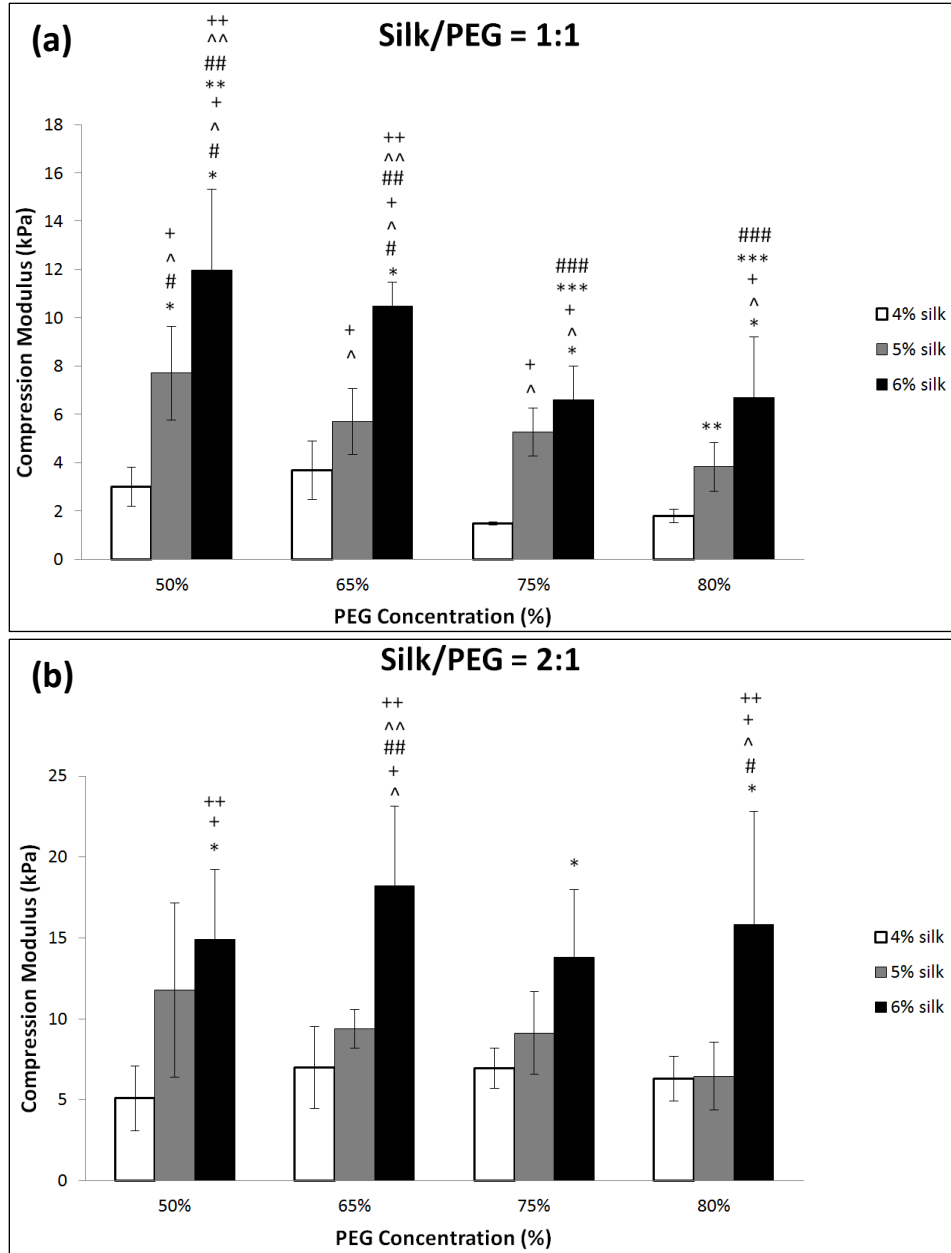
Figure 4- 8. Compressive modulus (kPa) of Silk/PEG composites with ratios 1:1 (a) and 2:1 (b). For silk/PEG composite ratios of 1:1, significantly higher compressive modulus was observed for 6% silk composites with 50% and 65% PEG over 4% silk composites with 50% PEG (*p<0.05), 65% PEG (#p<0.05), 75% PEG (^p<0.05) and 80% PEG (+p<0.05) and 5% silk composites with 50% PEG (**p<0.05), 65% PEG (##p<0.05), 75% PEG (^^p<0.05) and 80% PEG (++p<0.05). However, 6% silk composites with 75% and 80% PEG had lower compressive modulus compared with 50% PEG (***p<0.05) and 65% PEG (###p<0.05). For silk/PEG composite ratios of 2:1, significantly higher compressive modulus was observed for 6% silk composites as compared to 5% and 4% silk composites.
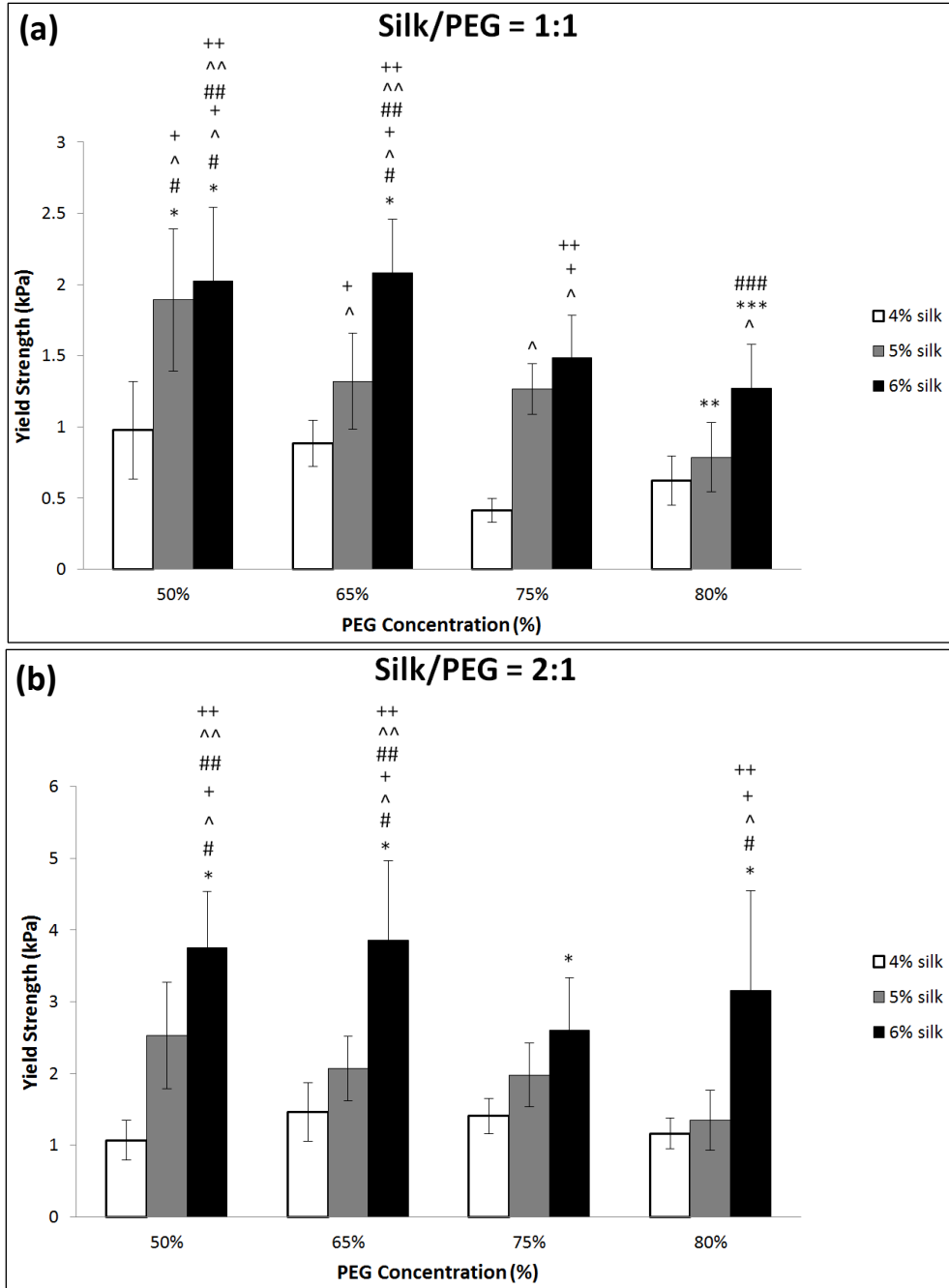
Figure 4- 9. Yield strength (kPa) of Silk/PEG composites with ratios 1:1 (a) and 2:1 (b). For silk/PEG ratios of 1:1, significantly higher compressive modulus was observed for 6% silk composites with 50%, 65% and 75% PEG over 4% silk composites with 50% PEG (*p<0.05), 65% PEG (#p<0.05), 75% PEG (^p<0.05) and 80% PEG (+p<0.05) and 5% silk composites with 50% PEG (**p<0.05), 65% PEG (##p<0.05), 75% PEG (^^p<0.05) and 80% PEG (++p<0.05). However, significantly lower compressive modulus was observed for 6% silk/80% PEG composites when compared with 50% PEG (***p<0.05) and 65% PEG (###p<0.05). For silk/PEG ratios of 2:1, significantly higher compressive modulus was observed for 6% silk composites as compared to 5% and 4% silk composites.

For silk/PEG composites of ratio 1:1, there was no significant difference in the compressive modulus and yield strength as the PEG concentration increased from 50% to 80% for 4% silk/PEG composites. However, when 5% silk was blended with PEG, there was a significant decrease in the compressive modulus and yield strength when PEG concentration was increased to 80% when compared with 50%. The compressive modulus and yield strength of the blend of 5% silk/50% PEG was observed to be significantly higher than that of 4% silk/PEG composites. Comparatively, when the SF concentration was increased further to 6%, composites with 50% PEG and 65% PEG were found to have significantly higher compressive modulus and yield strength as compared to the 4% and 5% silk/PEG composites. Within the 6% silk/PEG composite group, 75% PEG was observed to have significantly lower compressive modulus values while 80% PEG had significantly lower compressive modulus and yield strength as compared to composites with 50% and 65% PEG. Conversely, when the silk/PEG composites were blended in the volume ratio of 2:1, there was no significant difference in either the compressive modulus or the yield strength across all PEG concentrations when the silk concentration was increased from 4% to 5%. When SF concentration was increased further to 6% silk, there was a significant increase in the compressive modulus and yield strength as compared to the 4% silk/PEG composites with the exception of 6% silk/75% PEG blend in terms of yield strength. Particularly, 6% silk/65% PEG blend had the most significant increase in compressive modulus and both 6% silk/50% PEG and 6% silk/65% PEG had the most significant increase in yield strength when compared with 4% and 5% silk composites. There was no observable relationship between compressive modulus and the increase in PEG concentration within the 6% silk/PEG composites condition. Similarly, this was also observed for yield strength of the silk/PEG composites (**Figure 4- 9**). In general, the mechanical properties of silk/PEG composites with the ratio of 2:1 were higher than with the ratio of 1:1 (**Figure 4- 8** and **Figure 4- 9**).

(c)   Discussion

The presence of polar and ionogenic groups in SF enhanced its ability to react with other polar and functional groups. When PEG, a strongly hydrophilic polyalcohol, was blended with SF solution, the PEG molecules rapidly diffused to the hydrophilic regions of the SF molecules and formed abundant hydrogen bonds. This resulted in the breakage of the hydration layer around the SF molecules and with the competition for water molecules by the PEG molecules, increased the collision of SF and PEG molecules. In addition, with the separation of SF molecules into different phases, the folding of the hydrophobic regions of the SF molecules was induced. The breaking and reformation of hydrogen bonds promoted the SF molecules to intertwine and aggregate with each other. The end result was the transition of the random coil structure to the formation of β-sheets within the SF molecules, resulting in the gelation of silk/PEG composites [154-156]. As the concentration of SF increased, the local density of the silk molecules was higher which enhanced the silk/PEG intermolecular interactions and subsequently the silk self-assembly. Hence, the gelation time was observed to decrease as the concentration of SF in silk/PEG composites increased from 4% to 6% for both silk/PEG composites of ratios 1:1 and 2:1 [154]. At the same time, with increasing silk concentrations, the mechanical properties (i.e. compressive modulus and yield strength) increased, with 6% silk/PEG having significantly better mechanical properties compared to 4% and 5% silk/PEG composites.

Conversely, with concentration of SF held constant and increasing concentrations of PEG, the gelation time was observed to increase. This was because with a higher density of PEG molecules within the composite, the increase in the viscosity of the blend increased the volume of the separated phase for SF molecules. The increase in viscosity had 2

68

counter effects occurring simultaneously; while more SF molecules entrapped in the separated phase promoted SF molecules aggregation, the decrease in the collision rate of SF and PEG molecules due to increased viscosity [154] led to the decreased rate of aggregation of SF molecules. From the results observed from **Figure 4- 7**, it would seem that for silk/PEG composites in a 1:1 ratio, the viscosity of the solution and hence the collision rate effect was more prominent, leading to a slight increase in the gelation time as PEG concentration increased. This relationship was found to be even more prominent for silk/PEG composites of 2:1 ratio where the phase separation effect was even less prominent with the increase in the amount of SF molecules; leading to a sharp increase in gelation time across increasing PEG concentrations.

Another contributing factor to the slower gelation was also due to the concentration and molecular weight of PEG being used. In a similar study with silk/PEG microspheres, it was found that for PEG of molecular weights 4000 – 20 000, the addition of PEG to 8% (w/v) SF only formed particles [154]. In the current study of blending lower concentrations of silk (i.e. 4%, 5% and 6%) with PEG (MW 8000), the gelation that was observed could be a mixture of both particles and gel. Within the groups of same SF concentration, the increase in PEG concentration enhanced the formation of silk/PEG gel microparticles more than gels. Due to the uneven distribution in the highly viscous solution, the microparticles may be prevented from forming fiber gel networks due to the limited interaction in the increasingly viscous solution hence causing the increase in gelation time. The uneven distribution of the microparticles in the resultant silk/PEG composite also resulted in the much lower mechanical properties with increasing PEG concentrations within a fixed SF concentration group (i.e. 6%). However, the decrease in mechanical properties was only significant for PEG concentrations above 65% and above 75% for silk/PEG blend ratios of 1:1 and 2:1 respectively. These could be indicative of

69

the concentrations at which the viscosity was so high that rapid local gelation (i.e. aggregation) occurred instead of self-assembly; the lower amount of β-sheet structures led to the lower mechanical properties of the resulting silk/PEG micro-particle gel [154].

(d)   Conclusion

The rationale for choosing silk/PEG composites was because of PEG's ability in inducing rapid silk gelation by easily changing either SF or PEG concentrations or their mixing ratios. From the results above, the shortest gelation time achieved with 6% silk/50% PEG composites of ratio 2:1 was only 11 minutes. However, this was at the expense of the mechanical properties of the composite. Conversely, for silk/PEG composites of better mechanical properties (i.e. 6% silk/65% PEG composite of ratio 2:1 with highest compressive modulus and yield strength of 18.21 kPa and 3.86 kPa respectively), the gelation time was found to be much longer at approximately 39 minutes. Even so, the mechanical properties of these silk/PEG gels were still three orders of magnitude lower than that of the PolyJet material used in the sleeve design demonstrated above. Hence, silk/PEG composites are not an optimal material for the translation of the 3D printable device. Neither can it be considered as a 3D printable bio-ink due to its difficulty in achieving an optimal silk/PEG ratio that has both high mechanical properties and an extremely short gelation time for conventional 3D extrusion printing.

iii.   Silk-SDS

(a)   Material and Methods

8mM Sodium dodecyl sulfate (SDS) solution was made by dissolving SDS powder (Sigma Aldrich) in dH$_2$0. Thereafter, 6% (w/v) SF solution was blended with SDS solutions at varying ratios and triplicates of each silk/SDS ratio at a volume of 1ml were pipetted to a 96-well plate (Corning® Costar®, NY, USA). For monitoring of the gelation process and the determination of gelation time, turbidity of the silk/SDS

70

composites during gelation were measured spectrophotometrically at the absorbance

mode (wavelength of 550nm) with defined intervals using a microplate reader (Turner

Bio- systems, Sunnyvale, CA) at a temperature of 25˚C over a period of 2 weeks. 6%

(w/v) SF solution and 8mM SDS solution were the negative controls for this study. The

opacity of the silk/SDS gels will increase over time and the change in optical density will

quantify the turbidity change [150] and hence the gelation time of the silk/SDS gels. For

each silk/SDS condition, the optical density values were averaged to obtain the change in

optical density over time. The gelation time was then determined as the time at which the

optical density reached a value corresponding to half of the maximum optical density

obtained [150, 151]. At the same time, the silk/SDS composites were loaded into 3ml

syringe – moulds for the eventual formation of silk/SDS gels and left to undergo

complete gelation at room temperature. Thereafter, the silk/SDS gels (n = 5) were

removed from their moulds and subjected to unconfined compression testing with an

Instron machine (Instron, Norwood, MA, USA) between 2 compression platens with a

10N load cell and at a compression loading rate of 1mm/minute till fracture (**Figure 4- 6**).

After normalizing to sample geometries, the compressive modulus was determined from

the slope of the initial linear region of the stress-strain curve generated and yield strength

determined using a 2% strain offset from the initial linear region [138, 153].

(b)   Results
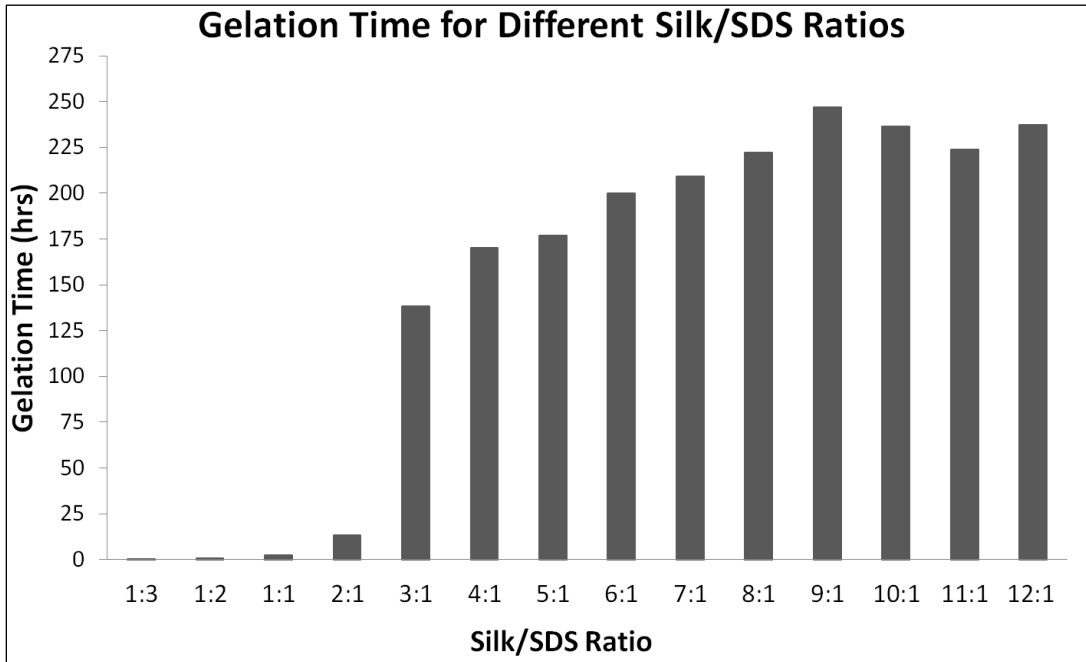
Figure 4- 10. Gelation times of silk/SDS composites. Gelation time increased as proportion of SDS decreased, with maximum gelation time at silk/SDS ratio of 9:1, before decreasing as SDS proportions decreased.

From **Figure 4- 10**, it was observed that when the proportion of SDS was in excess in the silk/SDS composites (i.e. silk/SDS ratio of 1:3 and 1:2); the gelation time was extremely short with the shortest gelation time of 8 minutes for silk/SDS ratio of 1:3. As the proportion of SDS decreased from 75% (i.e. silk/SDS ratio of 1:3) to 7.69% (i.e. silk/SDS ratio of 12:1), the gelation time increased from 8 minutes to a maximum of 10.29 days at 10% SDS (i.e. silk/SDS ratio of 9:1). No observable relationship between silk/SDS ratio and gelation time could be determined for proportions of SDS lower than 10%.
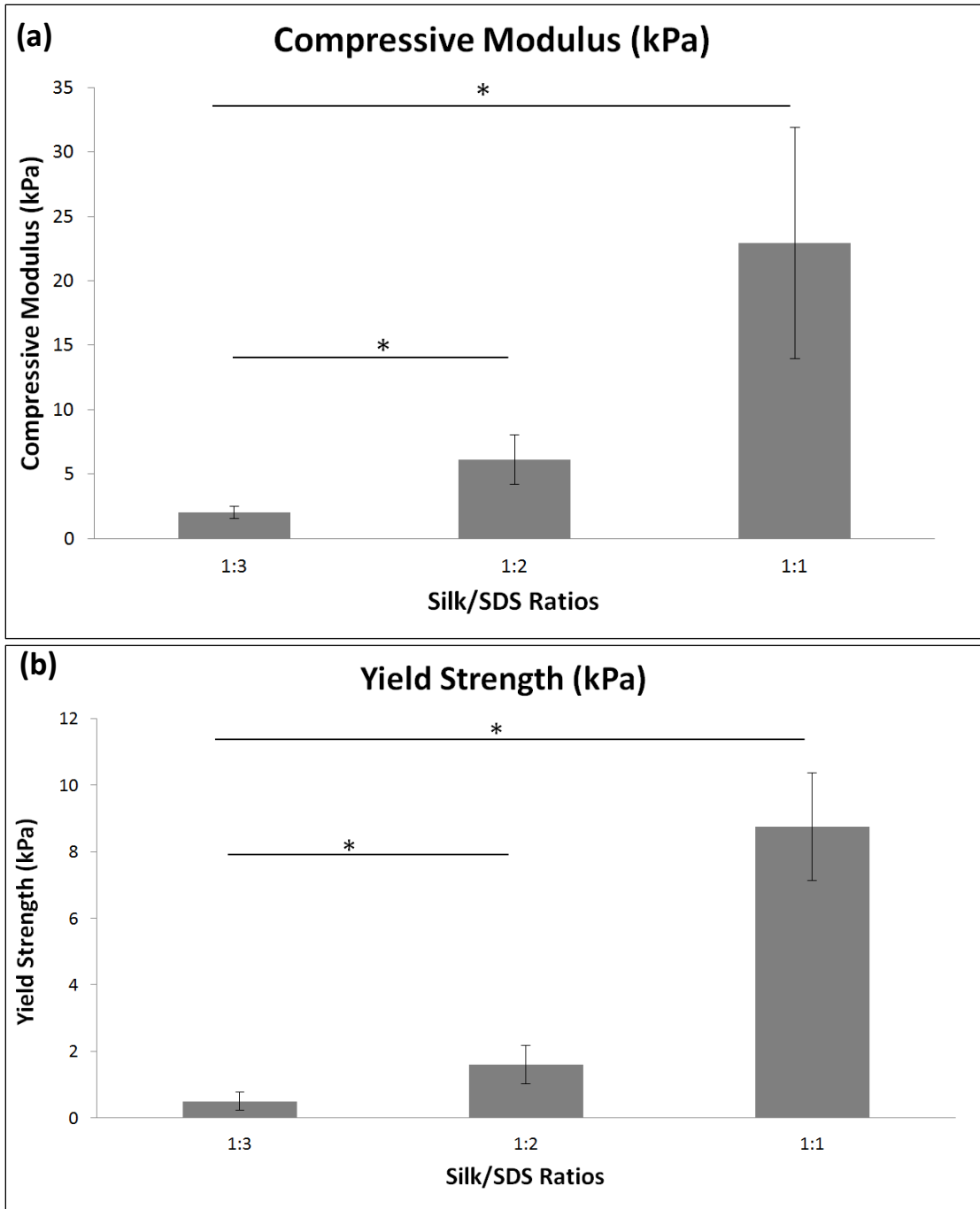
Figure 4- 11. Compressive modulus (kPa) (a) and yield strength (kPa) (b) of silk/SDS composites from ratios 1:3 to 1:1. Silk/SDS composites of ratio 1:1 and 1:2 had significantly higher compressive modulus and yield strength over composites of ratio 1:3 (*p<0.05).
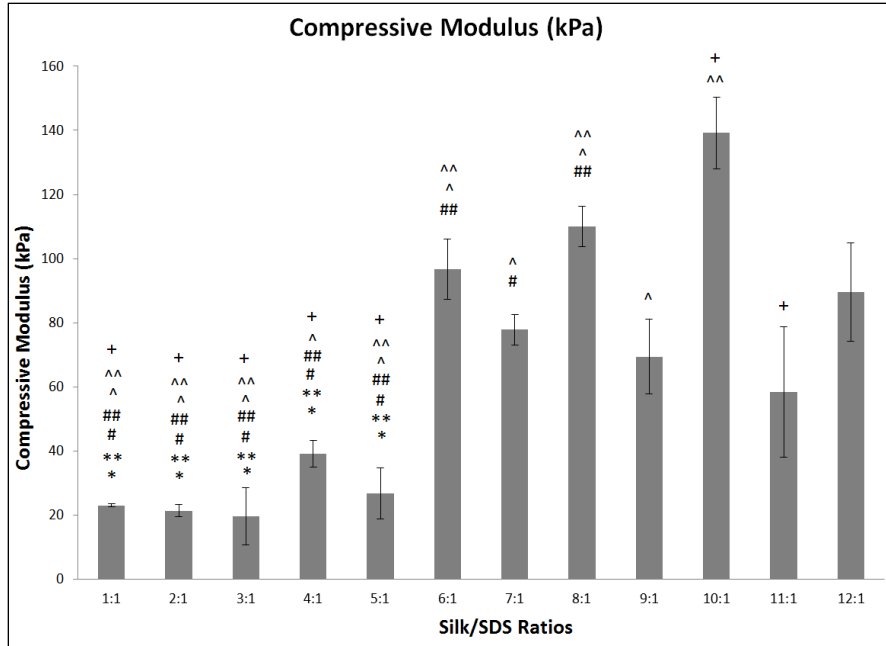
Figure 4- 12. Compressive modulus (kPa) of silk/SDS composites with ratios 1:1 to 12:1. Significantly lower compressive modulus was observed for silk/SDS composites from 1:1 to 5:1 as compared to their counterparts with ratio 6:1 (*p<0.05), 7:1 (**p<0.05), 8:1 (#p<0.05), 9:1 (##p<0.05), 10:1 (^p<0.05), 11:1 (^^p<0.05) and 12:1 (+p<0.05).
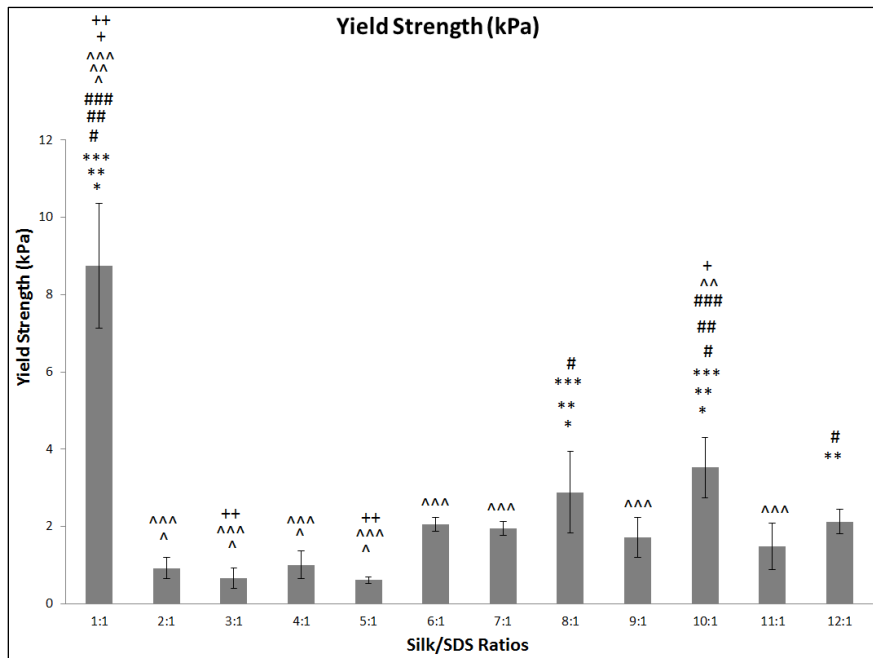
Figure 4- 13. Yield strength (kPa) of silk/SDS composites with ratios 1:1 to 12:1. Significantly higher compressive modulus was observed for silk/SDS blend of 1:1 as compared to their counterparts with ratio 2:1 (*p<0.05), 3:1 (**p<0.05), 4:1 (***p<0.05), 5:1 (#p<0.05), 6:1 (##p<0.05), 7:1 (###p<0.05), 8:1 (^p<0.05), 9:1 (^^p<0.05), 10:1 (^^^p<0.05), 11:1 (+p<0.05) and 12:1 (++p<0.05).

As the percentage of SDS decreased from 50% to 7.69% (**Figure 4- 12**), there was an observable increase in compressive modulus with the maximum compressive modulus of (139.18 ± 15.40) kPa observed at 9.09% SDS (i.e. silk/SDS ratio of 10:1). In general, for odd silk/SDS ratios of 2:1, 4:1, 6:1, 8:1, 10:1 and 12:1, the compressive modulus was found to be much higher than that of even silk/SDS ratios of 1:1, 3:1, 5:1, 7:1, 9:1, 11:1. Significantly lower compressive modulus was also observed for silk/SDS composites with 16.67% - 50% SDS as compared to their counterparts with 7.69% - 14.29% SDS. Conversely, as the percentage of SDS decreased from 50% to 7.69% (**Figure 4- 13**), there was a significant drop in yield strength when concentration of SDS dropped from 50% to 33.3% before increasing again for decreasing concentrations of SDS. The maximum yield strength of (8.75 ± 1.61) kPa was observed for silk/SDS composites with 50% of SDS. Thereafter, with decreasing proportion of SDS, the yield strength gradually increased till the next highest yield strength of (3.52 ± 0.78) kPa for silk/SDS blend ratio of 10:1.

(c)   Discussion

The rationale of blending silk with SDS was because even under mild conditions of 37˚C body temperature and pH 7, SDS as an anionic surfactant allows for accelerated fibroin aggregation and gelation [151]. 8mM SDS concentration was chosen because high concentrations of SDS (i.e. beyond 8mM) in the silk/SDS composites were believed to hinder gelation. It had been shown that the anionic groups present in SDS caused increased dehydration or salting out of silk fibroin. Due to the electrostatic repulsion, the negatively charged sulfonate groups outside of the SF molecules removed the surrounding water molecules. Hence, the intermolecular hydrophobic interactions between SF molecules and the long alkyl chains of SDS were promoted [157]. This facilitated the conformational change in structure from random coils to stable β-sheets.

75

The gelation time was also found to be dependent on the dehydration rate by the anionic surfactant and hence the concentration of anionic surfactant present [151, 157]; with decreasing SDS concentration, the dehydration rate was lower, leading to a longer gelation time as observed in **Figure 4- 10**. Beyond 10% SDS, there was only a slight decrease in gelation time attributed to the formation of more hydrophobic micro domains within the silk/SDS system because the concentration of SDS had reached its critical micellar concentration [151].

Stable gel formation was associated with SDS-induced gelation of silk. The combination of hydrophobic and electrostatic forces led to rapid protein folding and particle association with the eventual formation of an organised gel network [158] with conglomerate silk particles of micro sizes. With the decrease in concentration of SDS and hence the increase in concentration of SF solution, the final content of parallel β-sheets formed increased [159, 160]. Hence, there was an observed increased in the compressive modulus of the silk/SDS gels with the maximum modulus observed for 10% SDS concentration. This modulus was comparable to the compressive modulus of silk gels fabricated in other studies [139].

However, the positive linear relationship between β-sheet content and yield strength was not observed. This could be primarily due to the large slenderness ratio of the gel network which favoured the interconnection of clusters with each other. These physical cross-links were found to produce numerous cracks amongst the clusters [151]. As the concentration of SDS decreased, the increase in β-sheets formation increased the stiffness in the gels [161]. At the same time, the hydrophobic interactions were more dominant and the increase in water molecules led to weakened hydrogen bonds formed between β-chains. This decreased stability in the β-sheets could be the reason behind the lower yield

76

strength as SDS concentration decreased [162]. Conversely, at high SDS concentrations (i.e. 50% - 75%), the electrostatic repulsion amongst micellar aggregates became increasingly dominant [151]. Hence, as SDS concentration decreased from 75% to 50% and the number of negatively charged sulfonate groups and hence repulsion decreased, micellar aggregation was increased and promoted the gelation of silk. The increase in β-sheet content was reflected from the increase in yield strength.

(d)   Conclusion

Surfactants especially anionic surfactants are known to induce more rapid gelation of silk fibroin as compared with silk-polymer composites like silk/PEG with its properties of volume exclusion effect and silk/PVA which have to undergo multiple freeze-thaw cycles over days for complete gelation [158]. Compared with harsh and nonphysiological gelation methods like low pH and high temperature, SDS additives effectively shorten the gelation time without harmful effects as long as the concentration of SDS used is below the human lethal dose value of $500 - 5000$ mg kg^{-1} body weight [151]. From the results above, the shortest gelation time achieved with silk/SDS ratio of 1:3 was only 8 minutes; shorter than that for silk/PEG composites. However, the resultant silk/SDS gel has extremely weak mechanical properties. Conversely, for silk/SDS composites of higher mechanical properties (i.e. silk/SDS blend ratio of 10:1 with highest compressive modulus of 139.18 ± 15.40 kPa), the gelation time was found to be extremely long at approximately 9.85 days. The inverse relationship between gelation time and mechanical properties for silk/SDS composites does not make it an ideal bioink material. Therefore, another material capable of rapid gelation or the induction of rapid silk gelation has to be considered.

iv.   Silk-SDS Pluronic

(a)   Material and Methods

30% (w/v) Pluronic solution (i.e. Poloxamer 407, Sigma Aldrich) was blended with the

silk/SDS composite solutions (as above) at a ratio of 1:1. Thereafter, the

silk/SDS/Pluronic composites were then left at room temperature for a period of 2 weeks

for complete gelation before the composites were put to the extrusion test. Briefly, the

composites were loaded into 3ml syringes before being extruded through a 22G tapered

nozzle tip onto glass slides to form a rectangular construct. Thereafter, adopting a layer

by layer technique, more layers are extruded atop the previous layer to form a 3D

construct. For a preliminary examination of which silk/SDS/Pluronic composite ratios

had the potential to be a bioink, the following parameters were examined for the extruded

constructs over a period of 2 weeks:

During Extrusion	Post Extrusion
• Shear thinning • Thixotropy • Mechanical & Structural Integrity	• Mechanical & Structural Integrity • Rapid gelation

Using open source imaging software FIJI (2015), the dimensions of the extruded

constructs were measured and the percentage shrinkage in height of the constructs were

also calculated and plotted as shown in **Figure 4- 16**.

(b)   Results

In order to conduct a preliminary assessment of the silk/SDS/Pluronic composites that

would best fit the parameters above, the extruded constructs were assessed based on the

observations observed during and after extrusion and tabulated in **Table 4- 4**. Briefly, the

parameters of shear-thinning and thixotropy (i.e. time-dependent shear-thinning) of the

bioink material were assessed from possible nozzle clogging within the nozzle tip and the

"smoothness" of the extrusion. Post extrusion, the bioink material was then assessed

based upon the shape fidelity of construct formed and if the construct collapsed under the weight of the new extruded layers above and its stability at room temperature and conditions.

In general, the silk/SDS/Pluronic composites were observed to undergo complete gelation and had reached a stable state after a period of 21 days. With the Pluronic concentration held constant for all silk/SDS/Pluronic composites, as the concentration of SF solution increased, the ability of the bioink to form filamentous structures increased with no nozzle clogging observed. The extrusion was also smoother and the length of the extrudable fibres increased as compared with silk/SDS/Pluronic composites with lower concentration of silk which broke easily (**Table 4- 4**). The shape fidelity also increased with more stable 3D structures being formed; there was no visible collapse of the structure under the newly added layers and no visible spreading of the bioink material on the surface onto which the bioink material was extruded upon (**Figure 4- 15**). The constructs were observed to have good fusion between the layers and were increasingly stable at room temperature and pressure (**Table 4- 4**). When the constructs were left to dry for 24 hours at room temperature and pressure, there was 50% to 60% shrinkage in height across all groups with no significant difference between the groups (**Figure 4- 16**).
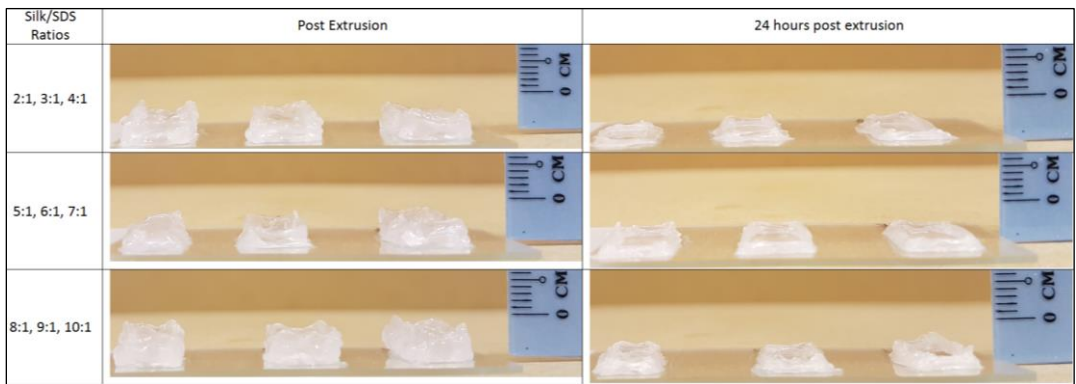
Figure 4- 14. Extruded constructs of silk/SDS/Pluronic composites of silk/SDS ratios of 2:1 to 10:1. The extruded constructs were observed to shrink in height 24 hours post extrusion.

Time (Days)	Extruded Constructs		
2			
5			
9			
21			
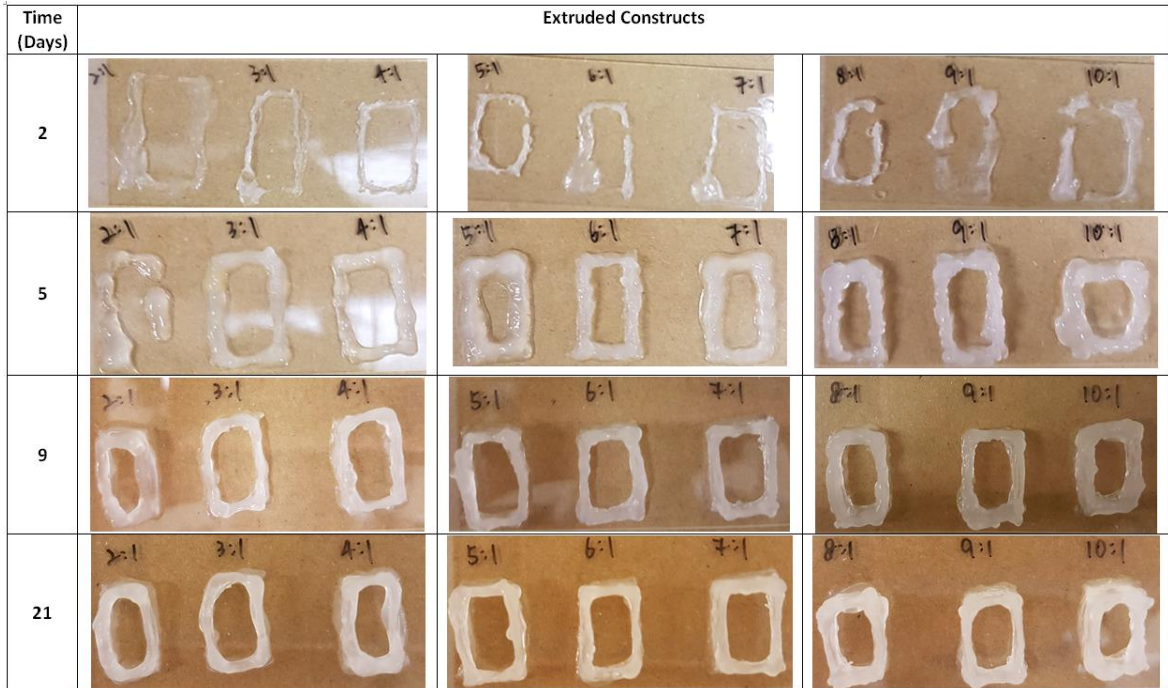
Figure 4- 15. Extruded constructs of silk/SDS/Pluronic composites of silk/SDS ratios of 2:1 to 10:1 over a period of 3 weeks. The shape fidelity, structural and mechanical integrity of the constructs improved with increasing silk concentration and increasing duration.
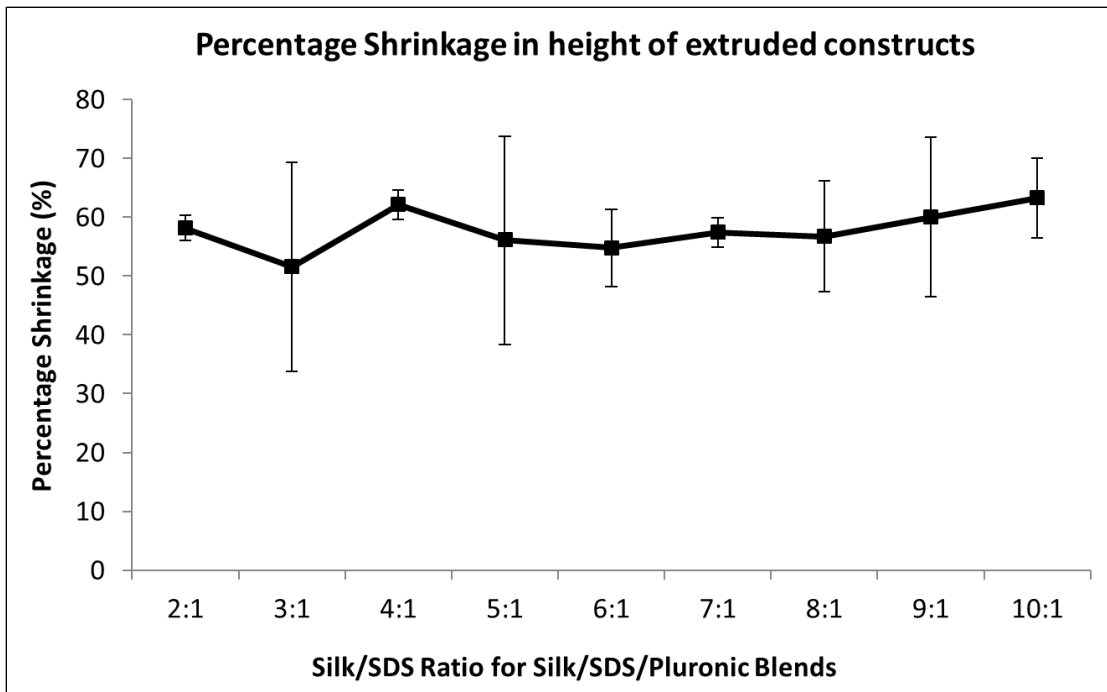
Figure 4- 16. Percentage Shrinkage in height of extruded constructs when left to dry for 24 hours at room temperature and pressure. Across all groups, the constructs had a shrinkage in height of between 50% to 60%.

Table 4- 4: Observable parameters of extruded constructs with silk/SDS/Pluronic composites of different silk/SDS ratios during and post extrusion. Y indicates yes while N indicates no.

Parameters	Silk/SDS Ratios (Silk/SDS composites are blended with Pluronic in a 1:1 ratio)								
	2:1	3:1	4:1	5:1	6:1	7:1	8:1	9:1	10:1
During Extrusion									
1.Nozzle Clogging	N	N	N	N	N	N	N	N	N
2.Smooth Extrusion	N	N	N	Y	Y	Y	Y	Y	Y
3.Formation of filament	N	N	Y	Y	Y	Y	Y	Y	Y
Post Extrusion									
1.Shape Fidelity	N	N	N	Y	Y	Y	Y	Y	Y
2.Construct collapse	Y	Y	N	N	N	N	N	N	N
3.Fusion between layers	Y	Y	Y	Y	Y	Y	Y	Y	Y
4.Stability at room temperature & pressure	N	N	Y	Y	Y	Y	Y	Y	Y

(c)   Discussion

Pluronic, also known as poloxamer 407, is a high molecular weight non-ionic surfactant. Due to the presence of hydrophobic interactions of its poly(propylene oxide) groups, it was able to undergo reversible gelation with a change in temperature. Hence, it has been often used as a sacrificial material in 3D bioprinting [163]. Conversely, due to the strong intermolecular hydrogen bonds present in SF, gelation of SF is irreversible [164]. When silk was blended with Pluronic, Pluronic caused a dehydrating effect when the hydrophilic groups of Pluronic removed the water molecules from the SF molecular chains and formed hydrophobic interactions with the chains because of its tendency for polymer binding, [157, 165]. Due to the enhanced hydrophobic interactions and hydrogen bonds between SF and Pluronic, not only was silk gelation accelerated, the reversal of gelation was also facilitated. It was suspected that Pluronic micelles formed did not influence silk fibroin gelation but instead, enhanced its own gelation [164]. With the addition of another ionic surfactant, SDS, to the silk/Pluronic blend, the critical micellar temperature of Pluronic was affected. In normal circumstances, at low temperatures, Pluronic is completely soluble in water and is thus liquid with its preference for polar conformation. As temperature increased, Pluronic-Pluronic interactions increased while Pluronic-water interaction decreased. This resulted in Pluronic forming a gel at room temperature. In the silk/SDS/Pluronic composite, SDS bound to Pluronic and suppressed this micellar formation. As SDS concentration increased, the amount of free Pluronic molecules decreased; hindering the aggregation of Pluronic molecules and the formation of micelles [165, 166]. Hence, there was no shape fidelity of the filaments formed and the bioink tend to spread on the printing substrate (**Figure 4-15**) because the Pluronic was unable to gel rapidly upon extrusion for

silk/SDS/Pluronic composites of high SDS concentrations (i.e. ratios of 2:1, 3:1). The gelation temperature of Pluronic was also increased such that the composites assumed a sol-gel form instead of the normal gel for Pluronic at room temperature. Nonetheless, with the shear thinning behaviour of both silk solution and Pluronic, no nozzle clogging was observed during extrusion.

After a period of 21 days, it was believed that with both SDS and Pluronic present as surfactants, the gelation of silk was accelerated which allowed for the formation of a soft gel which was extrudable yet able to maintain shape fidelity upon extrusion. The brittleness of normal silk gels was also found to be absent and this could be due to the presence of the surfactants which affected the gelation and hence the mechanical properties of the silk/SDS/Pluronic gel. Upon drying at room temperature, the composites were observed to undergo dehydration and this was evident from the 50% - 60% shrinkage in the constructs. This was an important feature to consider as the water swelling features of these composites will affect both the mechanical strength and the resolution of the eventual construct.

(d)   Conclusion

It can be concluded that the silk/SDS/Pluronic blend was able to form extrudable hydrogel of different extrudability and mechanical properties and may be a promising future bioink material. By changing the proportion of silk, SDS and Pluronic, the mechanical properties, viscosity and shear thinning properties can be optimised to have both mechanical strength and printability at the same time. The rationale behind this present study of simple observation and assessment of the workability of the silk/SDS/Pluronic composites was to conduct a preliminary selection and elimination of the composites that were not feasible. While further characterisation of the composites

such as viscosity, shear thinning properties, adhesion and surface tension properties is required, this study provided the basis for future investigation of parameters like Pluronic, silk and SDS concentrations, the ratios for the three solutions to be blended and how each parameter is related to each other for the development of a novel and ideal bioink suitable for biomedical applications.

5. Comparative Evaluation of Bioink materials

As discussed in Section 2.3.3 **Properties of a bio-ink,** there are many properties that a material has to have for it to be an ideal bioink. Five different materials were investigated in the present study and were compared and evaluated based on these performance metrics namely biocompatibility, compatibility with extrusion printing, biomimicry, resolution, scalability, practicality, mechanical and structural integrity, bioprinting and post-bioprinting processing time and degradability [102] in **Table 5- 1**and **Table 5- 2**.

At present, current 3D printing technologies are based on subsequent gelation post extrusion of the polymer solution. This fabrication technique is based on a layer-by-layer approach and in order for a solution to be self-supporting, it has to have high viscosity or able to gel rapidly on the printing surface [167].

Pure silk solution was initially considered as a bioink material because of its widespread use in ACL reconstruction applications and the ability to process SF solution into numerous material formats [137]. Low concentrations of silk solution have been known to have extremely slow rates of gelation under physiological conditions [151, 157, 168, 169]. This poses a challenge to the maintenance of the shape fidelity and resolution of the final construct post extrusion. In contrast, high concentrations of silk are highly viscous which help in the maintenance of the shape fidelity post extrusion. However, highly viscous SF solutions often have the problem of nozzle clogging during extrusion and a gelation rate too rapid for long term storage. Moreover, the results above have proved that the process of fabricating highly concentrated silk solution was non-reproducible due to the randomness and irreversibility of SF gelation and the yield was also extremely low. The extruded constructs were also not mechanically strong enough for further post

85

extrusion treatment. Further studies investigating the temperature responsiveness of silk

solutions also proved that freezing provided an alternative but temporary "gelation"

technique and thus maintenance of shape fidelity of the extruded filaments. Nonetheless,

when the temperature was raised to room temperature, the extruded SF filaments rapidly

thawed and were found to coalesce with adjacent filaments. For the formation of stable

silk filaments, the time consuming process of repeated freeze-thaw cycles were required.

Hence, these factors do not make pure silk solutions an ideal bioink material for 3D

extrusion applications.

Hydrogels are commonly used in 3D printing applications because they minimize the

collapse of the printed constructs by preserving their structures [167, 170-172]. Though

silk hydrogels have the potential to be developed as a potential bioink material, they are

too brittle for further applications [173, 174] and their gelation process is also random,

non-reproducible and non-uniform. Therefore, other methods of silk gelation have to be

considered; namely having silk-composite hydrogels like silk-PVA hydrogels or simply

having precipitating agents like large polymeric precipitating agent PEG, surface agents

like SDS surfactant and low molecular weight neutral additives like Pluronic [158]. There

are two general conditions required for the 3D printing of high-fidelity constructs. Firstly,

the extruded droplets must maintain their raised 3D profile instead of spreading

completely flat. Secondly, extruded droplets has to gel sufficiently to prevent the coalesce

of new extruded droplets adjacent or atop them [175].

In the first approach of silk-composite hydrogels, PVA was the chosen synthetic polymer

as it had been found to be effective in the improvement of physical properties of SF [176].

It had been widely reported in literature that through repeated freeze thaw cycles,

silk/PVA was able to form strong rubber-like gels [176, 177]. However, the current study

found that silk and PVA were immiscible and undergo macrophase separation when the silk/PVA composite films were cast and left to dry at room temperature. This resulted in the eventual delamination of the layers of the silk/PVA composite films which contributed to the inferior mechanical properties as compared to pure SF films. For homogenous silk/PVA composites, numerous time consuming freeze thaw cycles are required. Hence, silk/PVA composites did not fulfil the parameter of fast gelation for an ideal bioink.

An alternative polymer, PEG, was used as it can rapidly crosslink and induce the rapid gelation of SF [152, 178]. However, in the present study, when PEG was added in an equal proportion with SF, there was no reduction in gelation times observed. Gelation times even increased with increasing PEG concentration when half the proportion of PEG was added to SF. Composites of 6% silk/50% PEG of 2:1 ratio underwent rapid gelation but had extremely weak mechanical properties and thus structural integrity post extrusion. Though increasing the silk concentrations were found to have improved mechanical properties and faster gelation times, the final silk/PEG constructs did not have the mechanical strength for further post-extrusion processing. In addition, the constructs disintegrated upon contact with water due to the high solubility of PEG in water. Last but not least, blending other polymers (either PVA or PEG) to silk also affected the biocompatibility and biodegradability of silk fibroin [179].

Surface agents like SDS surfactants were then considered for the rapid gelation of SF. In the present study, SDS was shown to be an effective gelling agent with a significant reduction in gelation time to mere minutes when high concentrations of SDS was used. However, the higher the content of SDS present in the silk/SDS composite, the weaker the mechanical properties of the material. The extruded constructs were observed to lose

their structural integrity and the extrusion resolution was very poor. In addition, high concentrations of SDS (i.e. more than 1% SDS) are above the tolerance levels for human use and are thus toxic for tissue engineering applications [178]. Conversely, silk/SDS composites with low SDS content formed stable but irreversible, rubber-like gels at room temperature, had good mechanical properties but were non-extrudable through the nozzle. Therefore, in order to improve on the extrudability of the silk/SDS gels, an alternative material capable of rapid gelation had to be considered.

Pluronic, commonly used as a hydrogel or a sacrificial bioink for 3D printing applications, was studied for its interaction with silk/SDS gels. Due to its non-biodegradability in the human body, it has limited use for tissue engineering applications [180, 181]. However, Pluronic can be easily removed; thus, it was added to silk/SDS gels as a sacrificial material for the rapid gelation and the maintenance of shape fidelity of constructs post extrusion. This composite material was stable at room temperatures; it did not degrade over time and its extrudability remained even after 3 weeks at room temperature. Upon complete gelation of the silk/SDS/Pluronic constructs, Pluronic can then be leached out from the printed constructs and stable bioink materials were formed. One major concern with the addition of Pluronic was the significant decrease in the mechanical strength of the silk/SDS/Pluronic composites. Though the composites were now extrudable and were able to build up to form 3D structures, the mechanical and structural integrity of the constructs were limited. When the silk/SDS/Pluronic composites were removed from their moulds, its original form and structure was lost immediately and the composite material exhibited spreading on the printing surface. The extruded constructs were also observed to have 50% - 60% shrinkage in height when left to dry at room temperature. This shrinkage was significant as the water content of the extruded constructs may affect its eventual mechanical properties.

In conclusion, of all the silk and silk-composite materials investigated thus far, silk/SDS/Pluronic composite material showed the most potential of being a future biocompatible bioink due to its extrudability, mechanical and structural integrity at room temperature and pressure and its stability over time.

Table 5- 1: Comparison of silk and silk-based composites as potential bio-inks

	Parameters	Silk and Silk-based Composites					
		Concentrated SF	Temperature – sensitive SF	Silk/PVA	Silk/PEG	Silk/SDS	Silk/SDS/Pluronic
1	Biocompatibility	✓	✓	✓	✓	✓	✓
2	Compatibility with extrusion printing						✓
3	Biomimicry						
4	Resolution						✓
5	Scalability			✓	✓	✓	✓
6	Mechanical and Structural Integrity					✓	✓
7	Short Processing Time				✓		✓
8	Degradability	✓	✓	✓	✓	✓	✓
9	Practicality			✓	✓	✓	✓

Table 5- 2: Comparison of quantitative parameters of silk and silk-based composites as potential bio-inks

	Parameters	Silk and Silk-based Composites					
		Concentrated SF	Temperature – sensitive SF	Silk/PVA	Silk/PEG	Silk/SDS	Silk/SDS/Pluronic
1	Tensile Modulus (MPa)	N.A.*	N.A.*	16.9 ± 1.5	N.A.*	N.A.*	N.A.*
2	Ultimate Tensile Strength (MPa)	N.A.*	N.A.*	2.5 ± 1.4	N.A.*	N.A.*	N.A.*
3	Compression Modulus (kPa)	N.A.*	N.A.*	N.A.*	14.9 ± 4.3	2.0 ± 0.5	N.A.**
4	Yield Strength (kPa)	N.A.*	N.A.*	N.A.*	3.7 ± 0.8	0.5 ± 0.3	N.A.**
5	Gelation Time (Hours)	24	Months	N.A.***	0.183	0.134	Instantaneous

*No experimental results were obtained as these composites are not able to achieve a stable form for mechanical testing with the Instron machine.
**No experimental results were obtained as these composites were not stable for transfer between platforms for mechanical testing with the Instron machine.
***Inhomogeneous gelation occurs.

6. Conclusion and Recommendation for future work

6.1. Conclusion

ACL tears have a high rate of incidence amongst athletes. However, the native ACL has poor healing ability due to insufficient vascularization and this eventually leads to degenerative joint diseases. The current clinical treatment of surgical ACL reconstruction with biological grafts primarily focuses on mechanical fixation instead of the histological osteointegration of the graft within the bone tunnel. Hence, the aim of the present thesis was to design and develop a 3D printed device that will have its future application in ACL reconstruction surgery; a graft sleeve which helps in the promotion of osteointegration at the bone-tendon-graft interface within the bone tunnel.

Based on user needs of the graft sleeve and benchmarking it against a similar device, the tissue interface augmentation device for ligament or tendon reconstruction, various scaffold designs were explored and developed using Solidworks and subsequently printed with a 3D printer. The feasibility and efficacy of the designs were evaluated and improvements were made, with the final design being a hollow and porous cylinder with teethed protrusions regularly spaced along the interior wall of the scaffold. This design was found to have the grip strength to "bite" onto the tendon graft to ensure smooth pull-through of the graft – sleeve construct through a sawbone bone tunnel model without slippage of the graft out of the graft – sleeve construct.

In order to determine if the current design does indeed promote osteointegration at the graft and bone tunnel interface of *in vivo* ACL reconstruction, the graft sleeve has to be fabricated with a biocompatible material. Hence, concurrently, various silk-based materials were explored for the possibility of being a biocompatible 3D printable bioink

for its subsequent application as a biomaterial for printing of the graft sleeve. Initial studies with pure silk solutions showed that even though braided silk fibres were a comparable replacement for native ACL, as a potential bioink, its gelation time was too slow for mechanically and structurally stable constructs to be formed. Further studies with silk/polymer composites, namely silk/PVA and silk/PEG, similarly showed slow gelation times. While faster gelation times may be achieved with increased concentrations of these gelling agents, very often these composite materials have inferior mechanical properties. SDS surfactants were an alternative additive that was added to silk to induce rapid gelation. Silk/SDS gels with low surfactant content were found to be very stable and had superior mechanical properties though gelation time was extremely long. On the other hand, fast gelling silk/SDS constructs had the same limitation of having inferior mechanical properties as the silk-polymer gels. Hence, Pluronic as an alternative gelling agent and sacrificial material was added. It was found that this silk/SDS/Pluronic composite material had the extrudability and the mechanical strength required for the extrusion of stable 3D constructs. Thus, it is highly possible that this novel composite material can be further developed and optimised for its final application as a printable and biocompatible 3D printing bioink.

The studies in this thesis were divided into 2 main phases, the design and the material phase, with the objectives under each phase achieved and answered. Therefore, the overarching aim of this thesis, which was to design and develop a 3D printed graft sleeve for its future application in ACL reconstruction surgery to enhance osteointegration at the graft-bone interface, has been achieved.

6.2. Recommendations for future work

6.2.1. Recommendations for Design of Device

Further testing of the silk sleeve device on *in vitro* porcine bone models is required for a more accurate evaluation of the efficacy of the design as there are mechanical and morphological differences between sawbones models and porcine bone models. This can be done by drilling a bone tunnel through the porcine bone models similar to that of clinical ACL reconstruction surgeries and then pulling the silk sleeve-tendon graft construct through this tunnel. Through this study, the actual mechanical strength of the device and its grip strength on the tendon can be quantified and evaluated for its efficacy during the initial graft pull-through for ACL reconstruction surgeries. Thereafter, we expect more improvements to be made to the design of the device to address its current limitations.

6.2.2. Recommendations for Material of Device

Since this was a preliminary study to narrow down potential silk-composite materials ideal for bioprinting of the silk sleeve scaffold for ACL reconstruction surgeries, further characterisation and optimisation studies on the rheological, physical and chemical properties of the biomaterial and the blending ratios are required. It can be hypothesized that with a reduction in the concentration of Pluronic, the mechanical and structural integrity of the composite material will improve yet this may affect the subsequent extrudability of the material. Hence, a balance between Pluronic, silk and SDS concentrations and compositions of the composite material should be achieved in order to have a mechanically stable and extrudable bioink.

Further testing of the material should also be conducted with the printing of the bioink with commercial 3D extrusion printers to evaluate its compatibility with commercial 3D

printing technologies. The extrudability of the bioink material and the mechanical and structural integrity of the eventual construct are also highly dependent on the parameters of printing (i.e. splicing profile, strut density, strut thickness, distance between the layers in the z – direction). Hence, not only should the material compositions be optimised, the printing parameters of the 3D printing modality should also be studied and optimised. At the same time, the mechanical properties of the silk/SDS/Pluronic composite material and the final biomaterial should also be determined with the RSA3 Dynamic Mechanical Analyzer (TA Instruments, New Castle, DE) [123] and compared with the mechanical properties of conventional Rapid Prototyping material FLX9095 to ensure translatability of results.

In general, the results from the studies investigating the material of the device provided a stepping stone for the development of future silk-based bioinks compatible with commerical 3D printing technologies. At the same time, results from the design aspect of this thesis provided a cornerstone for the development of efficacious designs for future graft sleeve devices for applications relating to improved interfacial integration.

7. Bibliography

1.   Budny, J., et al., *Emerging Trends in Anterior Cruciate Ligament Reconstruction.* Journal of Knee Surgery, 2016.
2.   Duthon, V., et al., *Anatomy of the anterior cruciate ligament.* Knee surgery, sports traumatology, arthroscopy, 2006. **14**(3): p. 204-213.
3.   Petersen, W. and T. Zantop, *Anatomy of the anterior cruciate ligament with regard to its two bundles.* Clinical orthopaedics and related research, 2007. **454**: p. 35-47.
4.   Zantop, T., et al., *Anterior cruciate ligament anatomy and function relating to anatomical reconstruction.* Knee surgery, sports traumatology, arthroscopy, 2006. **14**(10): p. 982-992.
5.   LaBella, C.R., et al., *Anterior cruciate ligament injuries: diagnosis, treatment, and prevention.* Pediatrics, 2014. **133**(5): p. e1437-e1450.
6.   Leong, N.L., F.A. Petrigliano, and D.R. McAllister, *Current tissue engineering strategies in anterior cruciate ligament reconstruction.* Journal of biomedical materials research Part A, 2014. **102**(5): p. 1614-1624.
7.   Petrigliano, F.A., D.R. McAllister, and B.M. Wu, *Tissue engineering for anterior cruciate ligament reconstruction: a review of current strategies.* Arthroscopy: The Journal of Arthroscopic & Related Surgery, 2006. **22**(4): p. 441-451.
8.   Baxter, F., et al., *Augmentation of bone tunnel healing in anterior cruciate ligament grafts: application of calcium phosphates and other materials.* Journal of tissue engineering, 2010. **1**(1): p. 712370.
9.   Fu, F.H., et al., *Current trends in anterior cruciate ligament reconstruction part II. Operative procedures and clinical correlations.* The American journal of sports medicine, 2000. **28**(1): p. 124-130.
10.   Nau, T. and A. Teuschl, *Regeneration of the anterior cruciate ligament: Current strategies in tissue engineering.* World J Orthop, 2015. **6**(1): p. 127.
11.   Fu, F.H., et al., *Current trends in anterior cruciate ligament reconstruction part 1: biology and biomechanics of reconstruction.* The American journal of sports medicine, 1999. **27**(6): p. 821-830.
12.   Chang, S.K., et al., *Anterior cruciate ligament reconstruction: allograft versus autograft.* Arthroscopy: The journal of Arthroscopic & Related Surgery, 2003. **19**(5): p. 453-462.
13.   Marrale, J., M.C. Morrissey, and F.S. Haddad, *A literature review of autograft and allograft anterior cruciate ligament reconstruction.* Knee surgery, sports traumatology, arthroscopy, 2007. **15**(6): p. 690-704.
14.   Sherman, O.H. and M.B. Banffy, *Anterior cruciate ligament reconstruction: which graft is best?* Arthroscopy: The Journal of Arthroscopic & Related Surgery, 2004. **20**(9): p. 974-980.
15.   Haque, E., *A Systematic Review for Anterior Cruciate Ligament Reconstruction.* 2016.
16.   West, R.V. and C.D. Harner, *Graft selection in anterior cruciate ligament reconstruction.* Journal of the American Academy of Orthopaedic Surgeons, 2005. **13**(3): p. 197-207.
17.   Mascarenhas, R. and P.B. MacDonald, *Anterior cruciate ligament reconstruction: a look at prosthetics-past, present and possible future.* McGill Journal of Medicine, 2008. **11**(1): p. 29.

18.   Laurencin, C.T. and J.W. Freeman, *Ligament tissue engineering: an evolutionary materials science approach.* Biomaterials, 2005. **26**(36): p. 7530-7536.

19.   Legnani, C., et al., *Anterior cruciate ligament reconstruction with synthetic grafts. A review of literature.* International orthopaedics, 2010. **34**(4): p. 465-471.

20.   Vunjak-Novakovic, G., et al., *Tissue engineering of ligaments.* Annu. Rev. Biomed. Eng., 2004. **6**: p. 131-156.

21.   Altman, G.H., et al., *The Use of Long‐term Bioresorbable Scaffolds for Anterior Cruciate Ligament Repair.* Journal of the American Academy of Orthopaedic Surgeons, 2008. **16**(4): p. 177-187.

22.   Altman, G.H., et al., *Silk matrix for tissue engineered anterior cruciate ligaments.* Biomaterials, 2002. **23**(20): p. 4131-4141.

23.   Fan, H., et al., *Anterior cruciate ligament regeneration using mesenchymal stem cells and silk scaffold in large animal model.* Biomaterials, 2009. **30**(28): p. 4967-4977.

24.   Cristino, S., et al., *Analysis of mesenchymal stem cells grown on a three‐dimensional HYAFF 11®‐based prototype ligament scaffold.* Journal of Biomedical Materials Research Part A, 2005. **73**(3): p. 275-283.

25.   Hansson, A., et al., *In vitro evaluation of an RGD-functionalized chitosan derivative for enhanced cell adhesion.* Carbohydrate polymers, 2012. **90**(4): p. 1494-1500.

26.   Shao, H.J., et al., *The phenotypic responses of human anterior cruciate ligament cells cultured on poly (ϵ‐caprolactone) and chitosan.* Journal of Biomedical Materials Research Part A, 2010. **93**(4): p. 1297-1305.

27.   Shao, H.-J., et al., *Modulation of gene expression and collagen production of anterior cruciate ligament cells through cell shape changes on polycaprolactone/chitosan blends.* Biomaterials, 2010. **31**(17): p. 4695-4705.

28.   Majima, T., et al., *Alginate and chitosan polyion complex hybrid fibers for scaffolds in ligament and tendon tissue engineering.* Journal of Orthopaedic Science, 2005. **10**(3): p. 302-307.

29.   Majima, T., et al., *Chitosan-based hyaluronan hybrid polymer fibre scaffold for ligament and tendon tissue engineering.* Proceedings of the Institution of Mechanical Engineers, Part H: Journal of Engineering in Medicine, 2007. **221**(5): p. 537-546.

30.   Masuko, T., et al., *Chitosan–RGDSGGC conjugate as a scaffold material for musculoskeletal tissue engineering.* Biomaterials, 2005. **26**(26): p. 5339-5347.

31.   Yamane, S., et al., *Feasibility of chitosan-based hyaluronic acid hybrid biomaterial for a novel scaffold in cartilage tissue engineering.* Biomaterials, 2005. **26**(6): p. 611-619.

32.   Tovar, N., et al., *A comparison of degradable synthetic polymer fibers for anterior cruciate ligament reconstruction.* Journal of biomedical materials research Part A, 2010. **93**(2): p. 738-747.

33.   Lin, V.S., et al., *Ligament tissue engineering using synthetic biodegradable fiber scaffolds.* Tissue engineering, 1999. **5**(5): p. 443-451.

34.   Deehan, D. and T. Cawston, *The biology of integration of the anterior cruciate ligament.* Bone & Joint Journal, 2005. **87**(7): p. 889-895.

35.   Li, H., et al., *Functional regeneration of ligament-bone interface using a triphasic silk-based graft.* Biomaterials, 2016. **106**: p. 180-192.

36.   Moffat, K.L., et al., *Characterization of the structure–function relationship at the ligament-to-bone interface.* Proceedings of the National Academy of Sciences, 2008. **105**(23): p. 7947-7952.

37.   Thomopoulos, S., G.M. Genin, and L.M. Galatz, *The development and morphogenesis of the tendon-to-bone insertion What development can teach us about healing.* Journal of musculoskeletal & neuronal interactions, 2010. **10**(1): p. 35.

38.   Apostolakos, J., et al., *The enthesis: a review of the tendon-to-bone insertion.* MLTJ Muscles, Ligaments and Tendons Journal, 2014. **4**(3): p. 333-342.

39.   Connizzo, B.K., S.M. Yannascoli, and L.J. Soslowsky, *Structure–function relationships of postnatal tendon development: a parallel to healing.* Matrix Biology, 2013. **32**(2): p. 106-116.

40.   Atesok, K., et al., *Augmentation of tendon-to-bone healing.* J Bone Joint Surg Am, 2014. **96**(6): p. 513-521.

41.   Doschak, M. and R. Zernicke, *Structure, function and adaptation of bone-tendon and bone-ligament complexes.* J Musculoskelet Neuronal Interact, 2005. **5**(1): p. 35-40.

42.   Meyer, U., et al., *Fundamentals of tissue engineering and regenerative medicine.* 2009, Springer. p. 258-259.

43.   Zantop, T., W. Petersen, and F.H. Fu, *Anatomy of the anterior cruciate ligament.* Operative techniques in orthopaedics, 2005. **15**(1): p. 20-28.

44.   Benjamin, M. and D. McGonagle, *Entheses: tendon and ligament attachment sites.* Scandinavian journal of medicine & science in sports, 2009. **19**(4): p. 520-527.

45.   Paxton, J.Z., K. Baar, and L.M. Grover, *Current progress in enthesis repair: strategies for interfacial tissue engineering.* Orthopedic & Muscular System: Current Research, 2012. **2013**.

46.   Claudepierre, P. and M.-C. Voisin, *The entheses: histology, pathology, and pathophysiology.* Joint Bone Spine, 2005. **72**(1): p. 32-37.

47.   Lu, H.H. and S. Thomopoulos, *Functional attachment of soft tissues to bone: development, healing, and tissue engineering.* Annual review of biomedical engineering, 2013. **15**: p. 201.

48.   Villotte, S. and C. Knüsel, *Understanding entheseal changes: definition and life course changes.* International Journal of Osteoarchaeology, 2013. **23**(2): p. 135-146.

49.   Jin, S.-K., et al., *Enhancement of osseointegration of artificial ligament by nano-hydroxyapatite and bone morphogenic protein-2 into the rabbit femur.* Tissue Engineering and Regenerative Medicine, 2016. **13**(3): p. 284-296.

50.   Bunker, D., V. Ilie, and S. Nicklin, *Tendon to bone healing and its implications for surgery.* Muscles, ligaments and tendons journal, 2014. **4**(3): p. 343-350.

51.   Hao, Z.C., et al., *Stem cell therapy: a promising biological strategy for tendon–bone healing after anterior cruciate ligament reconstruction.* Cell proliferation, 2016.

52.   Mavrogenis, A., et al., *Biology of implant osseointegration.* J Musculoskelet Neuronal Interact, 2009. **9**(2): p. 61-71.

53.   Lui, P.P.-Y., et al., *Biology and augmentation of tendon-bone insertion repair.* Journal of orthopaedic surgery and research, 2010. **5**(1): p. 1.

54. Arnoczky, S.P., et al., *Biologic fixation of ligament prostheses and augmentations An evaluation of bone ingrowth in the dog.* The American journal of sports medicine, 1988. **16**(2): p. 106-112.

55. Wen, C.-y., et al., *Peri-graft bone mass and connectivity as predictors for the strength of tendon-to-bone attachment after anterior cruciate ligament reconstruction.* Bone, 2009. **45**(3): p. 545-552.

56. Chen, C.-H. and C.-H. Lee, *Biological fixation in anterior cruciate ligament surgery.* Asia-Pacific Journal of Sports Medicine, Arthroscopy, Rehabilitation and Technology, 2014. **1**(2): p. 48-53.

57. Dong, Y., et al., *Enhancement of Tendon–Bone Healing for Anterior Cruciate Ligament (ACL) Reconstruction Using Bone Marrow-Derived Mesenchymal Stem Cells Infected with BMP-2.* International journal of molecular sciences, 2012. **13**(10): p. 13605-13620.

58. Kiapour, A. and M. Murray, *Basic science of anterior cruciate ligament injury and repair.* Bone and Joint Research, 2014. **3**(2): p. 20-31.

59. Hirzinger, C., et al., *ACL injuries and stem cell therapy.* Archives of orthopaedic and trauma surgery, 2014. **134**(11): p. 1573-1578.

60. Rothrauff, B.B. and R.S. Tuan, *Cellular therapy in bone-tendon interface regeneration.* Organogenesis, 2014. **10**(1): p. 13-28.

61. Hays, P.L., et al., *The role of macrophages in early healing of a tendon graft in a bone tunnel.* The Journal of Bone & Joint Surgery, 2008. **90**(3): p. 565-579.

62. Lim, J.-K., et al., *Enhancement of tendon graft osteointegration using mesenchymal stem cells in a rabbit model of anterior cruciate ligament reconstruction.* Arthroscopy: The Journal of Arthroscopic & Related Surgery, 2004. **20**(9): p. 899-910.

63. Chen, C.-H., *Graft healing in anterior cruciate ligament reconstruction.* BMC Sports Science, Medicine and Rehabilitation, 2009. **1**(1): p. 1.

64. Chen, B., et al., *Enhancement of tendon-to-bone healing after anterior cruciate ligament reconstruction using bone marrow-derived mesenchymal stem cells genetically modified with bFGF/BMP2.* Scientific reports, 2016. **6**.

65. Pascher, A., et al., *Enhanced repair of the anterior cruciate ligament by in situ gene transfer: evaluation in an in vitro model.* Molecular Therapy, 2004. **10**(2): p. 327-336.

66. Steinert, A.F., et al., *In situ IGF-1 gene delivery to cells emerging from the injured anterior cruciate ligament.* Biomaterials, 2008. **29**(7): p. 904-916.

67. Ying, Z.-m., T. Lin, and S.-g. Yan, *Low-intensity pulsed ultrasound therapy: a potential strategy to stimulate tendon-bone junction healing.* Journal of Zhejiang University Science B, 2012. **13**(12): p. 955-963.

68. Walsh, W.R., et al., *Effects of low-intensity pulsed ultrasound on tendon–bone healing in an intra-articular sheep knee model.* Arthroscopy: The Journal of Arthroscopic & Related Surgery, 2007. **23**(2): p. 197-204.

69. Wang, C.J., et al., *The effect of shock wave treatment at the tendon–bone interface—an histomorphological and biomechanical study in rabbits.* Journal of orthopaedic research, 2005. **23**(2): p. 274-280.

70. Wang, C.-J., et al., *Shock wave treatment shows dose-dependent enhancement of bone mass and bone strength after fracture of the femur.* Bone, 2004. **34**(1): p. 225-230.

71.   Wang, C.-J., H.-Y. Huang, and C.-H. Pai, *Shock wave-enhanced neovascularization at the tendon-bone junction: an experiment in dogs.* The journal of foot and ankle surgery, 2002. **41**(1): p. 16-22.

72.   Thomopoulos, S., et al., *The effect of muscle loading on flexor tendon‐to‐bone healing in a canine model.* Journal of Orthopaedic Research, 2008. **26**(12): p. 1611-1617.

73.   Subramony, S.D., et al., *Combined effects of chemical priming and mechanical stimulation on mesenchymal stem cell differentiation on nanofiber scaffolds.* Journal of biomechanics, 2014. **47**(9): p. 2189-2196.

74.   Altman, G., et al., *Cell differentiation by mechanical stress.* Faseb Journal, 2002. **16**(2): p. 270-272.

75.   Brophy, R.H., et al., *Effect of short-duration low-magnitude cyclic loading versus immobilization on tendon-bone healing after ACL reconstruction in a rat model.* J Bone Joint Surg Am, 2011. **93**(4): p. 381-393.

76.   Fu, F.H. and S. Cohen, *Current concepts in ACL reconstruction*. 2008: SLACK Incorporated.

77.   Yilgor, C., P. Yilgor Huri, and G. Huri, *Tissue engineering strategies in ligament regeneration.* Stem cells international, 2011. **2012**.

78.   He, P., et al., *Enhanced osteoinductivity and osteoconductivity through hydroxyapatite coating of silk‐based tissue‐engineered ligament scaffold.* Journal of Biomedical Materials Research Part A, 2013. **101**(2): p. 555-566.

79.   Jiang, J., et al., *Enhancement of osseointegration of polyethylene terephthalate artificial ligament by coating of silk fibroin and depositing of hydroxyapatite.* Int J Nanomedicine, 2014. **9**: p. 4569-4580.

80.   Liu, C., Z. Xia, and J. Czernuszka, *Design and development of three-dimensional scaffolds for tissue engineering.* Chemical Engineering Research and Design, 2007. **85**(7): p. 1051-1064.

81.   Lu, T., Y. Li, and T. Chen, *Techniques for fabrication and construction of three-dimensional scaffolds for tissue engineering.* International journal of nanomedicine, 2013. **8**: p. 337.

82.   Zhu, N. and X. Chen, *Biofabrication of tissue scaffolds*. 2013: INTECH Open Access Publisher.

83.   Khan, F., M. Tanaka, and S.R. Ahmad, *Fabrication of polymeric biomaterials: a strategy for tissue engineering and medical devices.* Journal of Materials Chemistry B, 2015. **3**(42): p. 8224-8249.

84.   Pattanashetti, N.A., et al., *Chapter 21 Advances in Polymers and Tissue Engineering Scaffolds*, in *Green Polymer Composites Technology: Properties and Applications*. 2016, CRC Press. p. 343-354.

85.   Peltola, S.M., et al., *A review of rapid prototyping techniques for tissue engineering purposes.* Annals of medicine, 2008. **40**(4): p. 268-280.

86.   Mironov, V., et al., *Biofabrication: a 21st century manufacturing paradigm.* Biofabrication, 2009. **1**(2): p. 022001.

87.   Zhu, W., et al., *3D printing of functional biomaterials for tissue engineering.* Current opinion in biotechnology, 2016. **40**: p. 103-112.

88.   Jain, K., *Role of nanotechnology in developing new therapies for diseases of the nervous system.* 2006.

89. Rho, K.S., et al., *Electrospinning of collagen nanofibers: effects on the behavior of normal human keratinocytes and early-stage wound healing.* Biomaterials, 2006. **27**(8): p. 1452-1461.

90. Bourell, D., et al. *Solid freeform fabrication an advanced manufacturing approach*. in *Proceedings of the SFF Symposium*. 1990.

91. Jose, R.R., et al., *Evolution of Bioinks and Additive Manufacturing Technologies for 3D Bioprinting.* ACS Biomaterials Science & Engineering, 2016.

92. Murphy, S.V. and A. Atala, *3D bioprinting of tissues and organs.* Nature biotechnology, 2014. **32**(8): p. 773-785.

93. Pati, F., et al., *Extrusion Bioprinting*, in *Essentials of 3D Biofabrication and Translation*, M. Anthony Atala and M. James J. Yoo, PhD, Editors. 2015, Mica Haley. p. 123–152.

94. Dababneh, A.B. and I.T. Ozbolat, *Bioprinting technology: a current state-of-the-art review.* Journal of Manufacturing Science and Engineering, 2014. **136**(6): p. 061016.

95. Sundaramurthi, D., S. Rauf, and C. Hauser, *3D bioprinting technology for regenerative medicine applications.* International Journal of Bioprinting, 2016. **2**(2).

96. Prendergast, M.E., R.D. Solorzano, and D. Cabrera, *Bioinks for biofabrication: current state and future perspectives.* Journal of 3D printing in medicine, 2017. **1**(1): p. 49-62.

97. Carrow, J.K., et al., *Polymers for bioprinting.* Essentials of 3D Biofabrication and Translation; Atala, A., Yoo, JJ, Eds, 2015.

98. Chimene, D., et al., *Advanced bioinks for 3D printing: A materials science perspective.* Annals of biomedical engineering, 2016. **44**(6): p. 2090-2102.

99. Panwar, A. and L.P. Tan, *Current status of bioinks for micro-extrusion-based 3D bioprinting.* Molecules, 2016. **21**(6): p. 685.

100. Richards, D., et al., *3D bioprinting for vascularized tissue fabrication.* Annals of biomedical engineering, 2017. **45**(1): p. 132-147.

101. Ozbolat, I.T., *Scaffold-based or scaffold-free bioprinting: competing or complementing approaches?* Journal of Nanotechnology in Engineering and Medicine, 2015a. **6**(2): p. 024701.

102. Hospodiuk, M., et al., *The bioink: A comprehensive review on bioprintable materials.* Biotechnology Advances, 2017.

103. Chia, H.N. and B.M. Wu, *Recent advances in 3D printing of biomaterials.* Journal of biological engineering, 2015. **9**(1): p. 4.

104. Parker, S.T., et al., *Biocompatible silk printed optical waveguides.* Advanced Materials, 2009. **21**(23): p. 2411-2415.

105. Lewis, J.A., *Direct ink writing of 3D functional materials.* Advanced Functional Materials, 2006. **16**(17): p. 2193-2204.

106. Ghosh, S., et al., *Direct‐Write Assembly of Microperiodic Silk Fibroin Scaffolds for Tissue Engineering Applications.* Advanced Functional Materials, 2008. **18**(13): p. 1883-1889.

107. Kurland, N.E., et al., *Precise patterning of silk microstructures using photolithography.* Advanced Materials, 2013. **25**(43): p. 6207-6212.

108. Yucel, T., P. Cebe, and D.L. Kaplan, *Vortex-induced injectable silk fibroin hydrogels.* Biophysical journal, 2009. **97**(7): p. 2044-2050.

109. Schacht, K., et al., *Biofabrication of Cell‐Loaded 3D Spider Silk Constructs.* Angewandte Chemie International Edition, 2015. **54**(9): p. 2816-2820.

110. Brown, J.E., et al., *Injectable silk-based biomaterials for cervical tissue augmentation: an in vitro study.* American journal of obstetrics and gynecology, 2016. **214**(1): p. 118. e1-118. e9.

111. Stoppel, W.L., et al., *Elastic, silk‐cardiac extracellular matrix hydrogels exhibit time‐dependent stiffening that modulates cardiac fibroblast response.* Journal of Biomedical Materials Research Part A, 2016. **104**(12): p. 3058-3072.

112. Golding, A., et al., *A tunable silk hydrogel device for studying limb regeneration in adult Xenopus Laevis.* PloS one, 2016. **11**(6): p. e0155618.

113. Tao, H., et al., *Inkjet printing of regenerated silk fibroin: From printable forms to printable functions.* Advanced Materials, 2015. **27**(29): p. 4273-4279.

114. Applegate, M.B., et al., *Photocrosslinking of Silk Fibroin Using Riboflavin for Ocular Prostheses.* Advanced Materials, 2016.

115. Sun, Y.-L., et al., *Aqueous multiphoton lithography with multifunctional silk-centred bio-resists.* Nature communications, 2015. **6**.

116. Sun, L., et al., *Direct‐Write Assembly of 3D Silk/Hydroxyapatite Scaffolds for Bone Co‐Cultures.* Advanced healthcare materials, 2012. **1**(6): p. 729-735.

117. Heard, A.J., et al., *Silk-based injectable biomaterial as an alternative to cervical cerclage: an in vitro study.* Reproductive Sciences, 2013. **20**(8): p. 929-936.

118. Das, S., et al., *Enhanced redifferentiation of chondrocytes on microperiodic silk/gelatin scaffolds: toward tailor-made tissue engineering.* Biomacromolecules, 2013. **14**(2): p. 311-321.

119. Das, S., et al., *Bioprintable, cell-laden silk fibroin–gelatin hydrogel supporting multilineage differentiation of stem cells for fabrication of three-dimensional tissue constructs.* Acta biomaterialia, 2015. **11**: p. 233-246.

120. Ziv, K., et al., *A tunable silk–alginate hydrogel scaffold for stem cell culture and transplantation.* Biomaterials, 2014. **35**(12): p. 3736-3743.

121. Compaan, A.M., K. Christensen, and Y. Huang, *Inkjet Bioprinting of 3D Silk Fibroin Cellular Constructs using Sacrificial Alginate.* ACS Biomaterials Science & Engineering, 2016.

122. Jose, R.R., et al., *Polyol-silk bioink formulations as two-part room-temperature curable materials for 3D printing.* ACS Biomaterials Science & Engineering, 2015. **1**(9): p. 780-788.

123. Rodriguez, M.J., et al., *Silk based bioinks for soft tissue reconstruction using 3-dimensional (3D) printing with in vitro and in vivo assessments.* Biomaterials, 2017. **117**: p. 105-115.

124. Kamrani, A.K. and E.A. Nasr, *Engineering design and rapid prototyping*. 2010: Springer Science & Business Media.

125. Kamrani, A.K. and M.S. Sa'ed, *Product design for modularity*. 2002: Springer Science & Business Media.

126. GOH, C.H.J., et al., *Tissue interface augmentation device for ligament/tendon reconstruction*. 2015, Google Patents.

127. Nasr, E.A. and A.K. Kamrani, *Computer Based Design and Manufacturing*. 2007: Springer Science & Business Media.

128. Conte, E.J., et al., *Hamstring autograft size can be predicted and is a potential risk factor for anterior cruciate ligament reconstruction failure.* Arthroscopy: The Journal of Arthroscopic & Related Surgery, 2014. **30**(7): p. 882-890.

129. Darnley, J.E., et al., *Anterior Cruciate Ligament Reconstruction Using a Combination of Autograft and Allograft Tendon: A MOON Cohort Study.* Orthopaedic Journal of Sports Medicine, 2016. **4**(7): p. 2325967116662249.

130. Clatworthy, M., *Graft Diameter matters in Hamstring ACL reconstruction.* Orthopaedic Journal of Sports Medicine, 2016. **4**(7_suppl5): p. 2325967116S00082.

131. Yang, D.-L., et al., *A comparison of the fixation strengths provided by different intraosseous tendon lengths during anterior cruciate ligament reconstruction: a biomechanical study in a porcine tibial model.* Clinics in orthopedic surgery, 2014. **6**(2): p. 173-179.

132. Guan, J., et al., *Preparation and characterization of highly porous, biodegradable polyurethane scaffolds for soft tissue applications.* Biomaterials, 2005. **26**(18): p. 3961-3971.

133. Hsu, Y.Y., et al., *Effect of polymer foam morphology and density on kinetics of in vitro controlled release of isoniazid from compressed foam matrices.* Journal of Biomedical Materials Research Part A, 1997. **35**(1): p. 107-116.

134. Zhang, R. and P.X. Ma, *Poly (α-hydroxyl acids)/hydroxyapatite porous composites for bone-tissue engineering. I. Preparation and morphology.* 1999.

135. Loh, Q.L. and C. Choong, *Three-dimensional scaffolds for tissue engineering applications: role of porosity and pore size.* Tissue Engineering Part B: Reviews, 2013. **19**(6): p. 485-502.

136. Lu, S., et al., *Insoluble and flexible silk films containing glycerol.* Biomacromolecules, 2009. **11**(1): p. 143-150.

137. Rockwood, D.N., et al., *Materials fabrication from Bombyx mori silk fibroin.* Nature protocols, 2011. **6**(10): p. 1612-1631.

138. Wang, X., et al., *Sonication-induced gelation of silk fibroin for cell encapsulation.* Biomaterials, 2008. **29**(8): p. 1054-1064.

139. Kim, U.-J., et al., *Structure and properties of silk hydrogels.* Biomacromolecules, 2004. **5**(3): p. 786-792.

140. Hanawa, T., et al., *New oral dosage form for elderly patients: preparation and characterization of silk fibroin gel.* Chemical and pharmaceutical Bulletin, 1995. **43**(2): p. 284-288.

141. Ribeiro, M., et al., *The role of dialysis and freezing on structural conformation, thermal properties and morphology of silk fibroin hydrogels.* Biomatter, 2014. **4**(1): p. e28536.

142. Tsukada, M., et al., *Preparation and application of porous silk fibroin materials.* Journal of Applied Polymer Science, 1994. **54**(4): p. 507-514.

143. Oliveira, A., et al., *Aligned silk-based 3-D architectures for contact guidance in tissue engineering.* Acta biomaterialia, 2012. **8**(4): p. 1530-1542.

144. Nguyen, H.T., et al., *Investigate the Effect of Thawing Process on the Self-Assembly of Silk Protein for Tissue Applications.* BioMed Research International, 2017. **2017**: p. 16.

145. Wang, X., et al., *Silk nanospheres and microspheres from silk/pva blend films for drug delivery.* Biomaterials, 2010. **31**(6): p. 1025-1035.

146. Liu, Y., et al., *Structure and properties of the composite membrane of regenerated silk fibroin and PVA and ITS application to amperometric tetrathiafulvalene-mediating glucose sensor.* Journal of Macromolecular Science, Part A: Pure and Applied Chemistry, 1996. **33**(2): p. 209-219.

147. Li, M., et al., *Preparation of Porous Poly (vinyl alcohol)‐Silk Fibroin (PVA/SF) Blend Membranes.* Macromolecular Materials and Engineering, 2001. **286**(9): p. 529-533.

148. Dai, L., J. Li, and E. Yamada, *Effect of glycerin on structure transition of PVA/SF blends.* Journal of applied polymer science, 2002. **86**(9): p. 2342-2347.

149. Tanaka, T., et al., *Properties of silk fibroin/poly (vinyl alcohol) blend solutions and peculiar structure found in heterogeneous blend films.* Polymer international, 1997. **42**(1): p. 107-111.

150. Matsumoto, A., et al., *Mechanisms of silk fibroin sol– gel transitions.* The Journal of Physical Chemistry B, 2006. **110**(43): p. 21630-21638.

151. Wu, X., et al., *Sodium dodecyl sulfate-induced rapid gelation of silk fibroin.* Acta biomaterialia, 2012. **8**(6): p. 2185-2192.

152. Serban, M.A., B. Panilaitis, and D.L. Kaplan, *Silk fibroin and polyethylene glycol‐based biocompatible tissue adhesives.* Journal of Biomedical Materials Research Part A, 2011. **98**(4): p. 567-575.

153. Almany, L. and D. Seliktar, *Biosynthetic hydrogel scaffolds made from fibrinogen and polyethylene glycol for 3D cell cultures.* Biomaterials, 2005. **26**(15): p. 2467-2477.

154. Wu, J., et al., *Control of silk microsphere formation using polyethylene glycol (PEG).* Acta biomaterialia, 2016. **39**: p. 156-168.

155. Zhao, H., et al., *Comparison of gelation time and polyalcohol effect on hydrogels from domestic and wild silk fibroins.* Advances in Materials Science and Engineering, 2012. **2012**.

156. Xiong, S.-Y., et al., *Effect of Polyalcohol on the Gelation Time and Gel Structure of Silk Fibroin.* Journal of Fiber Bioengineering and Informatics. **3**(4): p. 236-243.

157. Park, J.H., et al., *Effect of surfactants on sol–gel transition of silk fibroin.* Journal of sol-gel science and technology, 2014. **71**(2): p. 364-371.

158. Floren, M., C. Migliaresi, and A. Motta, *Processing Techniques and Applications of Silk Hydrogels in Bioengineering.* Journal of Functional Biomaterials, 2016. **7**(3): p. 26.

159. Bai, S., et al., *Reversible hydrogel–solution system of silk with high beta-sheet content.* Biomacromolecules, 2014. **15**(8): p. 3044-3051.

160. Lu, S.Z., X.L. Wu, and M.Q. Luo. *Silk Fibroin Sol-Gel Transitions in Different Solutions*. in *Advanced Materials Research*. 2011. Trans Tech Publ.

161. Zhang, F., et al. *Excellent Cell Compatibility in Time Controlled Silk Fibroin Hydrogels*. in *Materials Science Forum*. 2014.

162. Cheng, Y., et al., *On the strength of β-sheet crystallites of Bombyx mori silk fibroin.* Journal of The Royal Society Interface, 2014. **11**(96): p. 20140305.

163. Müller, M., et al., *Nanostructured Pluronic hydrogels as bioinks for 3D bioprinting.* Biofabrication, 2015. **7**(3): p. 035006.

164. Kang, G.D., et al., *Effects of poloxamer on the gelation of silk fibroin.* Macromolecular rapid communications, 2000. **21**(11): p. 788-791.

165. Li, Y., et al., *Binding of sodium dodecyl sulfate (SDS) to the ABA block copolymer Pluronic F127 (EO97PO69EO97): F127 aggregation induced by SDS.* Langmuir, 2001. **17**(1): p. 183-188.

166. Hecht, E. and H. Hoffmann, *Interaction of ABA block-copolymers with ionic surfactants in aqueous-solution.* Langmuir, 1994. **10**(1): p. 86-91.

167. Rutz, A.L., et al., *A multimaterial bioink method for 3D printing tunable, cell‐compatible hydrogels.* Advanced Materials, 2015. **27**(9): p. 1607-1614.

168. Su, D., et al., *Enhancing the Gelation and Bioactivity of Injectable Silk Fibroin Hydrogel with Laponite Nanoplatelets.* ACS applied materials & interfaces, 2016. **8**(15): p. 9619-9628.

169. Deng, C.M., T.Y. Zhong, and B.Q. Zuo. *Surfactant-induced nanofibrous architecture of silk fibroin hydrogels*. in *Materials Science Forum*. 2013. Trans Tech Publ.

170. Highley, C.B., C.B. Rodell, and J.A. Burdick, *Direct 3D printing of shear‐thinning hydrogels into self‐healing hydrogels.* Advanced Materials, 2015. **27**(34): p. 5075-5079.

171. Hölzl, K., et al., *Bioink properties before, during and after 3D bioprinting.* Biofabrication, 2016. **8**(3): p. 032002.

172. Hong, S., et al., *3D printing of highly stretchable and tough hydrogels into complex, cellularized structures.* Advanced Materials, 2015. **27**(27): p. 4035-4040.

173. Partlow, B.P., et al., *Highly tunable elastomeric silk biomaterials.* Advanced functional materials, 2014. **24**(29): p. 4615-4624.

174. Park, S.-H., et al., *Silk-fibrin/hyaluronic acid composite gels for nucleus pulposus tissue regeneration.* Tissue Engineering Part A, 2011. **17**(23-24): p. 2999-3009.

175. Pataky, K., et al., *Microdrop Printing of Hydrogel Bioinks into 3D Tissue‐Like Geometries.* Advanced Materials, 2012. **24**(3): p. 391-396.

176. Li, M., et al., *Structure and properties of silk fibroin–poly (vinyl alcohol) gel.* International journal of biological macromolecules, 2002. **30**(2): p. 89-94.

177. Neo, P.Y., et al., *Characterization and mechanical performance study of silk/PVA cryogels: towards nucleus pulposus tissue engineering.* Biomedical Materials, 2014. **9**(6): p. 065002.

178. Wang, X., et al., *Injectable silk-polyethylene glycol hydrogels.* Acta biomaterialia, 2015. **12**: p. 51-61.

179. Li, Z., et al., *Robust Protein Hydrogels from Silkworm Silk.* ACS Sustainable Chemistry & Engineering, 2016. **4**(3): p. 1500-1506.

180. Yu, L. and J. Ding, *Injectable hydrogels as unique biomedical materials.* Chemical Society Reviews, 2008. **37**(8): p. 1473-1481.

181. Zhang, Z., et al., *Biodegradable and thermoreversible PCLA–PEG–PCLA hydrogel as a barrier for prevention of post-operative adhesion.* Biomaterials, 2011. **32**(21): p. 4725-4736.